

Nuclear Magnetic Dipole Transitions Excited by Backward Angle Scattering

LAWRENCE W. FAGG

*Linac Branch
Radiation Technology Division*

June 9, 1975



NAVAL RESEARCH LABORATORY
Washington, D.C.

UNCLASSIFIED

SECURITY CLASSIFICATION OF THIS PAGE (When Data Entered)

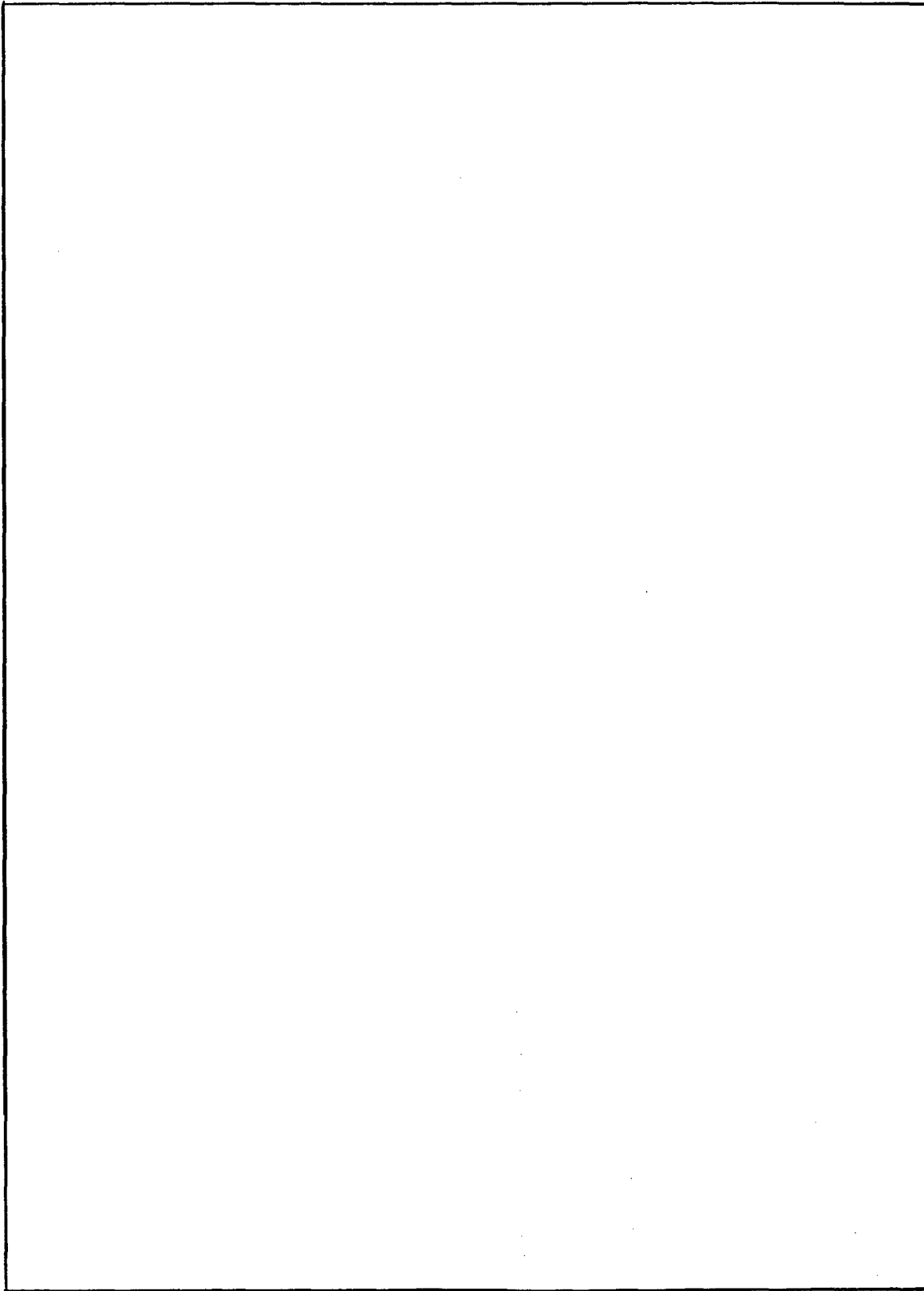
UNCLASSIFIED

REPORT DOCUMENTATION PAGE		READ INSTRUCTIONS BEFORE COMPLETING FORM
1. REPORT NUMBER NRL REPORT 7878	2. GOVT ACCESSION NO.	3. RECIPIENT'S CATALOG NUMBER
4. TITLE (and Subtitle) Nuclear Magnetic Dipole Transitions Excited by Backward Angle Scattering	5. TYPE OF REPORT & PERIOD COVERED Interim report on a continuing NRL problem	
	6. PERFORMING ORG. REPORT NUMBER	
7. AUTHOR(s) Lawrence W. Fagg	8. CONTRACT OR GRANT NUMBER(s)	
9. PERFORMING ORGANIZATION NAME AND ADDRESS Naval Research Laboratory Washington, D.C. 20375	10. PROGRAM ELEMENT, PROJECT, TASK AREA & WORK UNIT NUMBERS NRL Problem H01-09 Project RR 012-06-41-5005	
11. CONTROLLING OFFICE NAME AND ADDRESS Department of the Navy Office of Naval Research Arlington, Virginia 22217	12. REPORT DATE June 9, 1975	
	13. NUMBER OF PAGES 84	
14. MONITORING AGENCY NAME & ADDRESS (if different from Controlling Office)	15. SECURITY CLASS. (of this report) Unclassified	
	15a. DECLASSIFICATION/DOWNGRADING SCHEDULE	
16. DISTRIBUTION STATEMENT (of this Report) Approved for public release; distribution unlimited.		
17. DISTRIBUTION STATEMENT (of the abstract entered in Block 20, if different from Report)		
18. SUPPLEMENTARY NOTES		
19. KEY WORDS (Continue on reverse side if necessary and identify by block number). Electron scattering Nuclear magnetic dipole transitions		
20. ABSTRACT (Continue on reverse side if necessary and identify by block number) The field of electroexcitation of nuclear <i>M1</i> transitions is reviewed. The subject is introduced with an elementary description of the relationship between backward-angle electron scattering and <i>M1</i> excitation. Data analysis methods as well as 180° electron scattering techniques are also treated. The discussion of experimental results emphasizes the strength of the spin-flip transition, the concentration of <i>M1</i> strength in self-conjugate nuclei, the degree of fragmentation of this strength in other nuclei, and the response of odd-<i>A</i> rotational nuclei and heavy nuclei to 180° electron scattering.		

DD FORM 1473
1 JAN 73

EDITION OF 1 NOV 65 IS OBSOLETE
S/N 0102-014-6601

UNCLASSIFIED
SECURITY CLASSIFICATION OF THIS PAGE (When Data Entered)



CONTENTS

INTRODUCTION	1
THEORETICAL SURVEY	2
Relationship between Backward Angle Scattering and <i>M1</i> Transitions	2
Nuclear Properties Studied at Backward Angles	6
Radiation Tails and Radiative Corrections	18
SURVEY OF EXPERIMENTAL TECHNIQUES IN BACKWARD-ANGLE SCATTERING	22
Characteristic Experimental Problems in Backward- Angle Scattering	22
Significant Backward-Angle Scattering Techniques	24
Other Experimental Considerations	30
DISCUSSION OF EXPERIMENTAL RESULTS	35
Self-Conjugate Nuclei	35
Other Than Self-Conjugate Nuclei	57
Remarks on Some Closely Related Experimental <i>M1</i> Studies	68
CONCLUSIONS AND SUGGESTIONS FOR FURTHER STUDY	69
ACKNOWLEDGMENTS	69
REFERENCES	70
GLOSSARY OF SYMBOLS	81

NUCLEAR MAGNETIC DIPOLE TRANSITIONS EXCITED BY BACKWARD ANGLE SCATTERING*

INTRODUCTION

It has been the peculiar characteristic of backward angle electron scattering in general, and 180° electron scattering in particular, to selectively excite magnetic multipole transitions in nuclei. This has been especially true of magnetic dipole ($M1$) transitions amenable to excitation by the lower energy (<100 MeV) incident electron beams available at some Linac laboratories throughout the world.

This very selectivity has served to delimit a subfield of nuclear physics that can properly be called "Electroexcitation of Magnetic Dipole Transitions." Barber and his collaborators [2,3] essentially founded this field with their early survey results using backward angle electron scattering. Since that time there has been a steady growth in the productivity and accuracy of the experimental results in this field, along with a concurrent growth in the theoretical interest in these results.

Two articles that have to some extent reviewed this field were written by Barber [3] and by Goldemberg and Pratt [4] roughly a decade ago. The former article was actually a review of inelastic electron scattering in general at an early stage of its development and included discussions of pertinent scattering theory, experimental techniques, and the then-current experimental results. The latter paper, although dealing essentially with magnetic electron scattering, elastic and inelastic, was primarily devoted to theory and to extraction and interpretation of information on nuclear structure in general, with little discussion of results of work on specific nuclei.

More recently Theissen [5], reviewing the inelastic electron scattering from light nuclei, discussed the associated experimental apparatus, data analysis, and experimental results. Whereas his article indeed deals with some more recently electroexcited $M1$ transitions, its coverage is limited to the light nuclei, and the primary thrust of the article is not directed to magnetic inelastic scattering.

Under these circumstances it was felt that a review of the electroexcitation of $M1$ transitions in nuclei at this time would be useful. Furthermore, such a review would be quite timely since a summarization of the first major phases of the effort in this area could serve as a basis for the more precise work expected with the new round of higher resolution, higher current Linac facilities (e.g., Bates-M.I.T., Darmstadt, Amsterdam, Saclay) presently emerging. Thus, this report will present relevant theoretical considerations, survey current experimental techniques, and attempt as complete as possible a

Note: Manuscript submitted February 11, 1975.

*This report is a considerably expanded version of an earlier outline on this subject [1].

This work was done in part under the auspices of the Aspen Center for Physics, Aspen, Colorado.

coverage of electroexcited $M1$ transitions in nuclei at low-momentum transfers (<100 MeV/c). However, no claim of ultimate completeness is made.† The presentation throughout will be made from as elementary and conceptual a point of view as feasible.

Accordingly, a theoretical survey is presented in which considerable emphasis is placed on an examination of the intimate relationship between backward angle electron scattering and excitation of $M1$ transitions. The nuclear properties that can be studied in backward angle scattering along with Coulomb distortion effects are then discussed. Also, some remarks on radiative tails and corrections relevant to backward scattering are included. In the third section are mentioned some of the problems associated with 180° scattering and their solution in terms of some of the more significant 180° scattering techniques. The main body of the experimental results are discussed in the fourth section. Because of their uniqueness, the self-conjugate nuclei are the subject of a separate section prefaced with some appropriate theoretical remarks, again of a most elementary nature.

THEORETICAL SURVEY

Relationship Between Backward Angle Scattering and $M1$ Transitions

The capacity of backward angle electron scattering to selectively excite $M1$ transitions in nuclei was mentioned at the very beginning of the introduction. This intimate relationship between backward angle scattering and excitation of $M1$ transitions, being the foundation on which the field treated in this report is based, will be examined using an elemental and descriptive approach.

Focusing attention exclusively on the relationship between 180° electron scattering and $M1$ transitions will simplify the discussion. However, the remarks will, of course, also be applicable, but to a lesser degree, to scattering at backward angles not too far from 180° . Two features of this relationship will be highlighted: (a) assuming certain approximations, the longitudinal component of the scattering cross section vanishes at 180° , leaving only the transverse electric and magnetic components; (b) of the latter two components, the transverse magnetic usually dominates if the excitation energy is not too high compared to the incident electron energy.

To begin, it will be useful to define the distinction between the longitudinal and transverse components. If we regard the electromagnetic interaction as that between the nuclear charges and currents and the virtual photons generated by the electron in its trajectory, the two components can be defined in terms of the polarizations of these virtual photons. In particular, as shown in the extremely simplified diagram in Fig. 1, the longitudinal interaction results from those virtual photons polarized along the direction of the momentum transfer \vec{q} , whereas the transverse interaction results from those polarized perpendicular to this direction.

The distinction between these components is quite clear cut in the expression for the cross section in the plane-wave Born approximation (PWBA), where each term is

†For reviews of $M1$ transitions per se, see, for example, Hanna [6] and Yoshida [7].

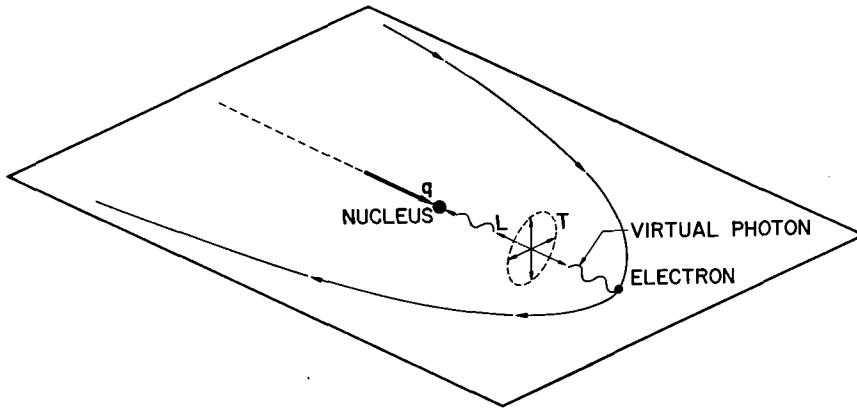


Fig. 1 — Definition of longitudinal and transverse virtual photon polarizations with respect to momentum transfer direction [1].

either longitudinal or transverse. However, in the distorted-wave expression (DWBA), interference terms dilute this distinction. Thus, again for the sake of conceptual simplicity, we will discuss the plane-wave expression which for a given multipolarity and for the two components can be written as

$$\frac{d\sigma_{\ell}}{d\Omega} = \frac{4\pi\alpha}{[(2L + 1)!!]^2} \frac{q^{2L}}{p^2} B(CL, q) V_{\ell}(\theta) \quad (1)$$

$$\frac{d\sigma_t}{d\Omega} = \frac{4\pi\alpha(L + 1)}{L[(2L + 1)!!]^2} \frac{q^{2L}}{p^2} [B(EL, q) + B(ML, q)] V_t(\theta) \quad (2)$$

with

$$V_{\ell} = \frac{\cos^2(\theta/2)}{4 \sin^4(\theta/2)}, \quad V_t = \frac{1 + \sin^2(\theta/2)}{8 \sin^4(\theta/2)}, \quad (3)$$

where q is the momentum transfer and p , the incident electron momentum. The expressions for V_{ℓ} and V_t are valid in the approximation that $p \gg \omega$ and m , where ω is the excitation energy and m the electron mass. $B(CL, q)$, $B(EL, q)$ and $B(ML, q)$ are the reduced transition matrix elements for longitudinal, transverse electric, and transverse magnetic interactions, respectively.

Inspection of Eq. (3) shows that at $\theta = 180^\circ$, $V_{\ell} = 0$; and thus $d\sigma_{\ell}/d\Omega = 0$. This is the first important feature of 180° electron scattering: that only the transverse electric and magnetic components of the cross section are nonzero, subject to the above assumptions.

An elementary visualization of the basis for the vanishing of the longitudinal component in the above equations can be given in terms of the conservation of helicity [8,9]. If it is assumed that the electron energy is large enough and the electron spin is thus aligned or opposite to its momentum direction, then the conservation of helicity should

be approximately valid. For helicity to be conserved in a 180° scattering as shown in Fig. 2, a spin-flip must occur. Since the longitudinal or Coulomb interaction cannot cause a spin-flip, only the transverse electric and magnetic interactions will remain active under these conditions.

Of these two interactions, it can be shown by means of two arguments that, for a given multipolarity, the magnetic generally dominates in a 180° scattering, if the excitation energy is not too high [10]. The first of these arguments is based on the order-of-magnitude estimates of the PWBA cross sections involved. For example, taking the reduced matrix element (as defined by Rosen [11]) $\langle J_f \parallel r^L \parallel J_i \rangle \approx (1.2A^{1/3} fm)L$, where fm is fermis and $q \approx 100$ MeV/c, typical for the relatively low-energy experiments discussed here, Überall [12] finds that

$$\sigma(M1)/\sigma(E1) \approx 3, \quad \sigma(M1)/\sigma(E2) \approx 25, \quad \sigma(M1)/\sigma(M2) \approx 8. \quad (4)$$

As will be seen in the fourth section, the estimate for $\sigma(M1)/\sigma(E1)$ is clearly lower than what is generally observed experimentally. Nevertheless, even in this crude approximation some dominance is indicated. A somewhat more refined approximation in closer general agreement with experiment observations has been made by Rosen [9] based on the independent particle model [13]. Assuming the same initial and final state spins, the same transition radii for the two kinds of transitions, and a $q = 100$ MeV/c, a ratio of

$$\sigma(M1)/\sigma(E1) \approx 16 \quad (5)$$

is obtained.

That this dominance of the $M1$ cross section should prevail in 180° scattering is supported by another, somewhat more fundamental argument [14,15] which we start by setting down the expressions for the four components of the electron current due to the beam electrons. Assuming $p, p' \gg m$, then it can easily be shown that

$$j_x = u_f^\dagger \alpha_x u_i \approx -2i (pp'/4m^2)^{1/2} \chi_f^\dagger \sigma_y \chi_i \quad (6)$$

$$j_y = u_f^\dagger \alpha_y u_i \approx 2i (pp'/4m^2)^{1/2} \chi_f^\dagger \sigma_x \chi_i \quad (7)$$

$$j_z = u_f^\dagger \alpha_z u_i \ll j_x, j_y \quad (8)$$

$$j_0 = u_f^\dagger u_i \ll j_x, j_y, \quad (9)$$

where p and p' are the incident and scattered electron momenta, respectively, and u_f, u_i and χ_f, χ_i are the 4-component and 2-component final and incident electron spin functions, respectively. Now j_x and j_y are only nonzero for a spin-flip; and j_z and j_0 , which are small relative to j_x and j_y , are neglected. Thus, if a spin-flip occurs in the 180° scattering, we have

$$\vec{j} = (pp'/m^2)^{1/2} e^{i\vec{q}\cdot\vec{r} - iq_0 t} \begin{pmatrix} 1 \\ i \\ 0 \end{pmatrix} \quad (10)$$

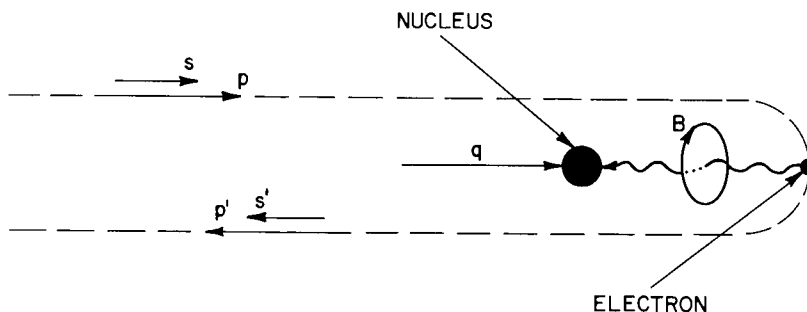


Fig. 2 — The circular polarization of the virtual photon in a 180° electron spin-flip scattering. The electron trajectory is shown for descriptive purposes and is not intended to depict the actual trajectory. (From Ref. 1.)

where \vec{q} is the 3-momentum transfer and q_0 is the zeroth component of the momentum transfer (approximately ω , neglecting recoil); and where the space-time part of the electron wave function has been included and the products of the spinors and Pauli matrices evaluated. Also, for the sake of simplicity, Eq. (10) has been calculated for the case of initial spin in the direction of the incident momentum. Solving the reduced Maxwell equation

$$\square^2 \vec{A} = \vec{j} \quad (11)$$

for the vector potential \vec{A} , we have

$$\vec{A} = \frac{1}{\vec{q}^2 - q_0^2} (pp'/m^2)^{1/2} e^{i|\vec{q}|z - iq_0 t} \begin{pmatrix} 1 \\ i \\ 0 \end{pmatrix}. \quad (12)$$

Now if the excitation energy ω is not too large, then $|\vec{q}| \gg q_0$, and we can state that

$$\vec{E} = \vec{\nabla} \cdot \vec{A} \approx \frac{-i q_0}{\vec{q}^2} (pp'/m^2)^{1/2} e^{i|\vec{q}|z - iq_0 t} \begin{pmatrix} 1 \\ i \\ 0 \end{pmatrix} \approx 0 \quad (13)$$

and

$$\vec{B} = \vec{\nabla} \times \vec{A} \approx \frac{i |\vec{q}|}{\vec{q}^2} (pp'/m^2)^{1/2} e^{i|\vec{q}|z - iq_0 t} \begin{pmatrix} -i \\ 1 \\ 0 \end{pmatrix}. \quad (14)$$

Thus, under the conditions of the approximation used for these last two expressions, only \vec{B} is nonzero and the transition is magnetic. Since a spin-flip is involved, the angular momentum change is 1. Thus assuming that the lowest orbital angular momentum involves the strongest interaction (which is true at the low-momentum transfers considered here), we see that an $M1$ transition will dominate. It should be remembered that the magnetic field expressed in Eq. (14) is that associated with a virtual photon and not a real magnetic dipole photon, which would have an accompanying electric field.

It needs to be stressed that (13) and (14) are valid only when $|\vec{q}| \gg q_0 \approx \omega$ (if the recoil is not too great), which, incidentally is the same approximation under which (3) is valid. When this is not the case and ω becomes comparable with $|\vec{q}|$, then the transverse electric field becomes effective. This explains why, for example, the 180° electron scattering spectra from ^{24}Mg and ^{28}Si (pages 49 and 55) in the giant resonance region (≈ 20 MeV) show many of the peaks due to $E1$ transitions that are observed with scattering at more forward angles as well as with photon scattering. This feature of 180° scattering will be treated further in the discussion of sd-shell nuclei (p. 47).

Perhaps the most interesting feature of the result expressed in Eq. (14) is, as an inspection of the phases of the components shows, that \vec{B} is circularly polarized. As mentioned earlier in calculating (10), the result in (14) is for the case when the electron spin is directed along the incident and scattered momenta. A little study of the relative phasing shows that the field in (14) is left-hand circularly polarized with respect to the direction of \vec{q} as shown in Fig. 2. If the incident and scattered spins were aligned in a direction opposite to the corresponding momenta, \vec{B} would be right-hand circularly polarized.

This means that even with an unpolarized incident beam the nucleus in a 180° scattering has effectively been subjected to a nuclear alignment (for definition of nuclear alignment see Ref. 16, p. 712). For example, suppose a nucleus with 0^+ ground-state spin undergoes an $M1$ transition as a result of 180° electroexcitation to a 1^+ excited state. Then the magnetic substates $m = \pm 1$ will be preferentially populated. This in turn means that the decay gamma ray will in general be plane polarized.

Nuclear Properties Studied at Backward Angles

Plane-Wave Born Approximation — Again for the sake of clarity, we confine our remarks on the study of nuclear properties to those determined by means of electron scattering at 180° only, using a PWBA analysis. A discussion of DWBA corrections to such PWBA analyses as well as direct DWBA analysis itself will be given in the next subsection. From the measured values of the experimental cross sections at 180° , three nuclear properties can in principle be determined (assuming $q \lesssim 100$ MeV/c): XL , the multipolarity of the transition excited ($X = E$ or M); R_{tr} , the transition radius; and Γ_o , the ground-state transition width. The value of the last quantity can often provide useful restrictions on nuclear wave functions (e.g., see p. 35). The question of the physical significance of R_{tr} will be discussed in the next subsection.

One general approach adopted in determining these three properties is to compare the experimental curve of cross section vs momentum transfer q to curves based on the corresponding theoretical PWBA expressions using trial multiplicities and reasonable transition radii (the use of the word "reasonable" here will be clarified below). Accordingly, a fit is made of the PWBA curve to the experimental curve extrapolated to $q=0$ and XL and R_{tr} are thereby determined. The value of the cross section at $q=0$ yields $B(XL, 0)$, from which Γ_o can be obtained.

We start the details of this analysis by first setting down the PWBA expression for transverse inelastic scattering at 180° :

$$\left(\frac{d\sigma}{d\Omega}\right)_{180^\circ} = \frac{\pi\alpha}{[(2L+1)!!]^2} \frac{L+1}{L} \frac{q^{2L}}{p^2} B(XL, q), \quad (15)$$

where L is the multipolarity, $X = E$ or M , q is the momentum transfer, p the incident electron momentum, α the fine structure constant, and $B(XL, q)$ the reduced nuclear matrix element. Incidentally, it should be remembered that at 180° , one has $q = 2p - \omega$, where ω is the nuclear excitation energy; thus the only means of varying q is by varying the incident electron energy since other angles are not available in most 180° systems. The reduced matrix element $B(XL, q)$ can be expanded in terms of q and the transition radii $R_{\ell X}$ ($\ell = 2, 4, 6 \dots$), which for the magnetic multipolarities is given by Rosen [11]:

$$B(ML, q) = B(ML, 0) \left[1 - \frac{L+3}{L+1} \frac{(qR_{2M})^2}{2(2L+3)} + \frac{L+5}{L+1} \frac{(qR_{4M})^4}{8(2L+3)(2L+5)} - \dots \right]^2, \quad (16)$$

where the first two transition radii $R_{\ell M}$ are defined as [11]

$$R_{2M}^2 = \frac{L+1}{L+3} \frac{\langle J || r^{L+2} || J_0 \rangle_m}{\langle J || r^L || J_0 \rangle_m} \quad (17)$$

$$R_{4M}^4 = \frac{L+1}{L+5} \frac{\langle J || r^{L+4} || J_0 \rangle_m}{\langle J || r^L || J_0 \rangle_m} \quad (18)$$

Initial and final states are here denoted by their spins, J_0 and J , respectively. In Eqs. (17) and (18)

$$\langle J || r^{L+\ell} || J_0 \rangle_m = \langle J || d^3 r [r^{L+\ell} \vec{j} \cdot \vec{Y}_{LL}(\hat{r}) + \vec{\mu} \cdot \vec{\nabla} r^{L+\ell} \vec{Y}_{LL}(\hat{r})] J_0 \rangle, \quad (19)$$

where \vec{j} and $\vec{\mu}$ are the nuclear charge current and magnetization density, respectively.

The reduced matrix element for the electric multipolarities is given by

$$q^2 B(EL, q) = \lim_{q \rightarrow 0} [q^2 B(EL, q)] \left[1 - \frac{L+3}{L+1} \frac{(qR_{2E})^2}{2(2L+3)} + \frac{L+5}{L+1} \frac{(qR_{4E})^4}{8(2L+3)(2L+5)} - \dots \right]^2 \quad (20)$$

where the first two transition radii are

$$R_{2E}^2 = \frac{L+1}{L+3} \frac{\langle J \| r^{L+2} \| J_0 \rangle_{ej} - 2(2L+3)R_c^2 \langle J \| r^L \| J_0 \rangle_{e\mu}}{\langle J \| r^L \| J_0 \rangle_{ej}} \quad (21)$$

and

$$R_{4E}^4 = \frac{L+1}{L+5} \frac{\langle J \| r^{L+4} \| J_0 \rangle_{ej} - 4(2L+5)R_c^2 \langle J \| r^{L+2} \| J_0 \rangle_{e\mu}}{\langle J \| r^L \| J_0 \rangle_{ej}} \quad (22)$$

where R_c is the charge radius of the nucleus. In Eqs. (21) and (22) the matrix elements due to nuclear charge currents and magnetization density, respectively, are

$$\langle J \| r^{L+\xi} \| J_0 \rangle_{ej} = R_c \langle J \| \int d^3 r \vec{j} \cdot \vec{\nabla} X r^{L+\xi} \vec{Y}_{LL}(\hat{r}) \| J_0 \rangle \quad (23)$$

and

$$\langle J \| r^{L+\xi} \| J_0 \rangle_{e\mu} = R^{-1} \langle J \| \int d^3 r r^{L+\xi} \vec{\mu} \cdot \vec{Y}_{LL}(\hat{r}) \| J_0 \rangle. \quad (24)$$

When the transition radius R_{tr} is referred to here, it is taken as equal to R_{2M} or R_{2E} , depending on the transition being discussed.

It should be noted that only the transverse electric and magnetic components of the cross section have been given above. This is motivated by the assumption that there is an insignificant contribution from the longitudinal component, as was discussed on page 1.

In principle a truly model-independent analysis of experimental results using the above expressions is possible only when all of the R_{qX} are determined. Of course, this would mean accurately measuring cross-section values at a large number of different values of the momentum transfer including very high ones. However, since the expansions (16) and (20) converge rapidly for low-momentum transfers and the lighter nuclei (which have smaller values of R_{qX}), in practice only a few measurements of the cross section at different momentum transfers are necessary for a virtually model-independent analysis. In general for heavier nuclei such an analysis, even though DWBA corrected, is not accurate, and direct DWBA cross-section calculations are then needed.

As an example of data reduction leading to values of XL , R_{tr} , and Γ_o , we describe the nearly model-independent analysis presently used [17] at the Naval Research Laboratory (NRL) for light ($A < 40$) nuclei (of course, subject to DWBA corrections discussed in the next subsection). This analysis is partially model dependent only in the sense that it is convenient to use initially the generalized Helm model [11] to help determine the transition multipolarity.

We start the multipolarity determination with the assumption that multipolarities $L \geq 3$ can be ignored. This seems valid, since thus far in the light nuclei at 180° and at low bombarding energies, such multipolarities have not been observed. Thus only $M1$, $M2$, $E1$, and $E2$ transitions need be considered. Next, curves of cross section vs momentum transfer for all four multipolarities are calculated using the generalized Helm model and are compared with the experimental curve.

With this technique usually unambiguous multipolarity assignments can be made or at least some possibilities can be eliminated. An example of how this technique rather unambiguously assigns the 7.63-MeV transition in ^{22}Ne an $M2$ character is shown in Fig. 3. On the other hand, in Fig. 4 this technique indicates that the 9.14-MeV transition in this nucleus is either $M1$ or $E2$ in character. In this last case often theoretical arguments can be used to resolve the ambiguity. For example, if the 9.14-MeV transition is assumed to be $E2$ and on this basis its transition width is calculated, this width turns out unreasonably larger than that of the shell model calculation [18]. Accordingly, an $M1$ assignment is made as being the most probable for this transition.

Another feature of these generalized Helm model calculations that plays a strong role in the multipolarity determination is the transition radius used. This quantity, according to the model, is given by expressions (42b) and (43b) in Ref. 11 for electric and magnetic multipole transitions, respectively. It has effectively become an empirical rule that at least for the light nuclei ($A < 40$) the transition radius must be of the order of the ground-state nuclear charge radius R_C .

That this is a necessary restriction on the transition radius can be seen from inspection of Fig. 5. This summary for the light nuclei given by Theissen [5] shows that for $M1$ and $E2$ transitions $R_{tr}/R_C = 1.09$ and 1.41 , respectively. Further comments on R_{tr} and its physical reality, especially in the case of $M1$ transitions, will be made in the next subsection.

Of course, multipolarity determinations can be made in a more model-independent way by using the expressions given above. The use of the Helm model for this phase of the analysis is a matter of simplicity and convenience. The resolution of any ambiguities that the Helm model approach cannot resolve, can, of course, always be attempted with a more model-independent approach.

In any event once the multipolarity is determined, then a best fit of the above expressions to the experimental data is undertaken by varying the values of the transition radii in (16) or (20). In doing this the experimental curve is extrapolated to $q=0$ and the curve based on the above expressions is fitted to this extrapolated curve. With the fitting procedure the value of R_{tr} can be determined. Then using the extrapolated value of the cross section at $q=0$, one can determine $B(XL, 0)$. This quantity can then be used to determine Γ_0 from the relation

$$\Gamma_0 = 8\pi \frac{L+1}{L} \frac{\omega^{2L+1}}{[(2L+1)!!]^2} \left(\frac{2J_0+1}{2J+1} \right) B(XL, \omega), \quad (25)$$

where $B(XL, \omega)$ can be found from (16) or (20) by inserting $q=\omega$, the excitation energy.

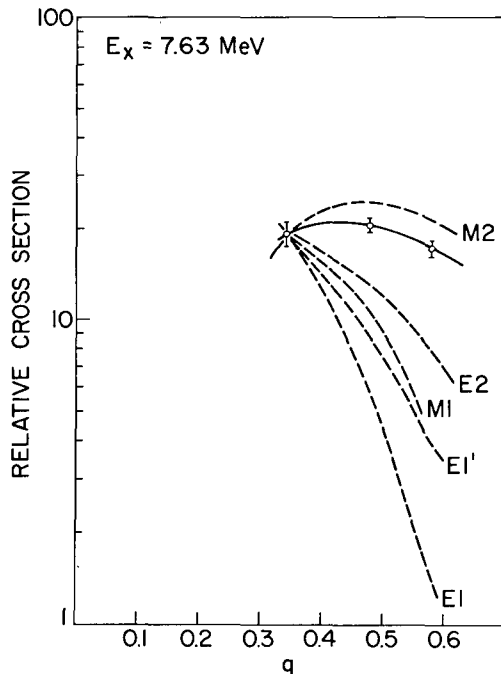


Fig. 3 — Comparison of the experimental curve of cross section vs q based on three data points with various generalized Helm model curves for the four multipolarity possibilities considered in the case of the 7.63-MeV transition in ^{22}Ne . The two curves $E1$ and $E1'$ represent the range of “reasonable” transition radii that were used.

The foregoing description of the analysis of 180° scattering data leading to values XL , R_{tr} , and Γ_0 is obviously only one of several possible variations. However, it would seem that all would have to be initiated by trial multipolarities as well as by fitting to determine R_{tr} . Obviously, since data are taken at only one angle (180°) as discussed here, occasional ambiguities in multipolarity assignment will occur, but these instances are usually in a small minority.

Such PWBA analysis procedures as the above, without DWBA corrections, are at present rarely used for nuclei with $Z > 6$, and if high accuracy is desired, corrections must be made even for the lightest of nuclei. It must also be remembered that the validity of the PWBA also depends on the incident electron energy as well as the multipolarity of the transition. A discussion of the Coulomb distortions that alter the PWBA approach and of the attendant considerations of model independence is given in the following subsection.

Distorted-Wave Born Approximation — The Coulomb field of the nucleus distorts both the initial and final wave of the electron in a scattering. Nuclear currents and magnetization densities also affect these wave shapes but to an extent that does not yet justify correction in view of the accuracy of most present-day measurements.

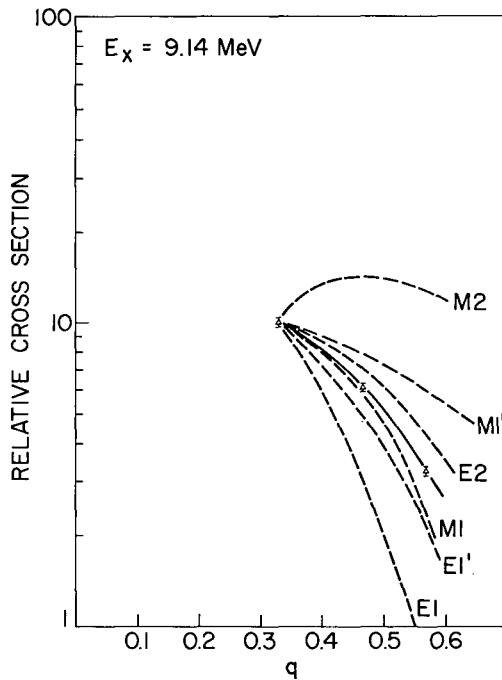


Fig. 4 — Comparison of the experimental curve of cross section vs q based on three data points with various Helm model curves for the four multipolarities considered in the case of the 9.14-MeV transition in ^{22}Ne . The two curves $E1$ and $E1'$ and the two, $M1$ and $M1'$, correspond to the ranges of “reasonable” transition radii that were used in each case.

Two approaches have been used in taking into account Coulomb distortion effects. The first, an approximate method, is to calculate, usually by partial-wave analysis in the DWBA, cross-section correction coefficients that can be applied to the experimental cross sections so that the corrected value can be related to PWBA expressions and analyzed accordingly. The second, an exact method, is to compare the experimental values directly with the appropriate DWBA calculation. The first method has the advantage of simplicity in that usually only elementary interpolations between tables of correction values need be made and that a PWBA analysis, which better highlights the nuclear properties involved, can be used. However, as discussed below, this method is inadvisable for use with heavier nuclei ($A \gtrsim 40$), in which case the direct DWBA calculation must be used.

The approximate or correction method uses a distorted-wave correction factor given by

$$f_c = (d\sigma/d\Omega)_{\text{DWBA}} / (d\sigma/d\Omega)_{\text{PWBA}} \quad (26)$$

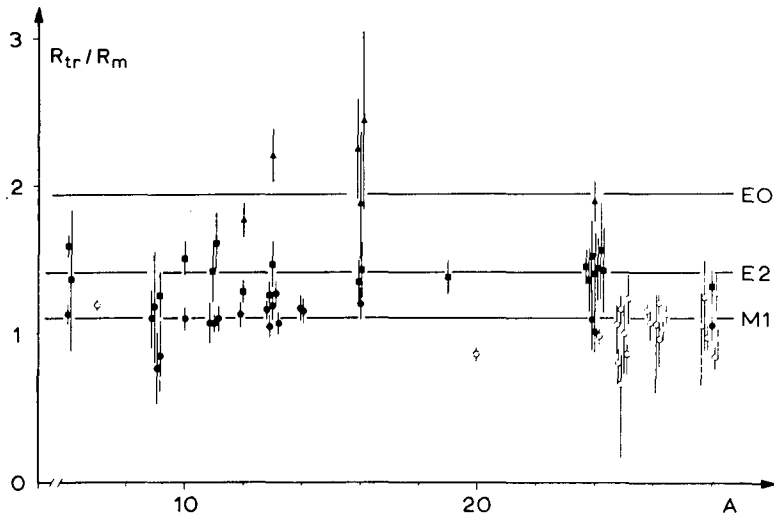


Fig. 5 — Transition radii R_{tr} divided by ground-state rms charge radius R_m as a function of mass number A . Of interest here is the $M1$ curve. Full symbols denote results from scattering $< 180^\circ$; open symbols denote results from 180° scattering. (From Ref. 5, © 1972 by Springer-Verlag, New York, N.Y. Used by permission.)

The experimental cross section is then divided by f_c :

$$(d\sigma/d\Omega)_{\text{PWBA}}^{\text{exp}} = (d\sigma/d\Omega)^{\text{exp}}/f_c \quad (27)$$

to give an “experimental PWBA” cross section which can be related to the theoretical PWBA expressions for analysis.

The principal problem encountered in the use of such a technique is performing it in a model-independent way. Essentially this problem reduces to separating the Coulomb distortion effects from the effects of the transition charge and current densities in the cross section. Roughly speaking, model independence will be valid if the PWBA cross sections are equal in the momentum transfer range under study for the various models considered [18]. Then the corresponding DWBA cross sections as well as the corresponding f_c will coincide. Such a situation will generally prevail for low-momentum transfers and $A < 40$ nuclei [5].

Using the second Born approximation, Schucan [19] was able to separate these effects and determine model-independent correction factors for longitudinal $C0$ and $C2$ transitions at low-momentum transfers. Duguay et al. [20] and Ziegler and Peterson [21] also showed that model independence prevailed in their cross sections for $C2$ transitions at small values of q calculated using the DWBA.

However, the matter of model-independent correction factors for cross sections involving transverse transitions, in particular $M1$ transitions, is a somewhat more difficult

problem. Intimately associated with this problem is the question of the model-independent physical meaning of an $M1$ transition radius [22] to be discussed below.

Using the Duke University DUELS [23] program which considers magnetization resulting only from orbital nuclear currents, Chertok [24-26] has calculated values of f_c for $M1$ excitation cross sections with $E < 140$ MeV and for nuclei with $Z \leq 20$. A linearity of the correction factor with Z is found at low incident electron energy ($E = 40$ MeV):

$$f_c = (1 + \alpha Z\beta) \quad (28)$$

where $\beta = 4.4$ and α is the fine structure constant. However, as the incident energy is increased there is a strong departure from linearity as is apparent in Fig. 6, which shows curves of f_c vs Z for various values of E and θ and for $\omega = 15$ MeV.

An idea of the extent to which model dependence influences $M1$ correction factor values, especially for backward scattering angles (or larger momentum transfers for a given constant E), can be seen in the example shown in Fig. 7. Here the correction factor is plotted vs scattering angle θ for the 11.42-MeV $M1$ transition in ^{28}Si at $E = 50$ MeV. The top curve was calculated by using the transition charge density $\rho_{tr} = \rho_0$, the ground-state Fermi density. The lower three curves were obtained by assuming that $\rho_{tr} = d\rho_0/dr$ and $t_{tr} = 0.8t$, t , and $1.2t$, respectively, in descending order, where t and t_{tr} are the Fermi and transition skin thicknesses, respectively. The 10% variation in f_c at 180° is apparent. It might be added that Chertok has also calculated with the same program $M2$ correction factors [26] again for low E and Z . These results along with $M1$ correction factors can be found in tables compiled by Chertok et al. [27].

The problem of the model dependence of f_c has been studied in some detail by Drechsel [22], who included in his calculation consideration of not only the nuclear orbital currents but also the nuclear magnetization. In conjunction with the study of f_c , the closely related problem of the model-independent physical meaning of the transition radius for $M1$ transitions is treated. It is pointed out that for longitudinal transitions there is a one-to-one correspondence between the moments of the transition charge density $\rho_L(r)$ and the expansion of the transition matrix element in terms of a transition radius (analogous to that given in Eqs. (16) and (20)). In this case then the transition radius can have physical significance. However, for transverse transitions more than one moment of the transition current and magnetization densities can appear in a term of the matrix element expansion. Thus the physical meaning of transition radii for such transitions is questionable.

This fact is amplified by calculating the transition radius using several different models. Drechsel starts by regarding the $M1$ transition radius (given in Eq. (16) for $L = 1$) as merely a convenient expansion parameter. He thus expands the experimental form factor, yielding

$$F_{\text{exp}} = q^L \sum_{n=0} (1)^n \alpha_n \exp q^{2n}, \quad (29)$$

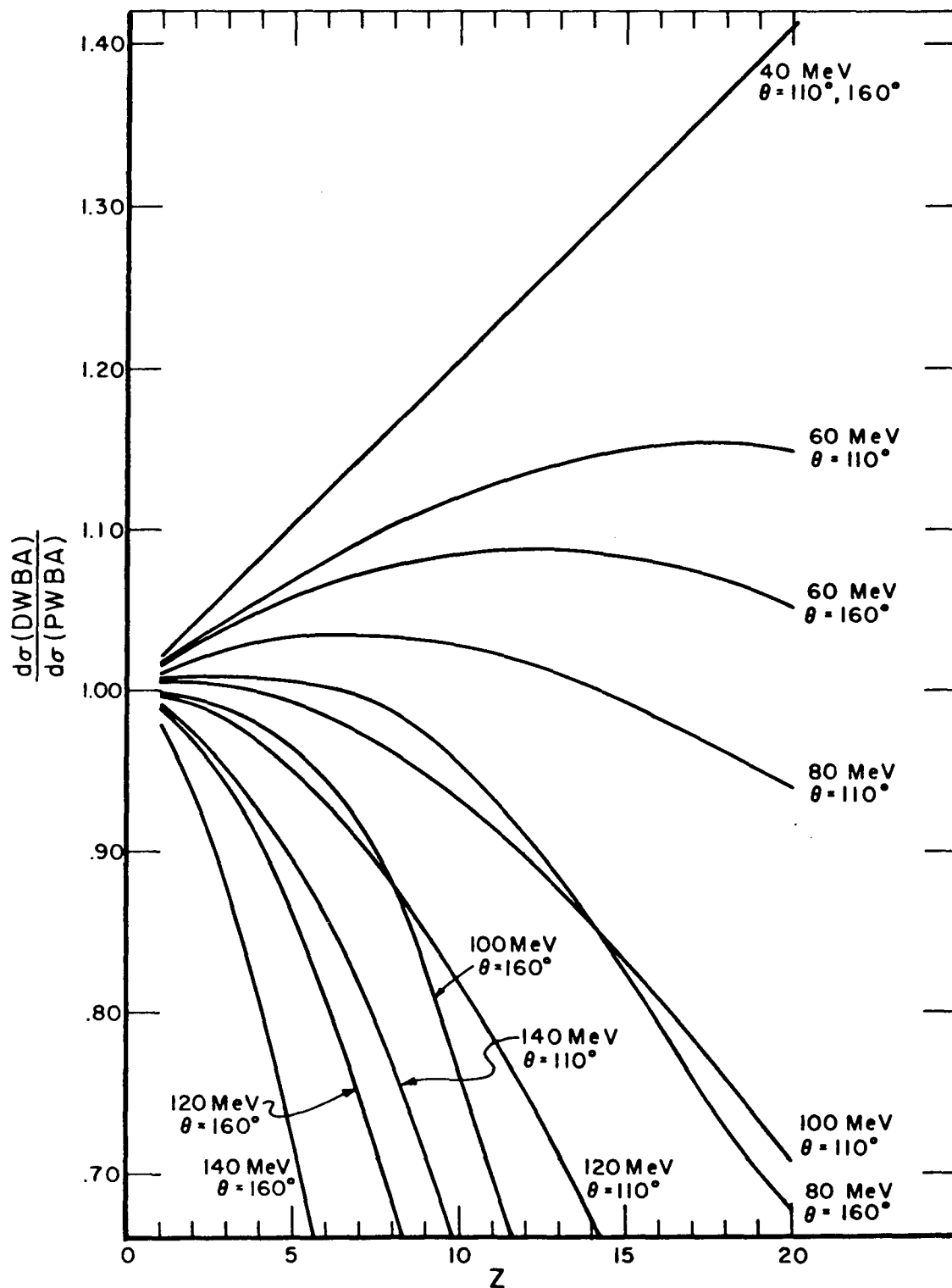


Fig. 6 — The correction factor $f_c = (d\sigma/d\Omega)_{DWBA}/(d\sigma/d\Omega)_{PWBA}$ vs Z , E_0 , and θ for $M1$ electroexcitation at 15 MeV (from Ref. 26).

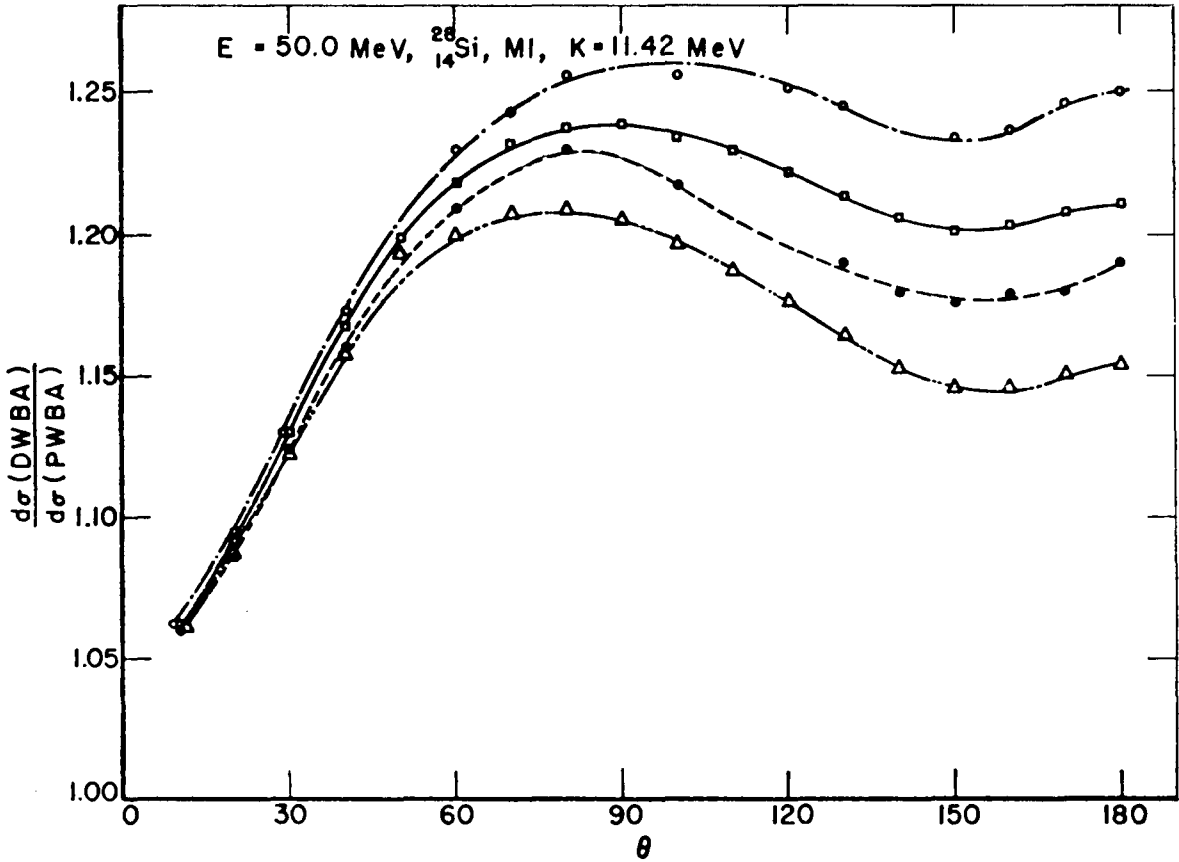


Fig. 7 — Values of $f_c = (d\sigma/d\Omega)_{DWBA}/(d\sigma/d\Omega)_{PWBA}$ vs scattering angle θ for the 11.42-MeV $M1$ transition in ^{28}Si . Fermi charge distribution parameters $c = 3.153$ fm and $t = 2.40$ fm were used. The four curves result from different parameters assumed for the nuclear convection current, $J = \rho_{tr} Y_{LL1}^M$, where ρ_{tr} is the transition density and Y_{LL1}^M is the vector spherical harmonic. In the top curve $\rho_{tr} = \rho_0$, the Fermi charge distribution. For the lower three curves $\rho_{tr} = d\rho_0/dr$, and, in descending order, $t_{tr} = 0.8t$, t , and $1.2t$, where t and t_{tr} are the Fermi and transition skin thicknesses, respectively. (From Ref. 25.)

where α_n^{exp} is a general expansion parameter. Then the five different nuclear models given in Table 1 are considered, two of which involve nuclear currents only and three of which involve nuclear magnetization only. Assuming the PWBA and that α_1^{exp} has been measured according to Eq. (29), the following values of transition radii are found from the models given in Table 1:

$$\alpha_1^{\text{exp}} = \frac{1}{10} R_A^2 = \frac{1}{3} R_B^2 = \frac{1}{6} R_C^2 = \frac{1}{5} R_E^2 . \quad (30)$$

This clearly questions the physical reality of $M1$ transition radii in terms of specifying in which region of the nucleus the transition takes place. However, in a model where, in the first few terms of the matrix element expansion, no more than one each current and magnetization moment appear in any one term, it may be meaningful to speak of two transition radii, one for current and one for magnetization, assuming, of course, that the model is physically applicable.

Table 1[†]
 Drechsel Current-Magnetization Models for Model Dependence Tests
 in $M1$ Transitions[‡]

Model	Current-Magnetization
A	$\vec{j} \approx \delta(R_A - r) \vec{Y}_{11\mu}^*$
B	$\vec{j} \approx r e^{-(3r/r_B)} \vec{Y}_{11\mu}^*$
C	$\vec{m} \approx \delta(R_C - r) \vec{Y}_{10\mu}^*$
D	$\vec{m} \approx \delta(R_D - r) \vec{Y}_{12\mu}^*$
E	$\vec{m} \approx \delta(R_E - r)$ $\times [2/3 \vec{Y}_{10\mu}^* + 1/3 \vec{Y}_{12\mu}^*]$

[†] From Drechsel [22].

[‡] \vec{j} , \vec{m} , \vec{Y}^* and μ are the nuclear current, nuclear magnetization, vector spherical harmonic, and magnetic quantum number, respectively.

The correction factors f_c are also calculated by Drechsel for different momentum transfers (or equivalently different scattering angles θ at a given E_0) as shown in Table 2. It can be seen that there is some model independence in f_c at low-momentum transfers (small angles). This is especially true for models B and F.

As a result of this study Drechsel suggests using an iterative procedure to determine a model-independent f_c at low-momentum transfers. First, determine the first few α_n^{exp} in Eq. (29) by evaluating the experiment in the PWBA. Then find any current and/or magnetization density that gives the same values of, say, α_0 , α_1 , and α_2 (for low-momentum transfers). Use these densities and calculate a correction factor. Apply the correction factor to the experimental cross section, then repeat the procedure. Convergence should occur rapidly.

As mentioned earlier, certainly for nuclei with $A > 40$ the correction factor approach must be abandoned and direct comparison with DWBA calculations must be undertaken. In fact this is more frequently becoming the case even with the light nuclei.

The first calculation that enjoyed any general use for electroexcitation of transverse magnetic transitions was that on which the Duke computer program DUELS [23] is based. This program treats the nuclear excitation through first-order perturbation theory but treats the Coulomb effects on the electron waves with a partial-wave analysis. As previously noted, in its original version it only accounted for magnetization due to nuclear orbital currents; i.e., only the convection current operator is used. The nucleus is regarded as an

Table 2[‡]
 Correction Factor f_c as Function of
 Scattering Angle θ for $M1$ Transitions^{||}

θ (deg)	Correction Factor f_c			
	A	B	C	D
15	1.175	1.175	1.175	1.175
20	1.23	1.23	1.23	1.23
30	1.325	1.33	1.32	1.33
40	1.39	1.40	1.38	1.40
60	1.46	1.48	1.43	1.48
80	1.45	1.485	1.405	1.49
100	1.39	1.45	1.33	1.46
120	1.32	1.385	1.24	1.42
140	1.25	1.35	1.16	1.38
160	1.205	1.32	1.10	1.36
180	1.19	1.305	1.08	1.35

[‡]From Drechsel [22].

^{||} For $E = 50$ MeV, $R_A = 4$ fm in model A, and R_B and R_C follow Eq. (30) in B and C. Model F is a combination of models C and D. The static charge is the Fermi distribution ($Z = 28$, $c = 4$ fm, $t = 2$ fm, where c and t are the Fermi radius and skin thickness parameters, respectively).

incompressible, irrotational liquid drop and parametrized accordingly. The transition current density in this model is proportional to the first derivative of the Fermi charge distribution, and it is assumed that the ground and excited states have approximately the same shape.

More recently, amended versions of the DUELS program [27-29] have been developed which take into account nuclear magnetization as well as convection currents. One technique used to accomplish this [29] is to bypass the DUELS subroutine that calculates the convection current transition density in the liquid drop model. Magnetization and current transition densities are thus calculated separately using any desired model, and these densities are fed into DUELS.

Independently developed or developing computer programs [22,30], useful for electroexcited magnetic transitions also exist. However, the program of Drechsel [22] is applicable only to $M1$ transitions. Andresen [30], presently developing a DWBA program, is studying a Coulomb gauge formulation to determine the extent to which separation of longitudinal and transverse components is possible in the DWBA.

Radiation Tails and Radiative Corrections — The frequently cited advantage of the electron as a nuclear probe, namely its use of the weak, well-known electromagnetic interaction, is offset by one serious disadvantage, its small mass. Because of this, it easily undergoes scatterings which in turn usually generate radiation. This results not only in the broadening of any spectral peak produced by an elastic or inelastic scattering but also in such peaks being accompanied by a low-energy radiation tail. The latter effect means that any inelastic peak must ride on top of a background produced by the radiation tails of the elastic peak as well as all inelastic peaks corresponding to lower energy nuclear excitations. At forward scattering angles the intensity of this tail background can be orders of magnitude larger than that of an inelastic peak under study. An advantage of 180° scattering is that generally these intensities are at least comparable.

Roughly speaking, the peak broadening is associated with soft-photon production as well as several other radiative effects assembled into the general category of radiative corrections, whereas the radiation tail results from hard-photon emission. No attempt will be made here to discuss comprehensively radiation tails and the three principal radiative corrections. Excellent reviews and treatments of these phenomena are now available in the literature [12, 31-33]. Maximon and Isabelle [31] treat radiative tails of both elastic and inelastic peaks produced by charge and magnetic scattering. Maximon [32] explains and classifies the basic terminology and phenomena contributing primarily to the Schwinger correction. Mo and Tsai [33], although generally emphasizing higher energy scattering than is discussed here, give comprehensive detailed procedures for radiative corrections in data treatment. Überall [12] presents a thorough discussion of both tails and corrections. Thus in this section, after defining more carefully the distinctions between tails and corrections, we will outline only those features germane to magnetic backward inelastic scattering.

The distinction between the radiation tail and the most important radiative correction, the Schwinger correction, has been very lucidly discussed by Maximon [32] and will only be outlined here. The contributions to the radiation tail are defined as arising from those scatterings involving emission of photons of energy $k > \Delta E$ (defined as hard photons), where ΔE is an arbitrary incremental energy, usually of the order of the peak width at half maximum. Specifically, ΔE is the energy difference between the electron energy of the peak (at maximum) and a lower arbitrary cutoff energy which serves to delimit the intensity of the peak and separate it from the tail.

The first of the radiative corrections, the Schwinger correction,[‡] corrects for the loss to the area under the peak of those electrons degraded in energy as a result of emission of any number of real soft photons of energy $k < \Delta E$ as well as the emission and absorption of virtual photons of any energy. Clearly, the larger the value of ΔE that is used in the calculation of this correction, the smaller will be the correction. One can further sharpen the distinction between the phenomena associated with this correction, and the hard-photon emission producing the tail, by considering one incremental segment of a tail, in the first approximation contributed to by a scattering accompanied by emission of a hard photon of a given energy. Then this phenomenon requires a

[‡]A particularly clear discussion of the Schwinger correction is given in Ref. 12.

Schwinger correction just as does the "radiationless" scattering contributing to the elastic peak. However, it should be noted that the distinction between correction and tail is not subscribed to by Mo and Tsai [33], who prefer to assemble all such phenomena into the category of corrections.

The Schwinger correction deals with quantum electrodynamical effects occurring during the scattering under study, whereas the second principal correction, the bremsstrahlung correction, corrects for effects due to small-angle scatterings from nuclei before and after this scattering. The third correction arises from ionization due to Landau straggling or multiple small-energy losses due to atomic ionization. The last two corrections are proportional to the square of the target thickness, whereas the Schwinger correction and the radiation tail intensity are linearly proportional to this thickness.

The two tail calculations presently most applicable to backward angle magnetic scattering are those of Ginsberg and Pratt [34] and Maximon and Isabelle [31]. Each of these are PWBA calculations which consider magnetic as well as charge scattering and which direct particular attention to 180° scattering. However, only the latter calculation [31] gives inelastic as well as elastic tails. The more recent calculation of Gargaro and Onley [35] is in DWBA but considers only elastic tails generated by charge scattering.

The features of such tail calculations that are related to 180° magnetic scattering and that will be briefly mentioned here are (a) even for a spinless nucleus (where charge scattering essentially vanishes at 180°) there is an elastic radiation tail due to charge scattering, (b) the presence of magnetic bremsstrahlung is more prominent at 180° . The first point is illustrated approximately by the radiation tail curve presented in Fig. 8 which is based on the rather simple expression which results [36] when 180° is substituted into the early PWBA expression of McCormick, Keiffer, and Parzen [37] for a point nucleus in the approximation that the incident electron energy $E \gg m$, the electron mass. The essential dependence in this expression is given by

$$\frac{d\sigma}{d\Omega dE} \approx (1 - \gamma - \gamma^{-1} + \gamma^{-2}), \quad (31)$$

where $\gamma = p'/p\gamma$, the ratio of the scattered to incident electron momenta. It can be seen from Fig. 8 that even though an elastic peak is not present, a tail is. Actually, when the electron mass is taken into account [38], a small elastic peak is indeed present. An experimental verification of this feature of 180° elastic scattering can be seen in the ^4He spectrum shown on page 59. Because of finite solid angle and small-angle target scattering effects, elastic peaks invariably appear in 180° scattering spectra for higher Z spinless nuclei. However, since charge scattering has a Z^2 dependence, the effect of interest here is well highlighted for a very light nucleus such as ^4He as is seen on page 59.

The second feature mentioned above, magnetic bremsstrahlung, was first treated by Ginsberg and Pratt [34]. At 180° the intensity of this bremsstrahlung is greatest near the elastic peak, tailing off with increasing excitation energy as shown in Fig. 9. Magnetic bremsstrahlung was first observed experimentally by Peterson and Barber [36] in scattering from hydrogen, and is clearly visible near the elastic peak in the ^3He spectrum also presented on page 59.

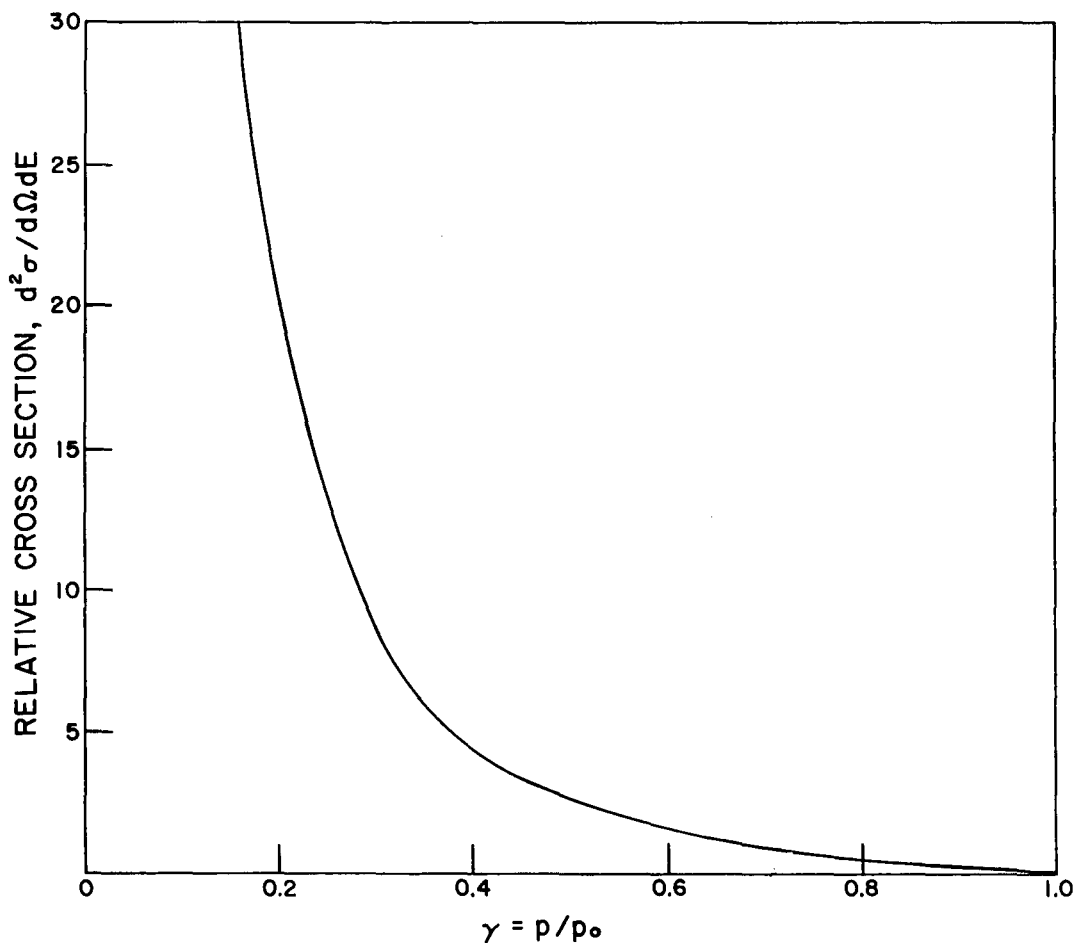


Fig. 8 — Relative cross section for radiation tail for a spinless point nucleus vs $\gamma = p'/p$, the ratio of the scattered to incident electron momenta. The curve follows a form used by Peterson and Barber [36] of a relation derived by McCormick et al. [37].

Perhaps the most pertinent aspect of the Schwinger correction of relevance here is answering the question of whether the correction as usually given for charge scattering is applicable to backward magnetic scattering. Rand et al. [39] give arguments to show that the same correction is valid, stating that, first, this result is implied in the cross-section calculations of Ginsberg and Pratt [34]. Second, they show that the correction is approximately proportional to the single photon exchange diagram, in part resulting from the fact that all the two-photon diagrams considered enter only as interference terms with the single-photon diagram. The correction is then independent of the interaction at the nuclear vertex. This result is also well explained in Maximon's review [32] and has been confirmed by actual calculations [40, 41].

Borie [41] has pointed out that for charge scattering at back angles the anomalous magnetic moment of the electron modifies the Schwinger correction. However, this does

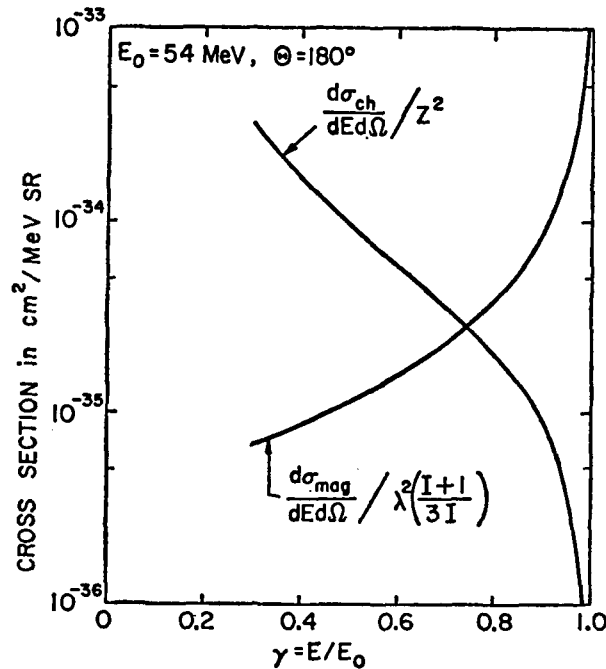


Fig. 9 — Relative contributions to the radiative tail of the elastic peak from a point charge and a point magnetic moment in the limit $E, E' \gg \theta = E^{-1}$ (from Refs. 4 and 34).

not occur for magnetic scattering. The modification occurs essentially because at 180° the approximation of neglecting the electron mass for charge scattering is no longer justified.

Concerning the remaining two corrections, bremsstrahlung and ionization, clearly the only unique consideration involved here is that reflection geometry obtains in backward scattering, with the average distance a back-scattered electron travels being that of the full target thickness. This is so since an electron in 180° scattering can traverse target material up to twice the target thickness. Finally, the existence of some helpful articles in addition to that of Mo [33] on the details of radiative corrections [42, 43] in experimental data treatment should be noted as well as a recent report on target ionization loss [44]. A discussion [45] on target multiple scattering, finite solid-angle, finite angular, and spatial incident beam effects in 180° scattering, and a treatment of curve-fitting [46] may also be helpful.

SURVEY OF EXPERIMENTAL TECHNIQUES IN BACKWARD ANGLE SCATTERING

Characteristic Experimental Problems in Backward Angle Scattering

Some of the most important problems characteristic of backward angle scattering are itemized in this section. Approaches to solutions of some of these problems are discussed in the following sections; however, a full comprehensive treatment of experimental techniques is not intended. Actually, the techniques discussed represent an art that is in a state of growth and clearly needs further refinement.

The most fundamental requirement of backward angle scattering, 180° scattering in particular, is that the incident and scattered beams must be separated. This necessitates the introduction of a separating or pretarget magnet of some form between the target and the spectrometer. The presence of this magnet generates a series of problems that must be considered.

- The object distance between the target and spectrometer must be increased beyond what it would be in more forward angle scattering by at least the path length used in traversing the separating magnet. This, of course, concurrently leads to a short spectrometer image distance with the result that often the effect of the spectrometer fringe field on the detectors in the focal plane, which is then closer to this field, must be dealt with. The increased object distance also results in a decreased spectrometer solid angle.

- The pole gap of this magnet must not be so small that the shape of the cross section of the scattered solid-angle envelope departs too far from a square or a circle. Otherwise, when scattering at 180° , the range of scattering angles accepted in the solid-angle envelope will vary azimuthally to an unacceptable extent. The pole gap must also not be so small that despite the presence of slits designed to prevent it, a significant number of backscattered electrons from the target scatter from the magnet pole faces (or more precisely, the vacuum chamber walls lining the pole faces). This could lead to unnecessary peak broadening and "instrumental" contributions to the radiative tails; this is especially true of the elastic peak.

- If inelastic scattering is being studied, then, after scattering from the target, the momentum dispersion of inelastic trajectories passing back through the separating magnet field will usually require moving the spectrometer so as to receive electrons of the desired energy as well as setting the spectrometer field appropriately. This leads to the further complication that the solid-angle acceptance of the separating magnet-spectrometer combination will vary with the inelastic electron energy.

- The presence of the separating magnet also complicates the adaptation of the 180° scattering system to the "energy loss" mode, discussed below.

- In general considerable care must be taken in the separating magnet design, for it must be magnetically matched to the spectrometer in what must be regarded as an integrated design.

- If only one pretarget magnet is used, the beam dump (Faraday cup) must be repositioned to accept the beam from its altered direction.

Problems similar to those associated with the separating magnet pole gap also exist with the choice of a pole gap for the spectrometer itself. If the spectrometer is mounted with the pole faces in a vertical plane, as is usually the case, then the ratio of the gap width to the width in the vertical plane (spectrometer median plane) must not be too small. More so than with the separating magnet, this could cause an unacceptable azimuthal variation of scattering angles about 180° as well as possible contributions from scattering off the pole face vacuum-chamber walls despite efforts at appropriate slitting.

The vacuum-chamber walls normal to the above-mentioned walls, i.e. normal to the spectrometer median plane, also present a background scattering problem. This is especially true of the outer wall, or wall of larger radius. For, when the spectrometer field is set to receive inelastic electrons of a given energy, the generally more numerous elastically scattered electrons are then striking this wall. This often produces a "ghost" or instrumental background peak in the inelastic spectrum. Of course, this particular problem is not unique to 180° scattering and, in fact, is usually more serious in the case of scattering at more forward angles where far more intense elastic peaks are observed.

Since many more electrons pass through the target than are backscattered into the spectrometer, some means must be found of trapping these electrons with minimum background production. This problem is complicated by the fact that after emerging from the target the beam is no longer a well-defined ray, but contains electrons scattered at all angles with, of course, a very strong predominance in the forward direction. Aside from the usual design considerations for beam dumps and Faraday cups that this situation requires, it is especially important in 180° scattering to ensure that a minimum of these electrons scattered from the Faraday cup stream back into the spectrometer and thus mask the intensity observed from the target.

The technique of relative cross-section determination often used in more forward-angle scattering involving comparison of the intensity of an inelastic peak with that of the corresponding elastic peak is usually not valid for the magnetic transitions observed at 180° . This is because, except for the very lightest nuclei, the experimentally observed elastic peak does not arise primarily from magnetic scattering, but from charge scattering produced by multiple scattering in the target and effects of finite solid angle and beam cross section.

Since an incident electron that undergoes a 180° scattering in the target may traverse an amount of target material from zero to twice the target thickness, thinner targets than used in more forward-angle scattering are often needed to achieve a desired resolution. Unfortunately, this requirement occurs at the very angle where cross sections are generally the smallest and counting rate statistics are already a problem.

Although a strong factor aiding in the accumulation of desired counting statistics for inelastic scattering studies is the low-intensity radiation tail encountered at back angles, this same low intensity then allows general background radiation to compete as a threat to statistical accuracy. That is, given a certain irreducible ambient background radiation, the statistical accuracy of the low counting rates characteristic of back-angle scattering is much more vulnerable than that of the higher rates experienced at more forward angles.

In the description of techniques that follows in the next two sections, the approaches to solutions of most of these problems will be apparent.

Significant Backward-Angle Scattering Techniques

All of the 180° scattering facilities thus far in operation have basically used the simple interjection of a separating magnet between the target and spectrometer. The earliest such system, operated at Stanford [8, 36, 47], which used a rectangular separating magnet, is shown in Fig. 10.

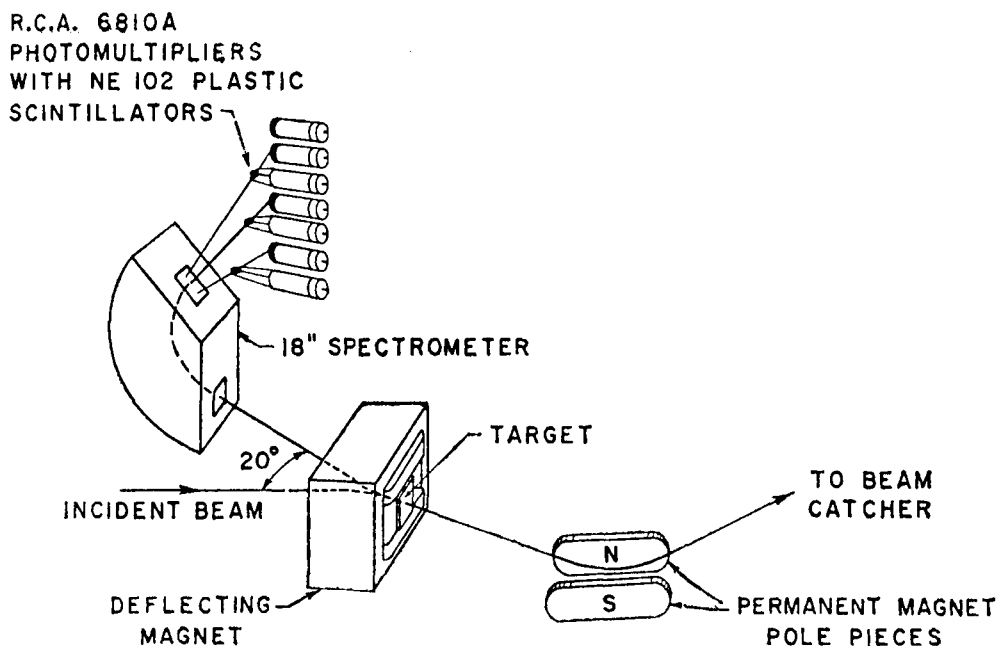


Fig. 10 — The early stanford 180° scattering system. (From Ref. 36).

A system using a circular magnet as proposed by de Vries [48] was designed and described in detail by Rand [45] and was also used at Stanford. Such a system has since found some use at Orsay [49-51] and extensive current use at NRL [52] and in Amsterdam [53]. Although the NRL system shown in Fig. 11 is typical, the most sophisticated system presently in operation is that in Amsterdam, shown in Fig. 12.

Some of the features of these two systems warrant some discussion. Common to both systems, of course, is the circular separating magnet which maintains a constant magnetic field at a given incident electron energy. A spectrum is obtained by rotating the spectrometer about the center of this magnet (not the target) in conjunction with setting the spectrometer field correspondingly. Also common to both systems is the use of an aperture between the target and separating magnet to absorb the backstreaming electrons scattered from the Faraday cup or beam dump, thus preventing their entry into the spectrometer.

NRL REPORT 7878
ELECTRON SCATTERING VACUUM SYSTEM

UNCLASSIFIED

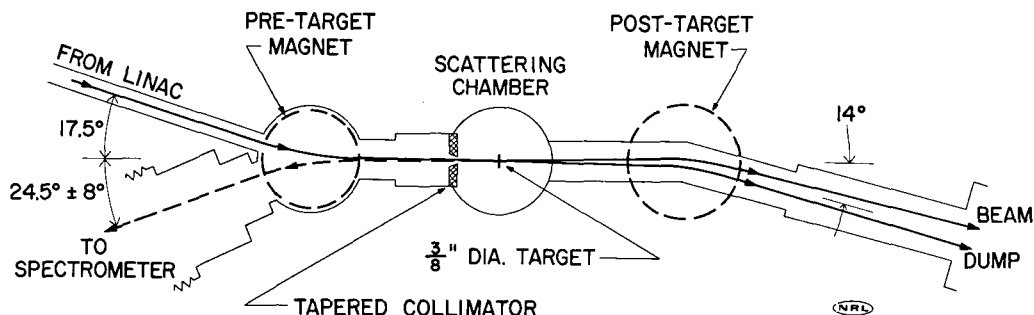


Fig. 11 — The 180° electron scattering system at the Naval Research Laboratory (NRL) (from Ref. 52).

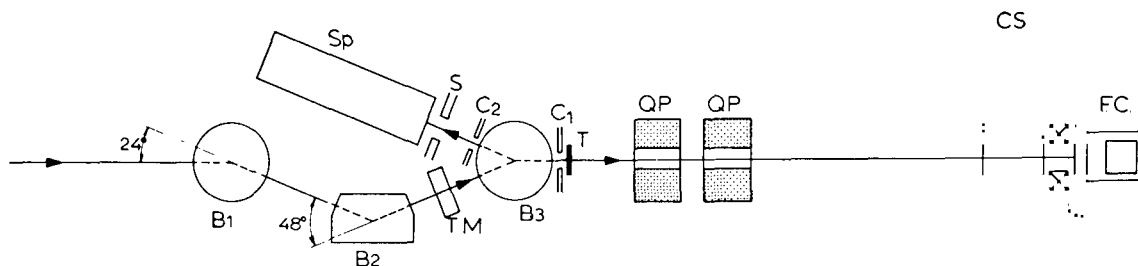


Fig. 12 — The 180° electron scattering system at Instituut voor Kernfysich Onderzoek (IKO) Amsterdam. B1, B2, and B3 are the magnets of the 3-magnet pretarget array; Sp and S are the spectrometer and spectrometer slit, respectively; TM and T are the current monitor and target, respectively; C1 and C2 are lead collimators; the QP's and CS are the quadrupoles and cement wall, respectively; and FC and B4 are the Faraday cup and Faraday cup trapping magnetic, respectively. (From Ref. 53, © 1971 by North-Holland Publishing Co., Amsterdam, The Netherlands. Used by permission.)

However, the means of trapping the electrons that have passed through the target are different in the two systems. Since the beam emerges from the target with a scattering pattern dominated by a strong forward cone of radiation, the effective solid angle subtended by the Faraday cup aperture must be as large as possible. Because of financial and space limitations, NRL gains this solid angle by placing the beam dump relatively close (about 1.2 m) to the target. However, a posttarget magnet is introduced between the target and beam dump to deflect electrons emerging from the dump away from the target and pretarget (separating) magnet. A more satisfactory system is used by the Amsterdam group, who are able to place the Faraday cup 6 m from the target through the use of two large quadrupole magnets that focus the scattered cone from the target into the cup. This larger distance as well as the concrete wall used by Amsterdam aids greatly in reducing background. Both NRL and Amsterdam use magnets in the immediate vicinity of the Faraday cup to augment its trapping capability (this magnet is not shown in Fig. 11).

The shortened spectrometer image distance resulting from the insertion of the separating magnet between the target and spectrometer poses no problem with the present NRL system, which uses a spectrometer of only 100° bending angle. It is more of a concern at Amsterdam, where a magic-angle spectrometer is used and a rather short image distance obtains. However, appropriate magnetic shielding of the scintillation and Cerenkov counters seem to have alleviated the problem.

There are two especially attractive characteristics of the Amsterdam system, each related to accommodation of scattering at more forward angles, which should be presented. The first pertains to the array of three magnets (including the separating magnet), which is upstream of the target (Fig. 12). The purpose of this array is to assure that the beam direction on striking the target is the same as that before entry into the 3-magnet array. After the spectrometer is rotated out of the way, this array, mounted on tracks parallel to the general beam direction, can be slid upstream so that the target can also be moved upstream to the spectrometer center of rotation. Therefore, conventional scattering at forward angles can be accommodated by deactivating the three magnets and installing a beam pipe directly across the array. This accommodation is made possible by the 3-magnet array because the beam direction is not changed by the separating magnet as in single-magnet systems such as the one at NRL. According to members of the Amsterdam group, the change from the conventional to the 180° scattering mode can be done in as little as half a day.

The other attractive feature of the Amsterdam system is that it accommodates backward scattering at angles in the vicinity of 180° . The method used is illustrated in Fig. 13, where, by laterally displacing the incident beam, a scattering angle different from 180° can be obtained. With the recent addition of an enlarged vacuum chamber for the 3-magnet array a range from about $170^\circ - 180^\circ$ can be covered.

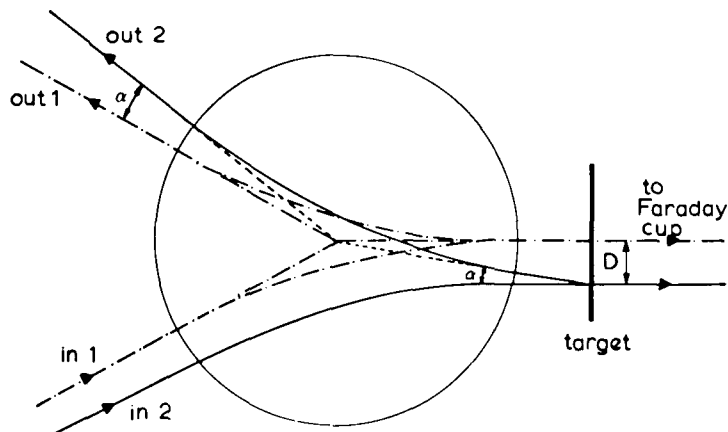


Fig. 13 — Illustration of the beam displacement technique used at IKO Amsterdam to study electron scattering at angles in the range $170^\circ - 180^\circ$. (From Ref. 53, © 1971 by North-Holland Publishing Co., Amsterdam, The Netherlands. Used by permission.)

There are other variations of this method; the earliest was that suggested by Rand [45], involving displacement of the target and separating magnet jointly as indicated in Fig. 14. Although Rand's Stanford apparatus is no longer in operation, it is nevertheless of interest here because in addition to variation in the vicinity of 180° , it illustrates another means of accommodating forward-angle scattering as indicated in Fig. 15, which shows the entire apparatus. Actually, for the angular variations near 180° the beam-ditching magnet or posttarget magnet is also movable jointly with the target and separating magnet along radial tracks. For the more forward angles and to calibrate the beam monitor, these three pieces can be moved entirely out of the way.

The 180° scattering systems mentioned thus far have either been in operation or are presently in operation. They all share the common handicap of requiring rotation of the spectrometer about the center of the separating magnet. Thus an angle setting in addition to the spectrometer field setting is required. However, far more serious is the problem of the variation of the solid angle with the spectrometer rotation angle (or scattered electron energy).

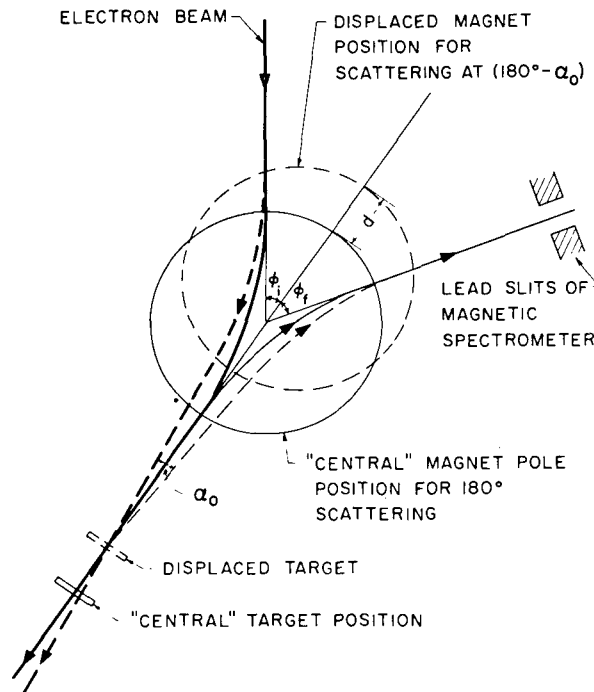


Fig. 14 — Illustration of the technique of Rand to study electron scattering at angles near 180° . The technique involves the joint displacement of the target and separating magnet. (From Ref. 45, © 1966 by North-Holland Publishing Co., Amsterdam, The Netherlands. Used by permission.)

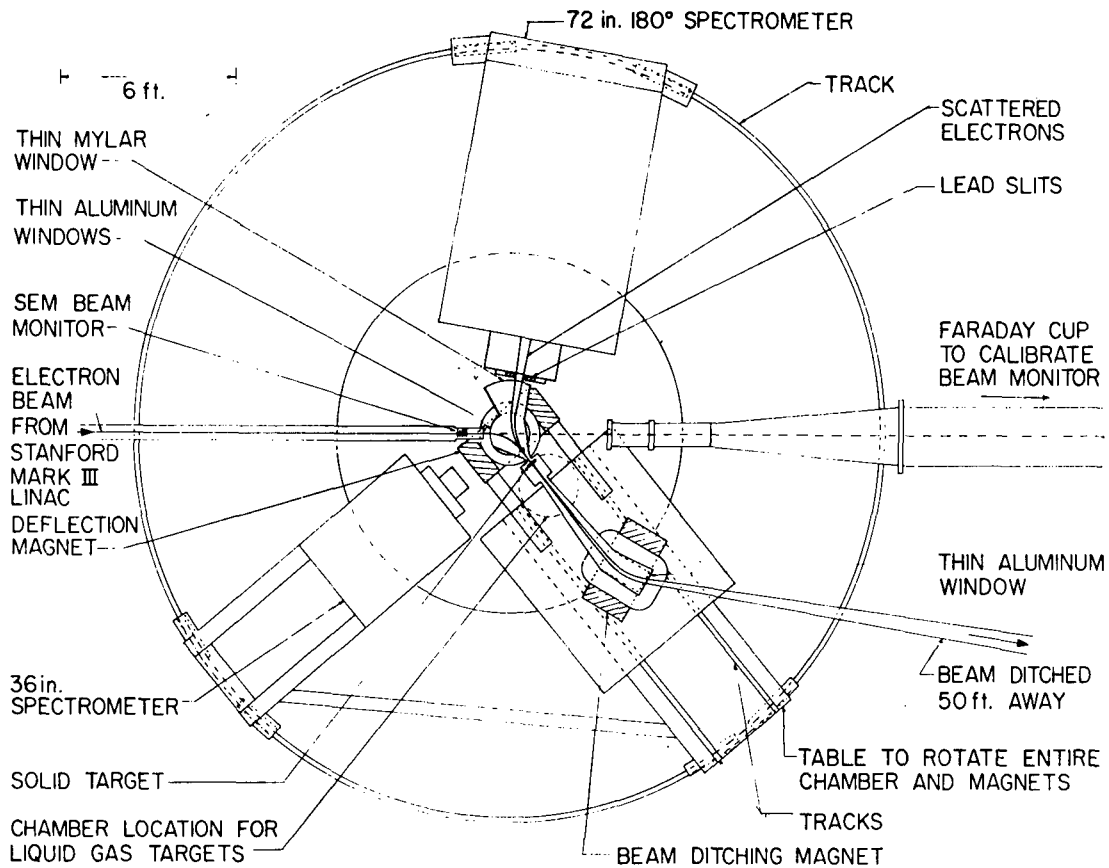


Fig. 15 — The 180° electron scattering system designed at Stanford by Rand. (From Ref. 45, © 1966 by North-Holland Publishing Co., Amsterdam, The Netherlands. Used by permission.)

There are at least three systems proposed to overcome the handicap of a variable solid angle. The one that has been taken most seriously is that suggested by Peterson [54], which is shown in Fig. 16. Here the spectrometer remains fixed and the four pretarget magnets are identical with identical fields at all times. At the field setting in the four magnets which renders the incident and scattered beam angles equal at the fourth magnet, the spectrometer observes elastically scattered electrons. An inelastic spectrum is then obtained by progressively decreasing the fields of the four magnets (as well as the spectrometer field proportionately), which in turn decreases the incident beam angle at the fourth magnet while the scattered beam angle, of course, remains constant.

If the four magnets have a large enough pole face area and the vacuum chamber of the 4-magnet array has a large enough lateral horizontal dimension, then an inelastic spectrum can be taken by progressively decreasing the fields in the array. However, if this is not the case then the two middle magnets can be moved laterally in order to produce the required incident trajectories. This system has the beauty of simplicity and economy in that the same field is maintained in each magnet.

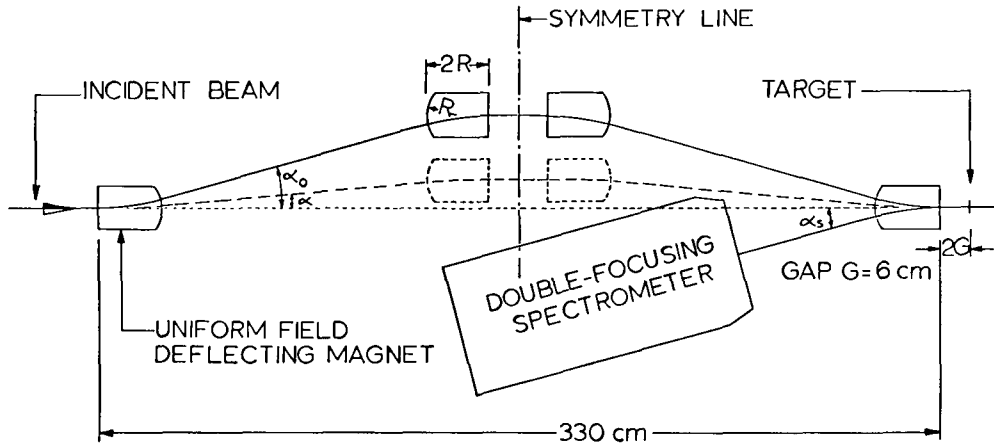


Fig. 16 — The 4-magnet system for 180° electron scattering suggested by Peterson. The elastic scattering trajectory (where $\alpha_0 = \alpha_s$) is shown with solid lines in an inelastic trajectory at one-third the incident momentum with the dotted lines. (From Ref. 54, © 1968 North-Holland Publishing Co., Amsterdam, The Netherlands. Used by permission.)

An obvious variation of this scheme is to replace the middle two magnets with one. This has the disadvantage of relinquishing two pole edges that could be useful in making trajectory corrections. Clearly, the one middle magnet would then have to maintain a field different from the outer two; i.e., it must produce twice the bending angle. However, a compelling reason for breaking the symmetry of the 4-magnet array is that, more often than not, the fourth magnet must be designed to integrate with the characteristics of the spectrometer, which usually renders the use of four identical magnets unfeasible. In fact, it is primarily for this reason that the 180° scattering system presently proposed by Peterson for the new Bates—M.I.T. Linac, as well as that being considered for the new NRL system, breaks this symmetry.

Another system that maintains a constant solid angle was proposed by Leconte [55] for the Saclay Linac and is depicted in Fig. 17. The unique feature of this system is its using the spectrometer itself as a separating magnet, passing the incident beam through a hole in the spectrometer yoke. To the best of the author's knowledge this system has not yet materialized.

A third constant solid-angle system is based on a principle of magnet design due to Koerts [56] and designed as a 180° system by Bergstrom [57]. To understand the principle on which this system is based, we consider a theorem of Koerts [56] that states that a charged particle, passing through a cylindrically symmetric magnetic field (vertical component B_z) which satisfies the relation

$$\int_0^{\infty} B_z r dr = 0 \tag{32}$$

has the same z (vertical) component of angular momentum in a field-free region near the magnet symmetry axis as it has in such a region outside the magnet. Thus, an electron approaching the magnetic field radially will intersect the axis of symmetry; conversely, an electron emerging from the axis of symmetry will leave the field radially. The system designed by Bergstrom is shown in cross section in Fig. 18.

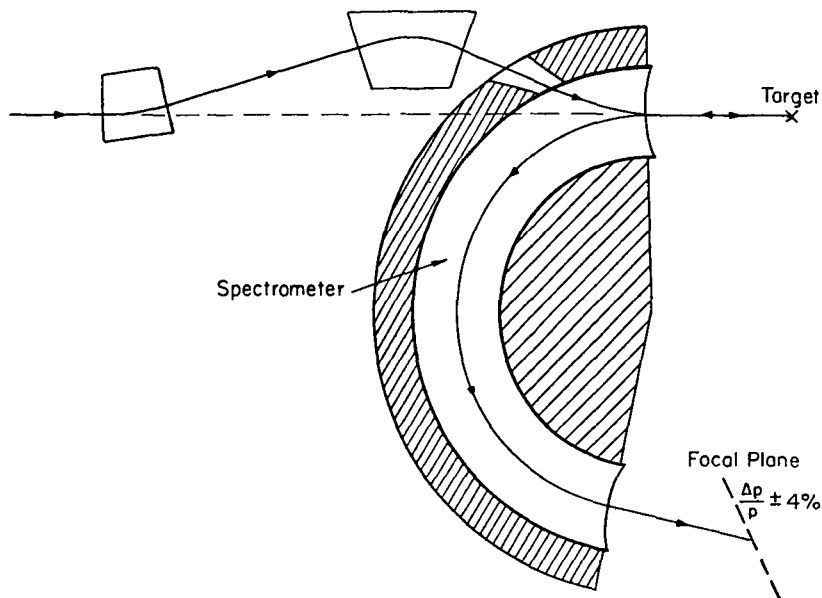


Fig. 17 — Schematic of the 180° electron scattering system suggested by Leconte (from Ref. 55).

There are two principal advantages of this system. First, since the target as well as the separating magnet symmetry axis is located at the center of rotation of the spectrometer, both 180° and more forward-angle scattering can be studied as indicated by the two outgoing trajectories in Fig. 18. Second, as implied earlier, the solid angle is constant, or more precisely, can be kept constant by appropriate variation of the magnet's field strength and the angle between the asymptotes of the incident and emergent electrons. A serious disadvantage of the system results from the vertical focusing that the electrons undergo in crossing the space between the inner and outer parts of the magnet. This causes a shift in the apparent position of the target as seen by the spectrometer. This shift could be neutralized by the introduction of a quadrupole magnet between the separating magnet and the spectrometer, but this in turn affects the double focusing of the spectrometer. It is the author's understanding that Bergstrom actually constructed a magnet based on the Koerts principle at M.I.T., but it has never been used.

Other Experimental Considerations

In this section a few remarks are offered about several miscellaneous residual items which should be mentioned. Perhaps the most important of these concerns the effect

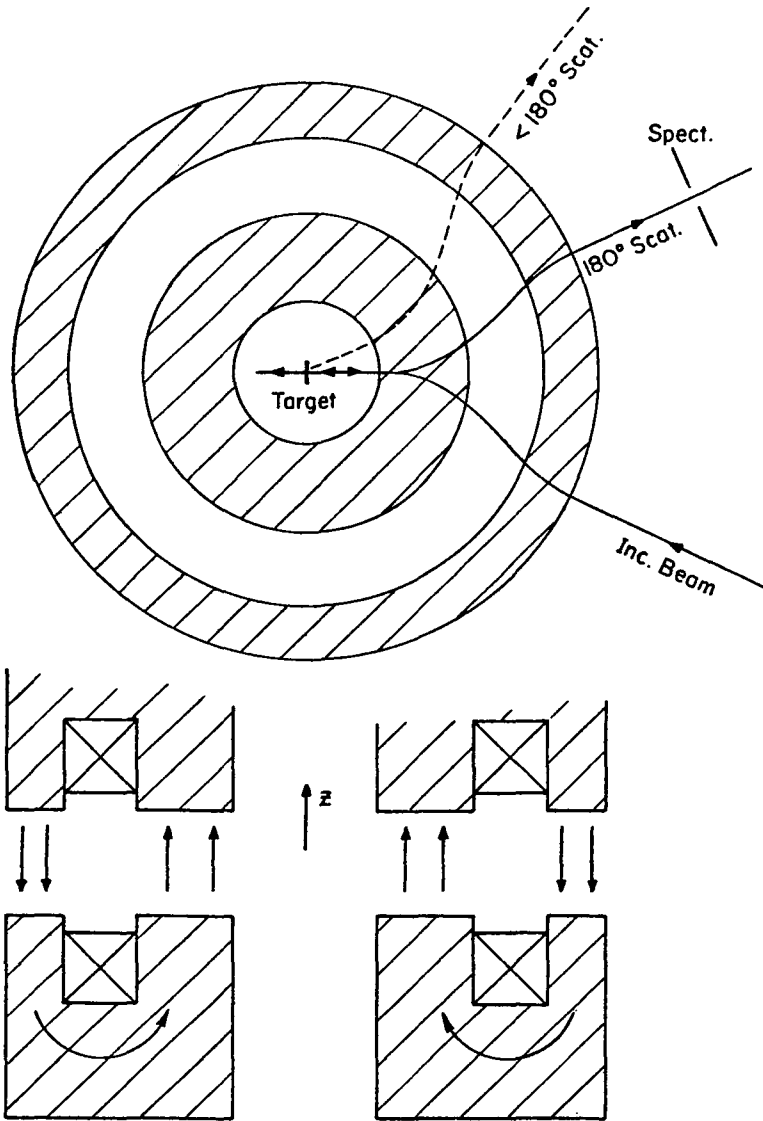


Fig. 18 — Schematic cross section of 180° electron scattering system designed by Bergstrom based on the Koerts magnet design [55]. Scattering at more forward angles can also be performed as indicated by the dotted-line trajectory. Relative direction of the fields in the two portions of the magnet are indicated in the lower part of the figure. (From Ref. 57).

of the pretarget magnet or magnets of a 180° system on operation in the so-called energy loss mode. Before discussing this, it may be useful to describe the basic principle of the energy loss method.

It is well known that two successive double-focusing magnets can be designed so that they perform in the following way. With an incident collimated electron beam which is chromatic over a certain momentum range, the first magnet essentially disperses the various

momenta by focusing each successive monochromatic increment of electrons at adjacent positions along its focal plane. The second magnet, assuming matched design, then focuses all these momenta at a given single position in its focal plane. In the energy loss mode, the role of the first magnet is usually played by the last one or two bending magnets of the beam-handling system and the momentum-dispersed beam is focused on the target. The spectrometer takes the role of the second magnet. If the electrons incident on the target within the dispersion range suffer an energy loss due to an inelastic scattering, e.g. nuclear excitation, then those electrons will be focused at a position on the spectrometer focal plane different from that reached by the elastically scattered electrons. Hence the name "energy loss." (Another name, perhaps more appropriate, is "dispersion matching.")

The clear advantage of such a system is that a much larger (up to the order of 100) momentum bin of electrons from the Linac can be used in the electron scattering study. This large increase in current can make it possible to take full advantage of the inherent resolution of the spectrometer. The disadvantage, that a larger target dimension is needed to accommodate the dispersed beam (roughly 2 to 4 cm in the dispersion direction), is offset somewhat by the fact that such a diffuse beam will not overheat or oblate the target as much as a well-focused beam. That is, it is a disadvantage for expensive isotopically enriched targets and an advantage for low-melting-point targets. The enlarged beam tubing required must also be dealt with. However, the most serious disadvantage is that most beam-handling systems disperse in a horizontal plane, whereas most spectrometers are mounted with their pole faces in a vertical plane. Thus, either special beam-handling magnets must be introduced to disperse the beam vertically (as done by the NBS and Mainz Linac groups) or the dispersion plane must be rotated to the vertical; e.g., by using five quadrupoles (as done by the Bates—M.I.T. group and the Darmstadt group) [58].

Obviously the problems encountered in realizing such a refined system are formidable enough without the introduction of the pretarget magnets used in the 180° scattering mode. Such magnets could have the effect of distorting the dispersion desired at the target. This is especially true of a system with a relatively large number of magnets, such as the 4-magnet Peterson system.

This problem has been investigated by Peterson and Vetter [59] using the TRANSPORT code in their design of the proposed 180° scattering system for the Bates—M.I.T. Linac. Their conclusion, as of this writing, is that in first order an appropriately designed 4-magnet array will not significantly distort the desired dispersion configuration at the target. In second order, due to vertical focusing effects, a loss in momentum resolution of one part in 10^{-5} at the target does occur. An additional part in 10^{-5} is lost by the time the scattered beam reaches the spectrometer (M.I.T. spectrometer) focal plane when one-half of the spectrometer solid angle is used. Thus, it should be possible to perform relatively high-resolution studies at 180° in the energy-loss mode with this system.

One of the problems associated with back-angle scattering and mentioned in pages 22 to 24 is the fact that for such an event in the target, the electron can traverse from zero to twice the target thickness. This enhances the energy spread due to target ionization loss and straggling effects. Rand [60] has devised an ingenious technique to compensate for the ionization energy loss suffered in the target by backscattered electrons.

In essence a short accelerating waveguide is inserted between the target and the separating magnet as indicated in Fig. 19. This accelerating structure is phased with the Linac so that electrons scattered from the downstream side of the target are accelerated while those scattered from the upstream side are retarded, thus compensating for the ionization energy spread. With this device the target thickness used can in principle be increased by as much as a factor of 20.

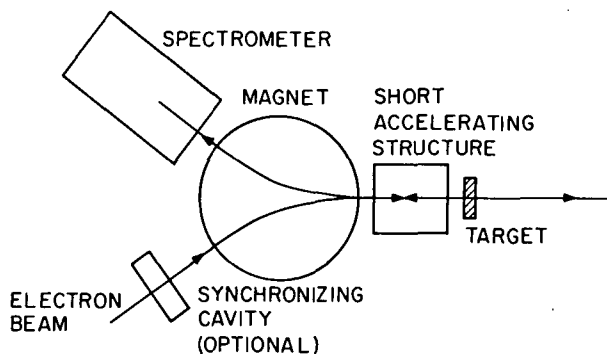


Fig. 19 — Simplified schematic of the system designed by Rand to compensate target ionization loss in 180° electron scattering experiments. Although not specifically mentioned in Rand's paper, the synchronizing cavity apparently further aids in phasing the short accelerating structure with the Linac. (From Ref. 60.)

Another target-related device useful for gaseous targets has been designed and used by Fagg et al. [61] and is depicted in Fig. 20. As can be seen an especially simple cylindrical geometry characterizes such an apparatus for 180° scattering. The gas chamber shown was 1 cm in diameter and used $6\text{-}\mu\text{m}$ havar foils at the entrance and exit apertures, which enclose a 5-cm path length of target gas. This gas was operated at pressures up to 4.4 atm and also could be refrigerated to liquid-nitrogen temperature by means of the cooling envelope indicated. Refrigeration to this temperature affords a target density gain of about a factor of three. A thermocouple (not shown) and pressure gauge measured the temperature and pressure, respectively, of the gas. Expensive isotopically enriched gases could be stored for reuse by a helium trapping system, also not shown in Fig. 20.

Since the report [61] describing this device was published, several improvements have been made [62]. The diameter of the chamber has been enlarged so that the number of backstreaming electrons scattered from the chamber walls could be diminished. For the same reason, the thickness of the walls separating the chamber from the cooling envelope as well as those supporting the exit foil has been minimized. A smaller relative contribution to the spectrum background from the foils is made possible by using $12\text{-}\mu\text{m}$ titanium foils (instead of Havar) which support pressures up to 15 atm. Last, a dry-ice and acetone mixture can now be pumped through the cooling envelope when higher cooling temperatures are needed for gases which liquefy at liquid-nitrogen temperature.

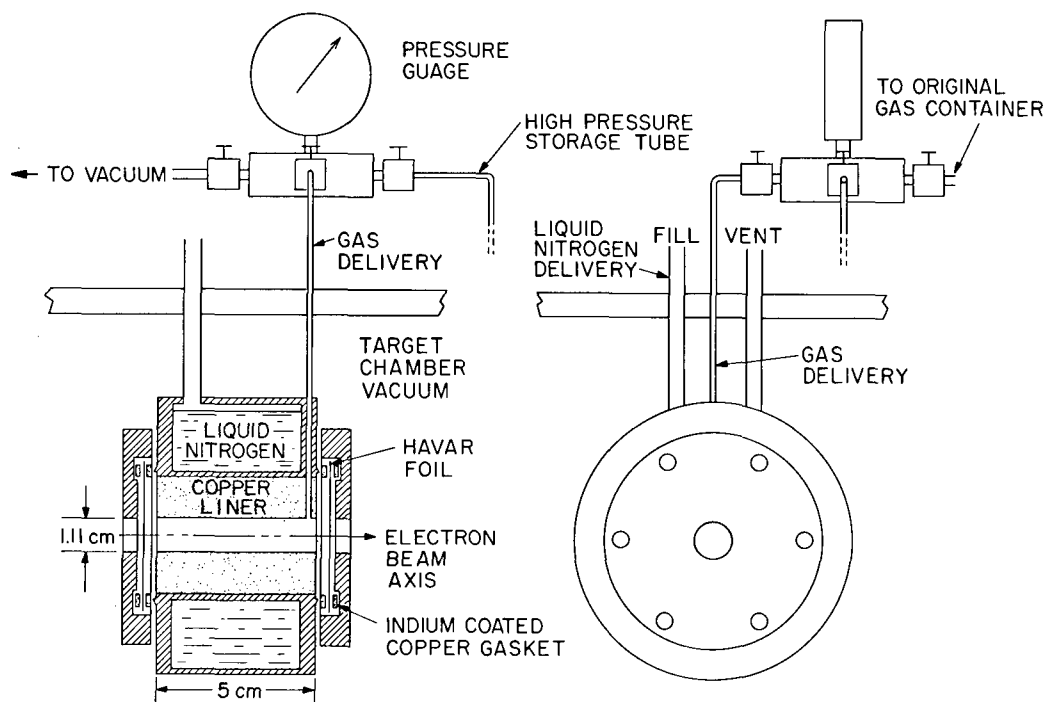


Fig. 20 — Early version of the NRL refrigerated gas target system for 180° electron scattering. The simple cylindrical symmetry about the incident beam direction is apparent. For more recent improvements on this system which include the removal of the copper cylinder [61], see the text. (From Ref. 61.)

As mentioned in pages 22 to 24 a “ghost peak” can appear in a spectrum, which is caused by the elastic electrons striking the outer diameter wall of the spectrometer vacuum chamber when the spectrometer field is at an inelastic setting. Although this is a more serious concern with the high elastic-scattering intensities occurring at more forward angles, it nevertheless has to be dealt with in 180° scattering. By far the best technique for solving this problem is that used at Mainz where the spectrometer pole gap essentially extends all the way to the outer perimeter of the yoke. A foil then constitutes the outer diameter wall of the vacuum chamber so that the elastically scattered electrons can escape and be trapped. An alternative is to line the outer diameter wall of the spectrometer vacuum chamber with appropriately designed baffles and absorbers [63].

Finally, reference was made in pages 22 to 24 to the unfeasibility of comparing inelastic peak intensities corresponding to $M1$ transitions to the elastic intensity for the purpose of relative cross-section determinations at 180° . Reasons were given for this being the case. Such a comparison technique at 180° , however, can be used for the very lightest of nuclei (^2D , ^3He , and perhaps $^6,7\text{Li}$) that have ground-state magnetic moments. For the heavier nuclei it has been found most useful to either make an absolute measurement or compare the $M1$ transition intensity under study with that of a very well-known $M1$ transition such as the one at 15.11 MeV in ^{12}C .

DISCUSSION OF EXPERIMENTAL RESULTS

Self-Conjugate Nuclei

Theoretical Preliminaries-Sum Rules — It will become apparent in the following theoretical outline that there are characteristics of the $M1$ transitions in self-conjugate nuclei which set them apart from those of other nuclei. For this reason we have chosen to deal with them separately and to give some prefatory theoretical remarks concerning them before discussing the relevant experimental results.

The mechanism that is more often responsible for the strongest $M1$ transitions in nuclei is the spin-flip mechanism. Its relative strength can be most easily theoretically demonstrated in the case of the self-conjugate nuclei where such transitions usually play a strong role. We start with the general expression for an $M1$ transition matrix element between states a and b as set down by Morpurgo [64]:

$$\langle a | \sum_{i=1}^A \left\{ \vec{L}^i \left(\frac{1+\tau_3^i}{2} \right) + \mu_p \vec{\sigma}^i \left(\frac{1+\tau_3^i}{2} \right) + \mu_n \vec{\sigma}^i \left(\frac{1-\tau_3^i}{2} \right) \right\} | b \rangle \quad (33)$$

where \vec{L}^i is the orbital angular momentum operator; $\vec{\sigma}^i$ and τ_3^i are the spin and isospin operators of the i th nucleon, respectively; and μ_p and μ_n are the proton and neutron magnetic moments, respectively. Expression (33) is valid in the limit $q \rightarrow \omega$, and thus should still be useful at low-momentum transfers. Rearranging terms and adding and subtracting $\frac{1}{2} \vec{\sigma}^i$ inside the sum, we have

$$\begin{aligned} \frac{1}{2} \langle a | \sum_{i=1}^A [\vec{L}^i + \frac{1}{2} \vec{\sigma}^i] | b \rangle + \frac{1}{2} \langle a | \sum_{i=1}^A (\mu_p + \mu_n - \frac{1}{2}) \vec{\sigma}^i | b \rangle \\ + \frac{1}{2} \langle a | \sum_{i=1}^A \tau_3^i \left\{ \vec{L}^i + (\mu_p - \mu_n) \vec{\sigma}^i \right\} | b \rangle . \end{aligned} \quad (34)$$

The first two terms of (34) constitute the isoscalar ($\Delta T = 0$) part of the transition, while the third term with the τ_3^i operator is the isovector ($\Delta T = 1$) part. However, the first term is the matrix element of

$$\vec{J} = \sum_{i=1}^A (\vec{L}^i + \frac{1}{2} \vec{\sigma}^i),$$

which vanishes due to the orthogonality of the two states (both being eigenstates of \vec{J}), so that only the second term gives the strength of the isoscalar transition. Since the $(\mu_p - \mu_n)$ term (the spin-flip term) of the isovector matrix element determines its order of magnitude, to compare the isoscalar and isovector strengths we can use

$$\frac{\mu_p + \mu_n + \frac{1}{2}}{\mu_p - \mu_n} = \frac{0.38}{4.7} . \quad (35)$$

When this ratio is squared, an intensity ratio of about 10^{-2} results. Here we have shown the general dominance of the spin-flip transition as well as outlined the derivation of a selection rule given by Morpurgo [64]. However, it is not to be implied that spin-flip transitions invariably dominate even in the self-conjugate nuclei. An exception is the 11.25-MeV $M1$ transition in ^{20}Ne which proceeds principally by orbital recoupling (see page 49 below).

From the foregoing outline we see that Morpurgo's rule states that $\Delta T = 0$, $M1$ transitions in self-conjugate (ground-state $T = 0$) nuclei are strongly inhibited. This rule yields two evident results: (a) there is a strong limitation in the number of $M1$ transitions experimentally observable in the self-conjugate nuclei, and (b) the remaining transitions, those with $\Delta T = 1$, are to relatively high energy states ($\gtrsim 10$ MeV) which are analogs of low-lying states in neighboring ($\Delta T_3 = \pm 1$) nuclei.

The number of $\Delta T = 1$ transitions in self-conjugate nuclei experimentally observed is, however, even further limited as a result of effects in the self-conjugate $4N$ and $4N + 2$ nuclei studied by Kurath [65]. Using the shell model with spin-orbit coupling and central force two-body interactions, he showed that most of the $M1$ transition strength in the self-conjugate nuclei of the p -shell is concentrated in the lowest few $\Delta T = 1$ transitions. He also derives an $M1$ sum rule starting with the ground-state expectation value of the double commutator of his Hamiltonian H with the z -component of the magnetic dipole operator μ_z :

$$\langle g | [\mu_z, [H, \mu_z]] | g \rangle, \quad (36)$$

where $|g\rangle$ denotes the ground state. H is given by

$$H = \sum_i H_0^i + a \sum_i \vec{\ell} \cdot \vec{s}^i + \sum_{j>1} V^{ji}, \quad (37)$$

where H_0^i is a harmonic oscillator Hamiltonian; a , the $\vec{\ell} \cdot \vec{s}$ coupling parameter; and V^{ji} , a standard central force two-body interaction.

The H_0 term commutes with μ_z and does not contribute to Eq. (36), while the $\vec{\ell} \cdot \vec{s}$ term gives the principal contribution. Giving arguments for choosing to ignore the V^{ji} term, Kurath then arrives at the sum rule:

$$\sum_k \omega_k B(M1)_k \approx -a (\mu_p - \mu_n + \frac{1}{2})^2 \langle g | \sum_i \vec{\ell} \cdot \vec{s}^i | g \rangle, \quad (38)$$

where $B(M1)_k$ and ω_k are the reduced transition probability and excitation energy of the k th level, respectively.

As an example of the concentration of the $M1$ strength into the lowest few $\Delta T = 1$ transitions as well as a justification for ignoring the two-body interaction term, Kurath calculates the $B(M1)_k$ for the lowest four $\Delta T = 1$, $M1$ transitions in ^{12}C as shown in Fig. 21. This is done for four different values of a/K , where K is a representative integral of the two-body interaction. The sum of the four transition probabilities is also shown as well as the value of the r.h.s. of Eq. (38). Particularly for values of $a/K = 4.5$ and 6.0 , the concentration of strength into the lowest $T = 1$ level is apparent. Also evident is the

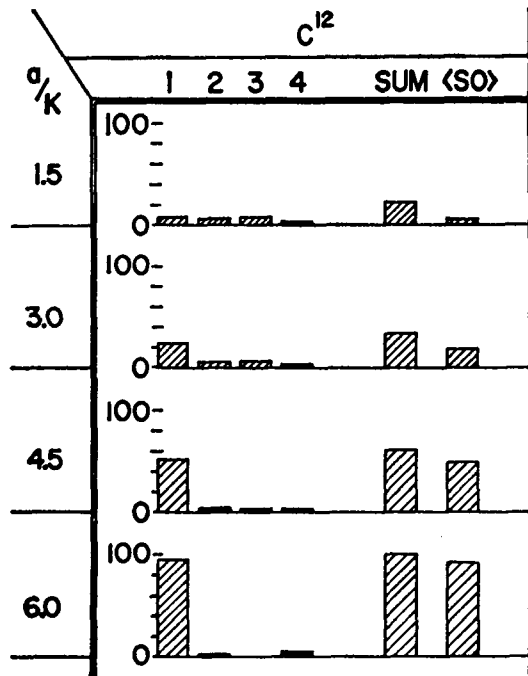


Fig. 21 — Contribution of the four lowest $\Delta T = 1$, $M1$ transitions in ^{12}C to the energy-weighted sum rule, their sum, and the ground-state expectation value of the spin-orbit term for different values of a/K (see text). (From Ref. 65.)

fact that the ground-state expectation value of the spin-orbit coupling nearly equals this sum, justifying Kurath's assumption that the two-body interaction term does not significantly contribute. That a/K should be high in value, although still not close to the jj limit is, of course, supported by the experimental results on ^{12}C . It is interesting to note [12] that the $M1$ strength is concentrated into the lower levels in contrast to the $E1$ giant dipole case where concentration is generally observed into the highest levels [13].

The above results, applicable to the self-conjugate ($4N$) nuclei, also apply to ($4N + 2$) nuclei, e.g., ^6Li , ^{10}B , and ^{14}N . As more accurate experimental results become available, it may be of interest to include consideration of the V^i term in Eq. (37).

Kurath also extrapolates the use of Eq. (38) to the sd shell, where, in some of the early experimental tests of the rule, Kuehne et al. [66], gave a version of the rule somewhat more useful to experimentalists:‡

$$\sum_k \left[\frac{\Gamma_{0k}(M1)}{3.395 \text{ eV}} \right] \left(\frac{10 \text{ MeV}}{\omega_k} \right)^2 = - \left(\frac{a}{2 \text{ MeV}} \right) \langle g | \sum_i \vec{l}^i \cdot \vec{s}^i | g \rangle \quad (39)$$

‡Dr. W. Bendel (NRL) notes a 4% error in denominator of the first factor of Eq. (39). It should be 3.259, not 3.395.

where Γ_{0k} is the ground-state transition width to the k th level in electron-volts. The beauty of this sum rule is the ease of its experimental use with the self-conjugate nuclei. Since the $M1$ transition strength is usually concentrated into a very few $\Delta T = 1$ transitions, the sum of the l.h.s. of Eq. (39) is easy to measure. Thus, when a reasonable value of the parameter "a" such as indicated for the sd shell from the $\vec{\ell} \cdot \vec{s}$ separation energy given by the 5.08-MeV state in ^{17}O is used, the ground-state $\vec{\ell} \cdot \vec{s}$ coupling expectation value ($\langle \sum \ell \cdot s \rangle$, hereafter) can be determined. This value can then be used to place some restriction on the ground-state wave function. This restriction often takes the form of a limitation on the possible ground state shapes a nucleus can assume, as will be discussed below.

For a spherically symmetric nucleus in the simple shell model the ground-state wave function $|g\rangle$ is an eigenfunction of the $\vec{\ell} \cdot \vec{s}$ operator, and the eigenvalue is given by

$$\vec{\ell} \cdot \vec{s} = \frac{1}{2} [j(j+1) + \ell(\ell+1) - s(s+1)] , \quad (40)$$

where j , ℓ , and s are the total, orbital, and spin angular momentum quantum numbers, respectively, of a given nucleon. Using Eq. (40) one can obtain an approximate idea of the expected pattern of total $M1$ strength among the self-conjugate nuclei in the sd shell. As a specific example, to calculate the sum in ^{20}Ne where, in the shell model, the $d_{5/2}$ level is being filled, one substitutes $j = 5/2$, $\ell = 2$, and $s = 1/2$ to obtain $\vec{\ell} \cdot \vec{s} = 1$ in Eq. (40). This is the value for one nucleon; since there are four nucleons in this subshell for ^{20}Ne , $\langle \sum \ell \cdot s \rangle = 4$. Proceeding accordingly with the other self-conjugate nuclei in the shell, we obtain the results given in Table 3. Since $\langle \sum \ell \cdot s \rangle$ gives values of zero and $-3/2$ for the $2s_{1/2}$ and $d_{3/2}$ levels, respectively, the behavior for ^{32}S and ^{36}Ar in the table can be understood. Of course, zero is obtained for ^{16}O and ^{40}Ca .

Table 3
Values of the Kurath Sum Rule for sd Shell
Self-Conjugate Nuclei Assuming a Spherically
Symmetric Nucleus in the Independent
Particle Shell Model

Nucleus	$\langle \sum \ell \cdot s \rangle$
^{16}O	0
^{20}Ne	4
^{24}Mg	8
^{28}Si	12
^{32}S	12
^{36}Ar	6
^{40}Ca	0

Since the sd shell nuclei are in general deformed, a much more sensitive indication of how the $M1$ strength sum varies among these nuclei can be obtained by using the Nilsson model. Nilsson gives tables of deformed wave functions from which the value of $\langle \Sigma \ell \cdot s \rangle$ as a function of the deformation parameter η can be determined. One particularly interesting such curve is presented in Fig. 22 for ^{32}S where the crossing of Nilsson levels 8 and 9 causes a discontinuity at $\eta = -4$. It will be noted that the maximum value of this curve is equal to that for a spherical shape given in Table 3 for ^{32}S . The shape of such curves clearly suggests that, in some cases, if sufficiently accurate experimental values of the $M1$ sum strength can be obtained, then something can be said about the ground-state nuclear shape. Further use will be made of this approach in the discussion of some of the self-conjugate nuclei in the next section.

Kurath's sum rule as well as others can also be used to say something about nucleon occupation numbers. The configuration mixing that is present, especially in some of the sd shell nuclei, will tend to decrease the sum strengths based on the pure independent particle shell model, such as those given in Table 3 (just as shown above with the Nilsson model). The amount of this decrease can be related to the nucleon occupation numbers. Using the project Hartree-Fock method, occupation numbers in the even sd shell nuclei have been calculated [68] and compared with experimental numbers using French's sum

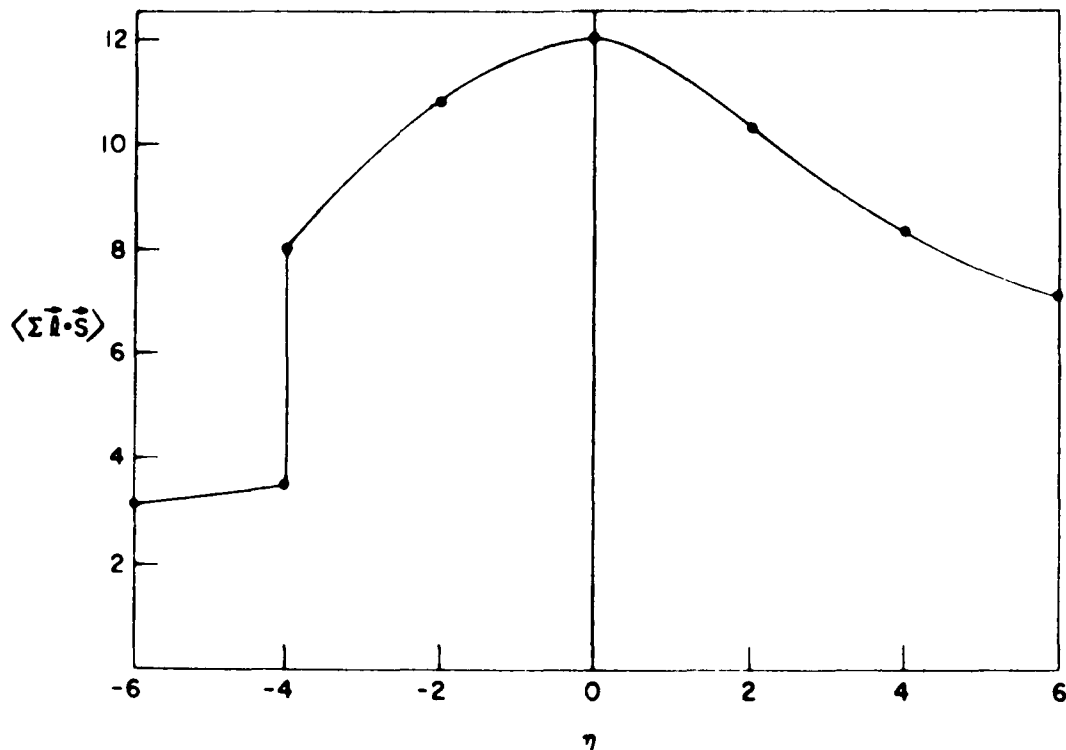


Fig. 22 — Curve of $\langle \Sigma \ell \cdot s \rangle$ vs η , the deformation parameter in the Nilsson model. The discontinuity of $\eta = -4$ is due to the crossing of Nilsson levels 8 and 9. (From Ref. 67.)

rule [69]. Castel et al. also use their calculated occupation numbers to calculate in turn $\langle \Sigma \ell \cdot s \rangle$ using Kurath's sum rule, and find good agreement with the photon scattering results [66] for $M1$ strengths in ^{24}Mg and ^{28}Si .

Other sum rules have been applied to the self-conjugate nuclei. Nang [70] in studying the validity of $SU(4)$ symmetry in light nuclei, shows that the $\Delta T = 1$, $M1$ transitions in self-conjugate nuclei result from symmetry breaking of $SU(4)$, and gives sum rules for the $4N$ and $4N + 2$ nuclei. Kurath [71] in a study of triaxial shapes in sd shell nuclei, gives a closure sum rule in the adiabatic model.

Two additional comments seem warranted. First, although usually weaker by about two orders of magnitude, $\Delta T = 0$, $M1$ transitions in self-conjugate nuclei have been detected with 180° electron scattering [72]. Where this is the case some determination of the isospin mixing between the $T = 0$ and $T = 1$ levels can be made. Second, although the $M1$ transitions especially in the self-conjugate nuclei are often referred to as " $M1$ giant resonances," this should not be considered true in any purely collective sense. Lipas [73] has shown that $M1$ transitions in even nuclei, whether spherical or deformed, cannot be of simple collective origin. However, this conclusion is being reexamined by Murphy and Úberall [74], e.g., by foregoing the usual assumption of irrotationality of the nuclear fluid.

The Deuteron — Because of the voluminous literature that has accumulated on the magnetic aspects of the deuteron, it could easily be the subject of a review in its own right. Accordingly, it is felt that an attempt at a comprehensive treatment would be out of place here. Thus, only selected references primarily germane to back-angle electro-excitation of the $M1$ transition at low-momentum transfer (<100 MeV/c) will be discussed.

Clearly the deuteron is the most fundamental of all self-conjugate nuclei. In back-angle scattering, it can be excited via the pure spin-flip $\Delta T = 1$ transition from the 3S_1 ground state to the 1S_0 state at breakup threshold. A visual idea of the strength of this spin-flip transition compared to that of the elastic scattering can be seen in Fig. 23, which shows a 180° scattering spectrum taken at NRL [75].

The first quantitative study of the inelastic cross section of the deuteron at 180° was performed at Stanford by Peterson and Barber [36] using a solid CD_2 target. The experimental results were compared with the impulse approximation theory of Jankus [76], which assumes point nucleons and point magnetic moments. After correction for instrumental contributions to the high-energy tail, the experimental cross section in this region was still found to be about 10% higher than that given by the Jankus theory. It was suggested that possible meson exchange effects could explain the discrepancy. Shortly thereafter, in another Stanford experiment performed with a deuterium gas target [10], agreement with the Jankus theory was obtained.

However, in a third Stanford experiment [77] using a liquid deuterium target, disagreement was found with the Jankus theory as well as that of Durand [78] on taking the final-state interaction of the two nucleons into account. In fact the experimental curve was about a factor of 2 higher than the curve obtained from the Durand theory, again in the tail region. The authors suggested that the discrepancy might be attributed

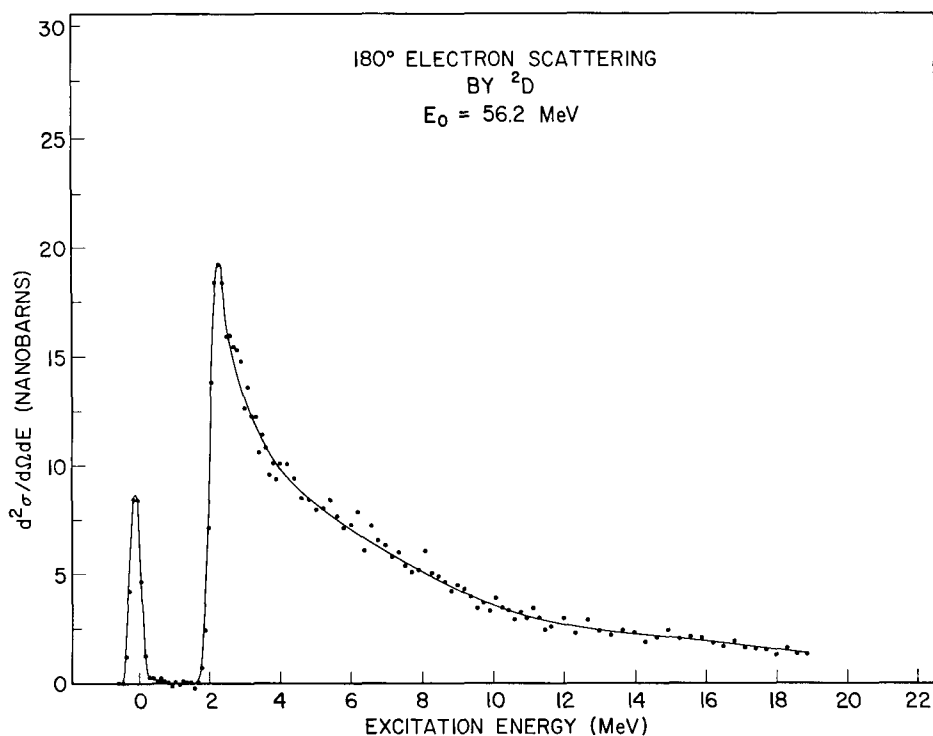


Fig. 23 — Spectrum of 56.2-MeV electrons scattered at 180° from deuterium gas (From Ref. 75.)

to inadequate treatment of the final-state interaction or to contributions from meson exchange currents. More recently Ganichot et al. [51] using a gas target have measured the 180° inelastic scattering cross section at several incident electron energies below 280 MeV. Although strictly speaking only their 70-MeV data are relevant to this paper, they find essential agreement using the theories of Jankus and Durand.

The works thus far mentioned [10, 36, 51, 74, 76], to the author's knowledge, constitute the entirety of the 180° inelastic scattering study of the deuteron at low-momentum transfer q . In fact the only additional inelastic work at 180° even at values of high q is that of Rand et al. [79]. Throughout the discussion of the low- q experiments there has been a persistent controversy over the extent of the contribution of meson exchange currents. Especially since Bosco et al. [80] have emphasized their importance, the use of 180° inelastic scattering from deuterium to examine the role of meson exchange currents has been at least a partial motivation for these experiments. Further incentive has been furnished by concurrent calculations of the exchange effects [81-83].

The elementary theoretical basis for interest of such magnetic transition measurements to determine meson exchange effects derives from the use of Siegert's theorem [84]. According to the theorem the effect of exchange currents on the electric transitions disappears as $q \rightarrow \omega$. However, this is not the case with magnetic transitions, and

thus such effects should be detectable if present, especially in the deuteron and other very light nuclei where other effects, such as configuration mixing, are not a problem.

However, meson current contributions increase with increasing q [12]. Therefore, although more accurate low- q 180° inelastic experiments on the deuteron would be most useful, the preponderant recent interest has been in the work at higher values of q . This interest is reflected in such work as that of Hockert et al. [85] and Riska [86], which account for the high- q cross-section discrepancies using meson exchange currents, and that of Rand et al. [87], which reviews the status of magnetic electron-deuteron scattering. Nevertheless, relatively recent work covering the low- q region has been done by Hadjimichael [88], who points out that meson exchange effects are more observable in the polarization of the breakup proton and neutron, and by Smirnov and Trubnikov [89], who calculate the 180° inelastic cross section taking into account final-state interaction but not meson exchange. Of general interest are the results given by Miller and Arenhovel [90], who find improved agreement with the photo-disintegration cross section at intermediate energies by allowing admixture of nucleon isobar configurations in the n-p system.

p-Shell Nuclei — Ever since the early survey work on electroexcited $M1$ transitions in these nuclei at Stanford, they have been studied extensively at several laboratories. The bulk of the subsequent, more accurate, studies have been performed by the group at Darmstadt, but quite significant contributions have been made by groups at the National Bureau of Standards, M.I.T., the University of Massachusetts, Glasgow, Saskatoon, Mainz, Catholic University, and NRL. The nuclei will be discussed generally in order of increasing A .

Since some of the early work [2, 91-93] on the transition to the 0^+ , $T = 1$ level at 3.56 MeV in ${}^6\text{Li}$ (ground-state spin, 1^+), considerable electron scattering study [94, 95] has been devoted to it as well as to the transition to the 2^+ , $T = 1$, level at 5.36 MeV. The strong 3.56-MeV transition is virtually pure $M1$, whereas the 5.36-MeV transition has a predominant $M1$ component. Eigenbrod [96] has made an accurate measurement of the 3.56-MeV ground-state transition width, $\Gamma_0 = 8.31 \pm 0.36$ eV, while Hutcheon et al. [97] have studied the 5.36-MeV transition. They find it to be primarily $M1$, with some $E2$ and $M3$ admixture, and give values of $\Gamma_0 = 0.19 \pm 0.04$ eV or 0.08 ± 0.04 eV depending on model parameters used.

Neuhausen and Hutcheon [98] have conducted a careful study of these two transitions and their form factors. They find the form factors, especially that for the 3.56-MeV transition, to be sensitive to the radial distribution of the outer nucleons of the nucleus. Using an intermediate coupling model, they conclude that the 3.56-MeV transition is an almost pure $M1$ spin-flip transition, 96% of the strength coming from the ${}^3S_1 \rightarrow {}^1S_0$ component of the transition, in agreement with an earlier suggestion of Barker [99] using a shell model analysis. They note that if they had fitted their data with an α - d model in which the alpha and deuteron were in a relative s -state and the deuteron changed from a triplet to a singlet state, the same overlap of ground- and excited-state radial-wave functions would have occurred as with the shell model.

All of the foregoing work on ${}^6\text{Li}$ has been at scattering angles $\theta \leq 160^\circ$ (except the 180° work of Goldemberg et al. [93]). A more recent study of the higher excitation energy region has been made by Fagg et al. [100] using 180° scattering, obtaining the spectrum shown in Fig. 24 which compares the intensity of the excitation region from 8 to 18 MeV with that of the 3.56-MeV peak. The strength of this peak is visually quite apparent, especially if it is noted that the elastic peak, not shown, is about one-third as intense. However, the prime motivation of this experiment arose from work of Fowler [101] and Fetisov and Kopysov [102], who suggested that the existence of a narrow 0^+ resonance state at about 11.5 MeV in ${}^6\text{Be}$ (i.e., at the ${}^3\text{He} + {}^3\text{He}$ separation energy) could explain why the high-energy solar neutrino flux is almost an order of magnitude lower than predicted [103, 104]. Hence the search was made for the analog of this state in ${}^6\text{Li}$, expected at about 15.2 MeV and reached by an $M1$ transition. From the results shown in Fig. 24, if a 0^+ state at 15.2 MeV is assumed as well as an $M1$ form factor equal to that of the 3.56-MeV transition [96], an upper limit of 3 eV can be placed on its ground-state transition width. This result is supported by electron scattering work in this excitation region at more forward angles [105, 106]. These recent studies of Fagg et al. [100] Cardman et al. [105], and Bishop [106] all disagree with those of Barber et al. [10] who show peaks at 9.3, 14.0 and 15.8 MeV in their spectrum.

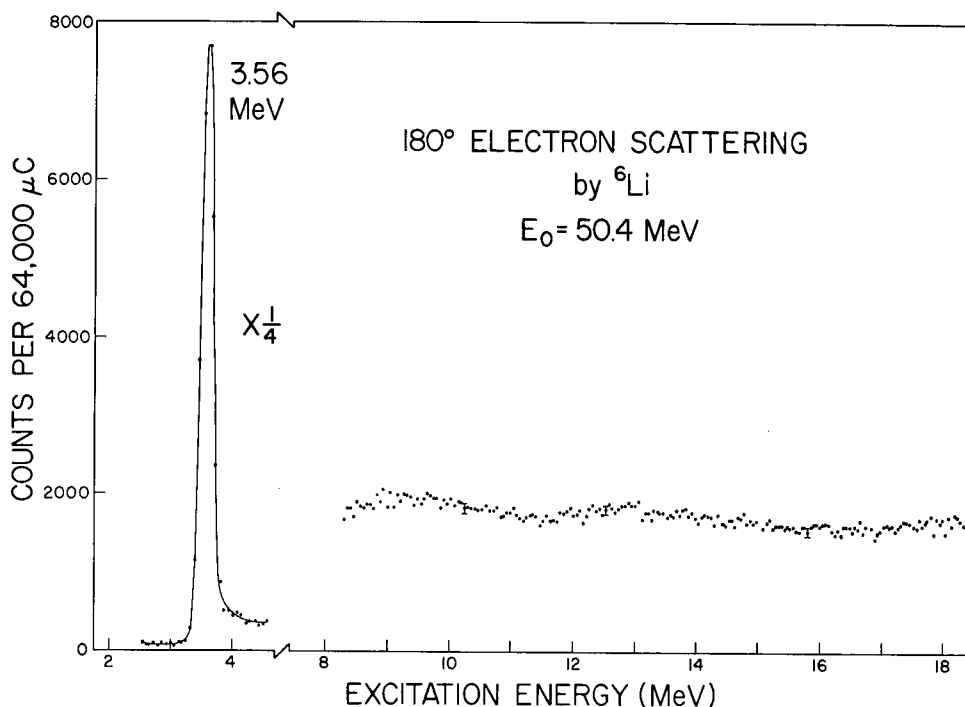


Fig. 24 — Spectrum of 50.4-MeV electrons scattered at 180° from ${}^6\text{Li}$. The peak at the left is due to the $M1$ transition at 3.56 MeV. (From Ref. 99.)

This dearth of $M1$ strength in the higher excitation region leaves virtually all of it in the 3.56- and 5.36-MeV transitions, largely the former. Therefore ${}^6\text{Li}$ is a prototype for the kind of $M1$ strength concentration Kurath has predicted.

Edge and Peterson [47] first studied ${}^{10}\text{B}$ (ground-state spin, 3^+) by means of 180° scattering and reported transitions to levels at 7.9, 11.8, and 14.0 MeV. With a Helm model analysis they suggested that all three transitions were $M1$; however, these results have not since been confirmed. At scattering angles $\leq 165^\circ$, Spamer and Gudden [107], motivated by Kurath's [108] prediction of a 2^+ , $T = 1$, level at 7.4 MeV, found a transition at 7.48 MeV which they definitely identified as $M1$. The existence of a known 2^- level at this energy [109] did not result in any measurable contribution of $M2$ strength according to their shell model [110] analysis, and thus they were able to report $\Gamma_0 = 11 \pm 2$ eV for the transition. Spamer [111] later reexamined this transition and, using an essentially model-independent analysis, reported a revised value of $\Gamma_0 = 12.0 \pm 2.2$ eV. Kossanyi-Demay and Vanpraet [112] in a 180° scattering study report peaks at 3.58 and 7.5 MeV which they suggest correspond to $M1$ transitions; however, the results on the 3.58-MeV transition have also not since been confirmed. Clearly, more study of this nucleus at back angles would be useful. Nevertheless, the strength of the 7.48-MeV transition, coupled with the fact that the Darmstadt group [107, 111] reported no other $M1$ transitions up to an excitation energy of 20 MeV, again gives general support to Kurath's predictions of strength concentration.

The $M1$, $\Delta T = 1$, transition at 15.11 MeV in ${}^{12}\text{C}$ has probably undergone more back-angle electron scattering study than any other in all the nuclides and is a classic example of the Kurath-type $M1$ strength concentration. As a result it has been subject to progressively more accurate measurements, and accordingly often serves as a reference for relative measurements on transitions in other nuclei. No attempt at a complete history of these measurements will be made here; only some selected highlights will be mentioned. The primary emphasis will be on more recent measurements and their ramifications.

The early Stanford investigations [2, 47, 93, 113] of this transition, by means of shell model, Helm model, and model-independent analyses, corroborated its $M1$ character. Further studies were also conducted at Stanford as well as at other laboratories [49, 78, 114, 115]. An early measurement of the ground-state transition width was made by Gudden [116] who reported $\Gamma_0 = 34.4 \pm 3.4$ eV, using a shell model analysis. Later Peterson [117], reporting slightly higher accuracy, found $\Gamma_0 = 36 \pm 3$. More recently, the status of the measurements on this Γ_0 was reviewed by de Vries [118] who reported the result of an Amsterdam—Darmstadt collaboration [119] giving $\Gamma_0 = 35.74 \pm 0.86$ eV.

However, the most recent value of this quantity has been obtained by Chertok et al. [46]. They were motivated not only by a wish to determine a value of Γ_0 that would serve as a benchmark for low- q measurements, but also by a desire to exploit the physical unity of weak and electromagnetic processes found in the $A = 12$ system [120] by using Γ_0 to increase the exactness of the weak magnetism test in β -decay as well as μ -capture. Specifically, this test, using the conserved-vector-current (CVC) theory, predicts for β -decay that the electromagnetic matrix element for the 15.109-MeV decay in ${}^{12}\text{C}$ determines the strength of the weak matrix element in ${}^{12}\text{B} \rightarrow \beta^- + {}^{12}\text{C}$ and ${}^{12}\text{N} \rightarrow \beta^+ + {}^{12}\text{C}$

for the V-A interference [121]. Actually, a third corollary motivation was to resolve the apparent discrepancy between a weighted average of (γ, γ') measurements of $\Gamma_0 = 45.8 \pm 2.6$ eV and that of (e, e') measurements, $\Gamma_0 = 32.6 \pm 3.5$ eV, the latter of which were corrected for Coulomb distortion effects.

Chertok et al. took measurements of $B(M1, q)$ at eight different values of q and used the Yale [117] and Orsay [122] results as well in order to obtain values over a range of q sufficient for a curve-fitting that would lead to an accurate extrapolation to $q = 0$ for a determination of $B(M1, 0)$. As shown in Fig. 25, they fit these points best to a curve based on a $1p$ -shell harmonic oscillator model. This extrapolated value of $B(M1, 0)$ leads to the result, $\Gamma_0 = 37.0 \pm 1.1$ eV, still in disagreement with the above average (γ, γ') value. However, it was concluded that this (e, e') measurement effected a fourfold and 30% reduction (compared to previous work, see Chertok [46, p. 32]) in the uncertainties of the basic electromagnetic parameters used in the weak magnetism tests in β -decay and μ -capture, respectively.

In another recent study of ^{12}C [72] using the NRL 180° system, a value of $\Gamma_0 = 0.35 \pm 0.05$ eV was determined for the $\Delta T = 0, M1$ transition at 12.71 MeV. The spectrum presented in Fig. 26 shows the intensity contrast between the above transition and the

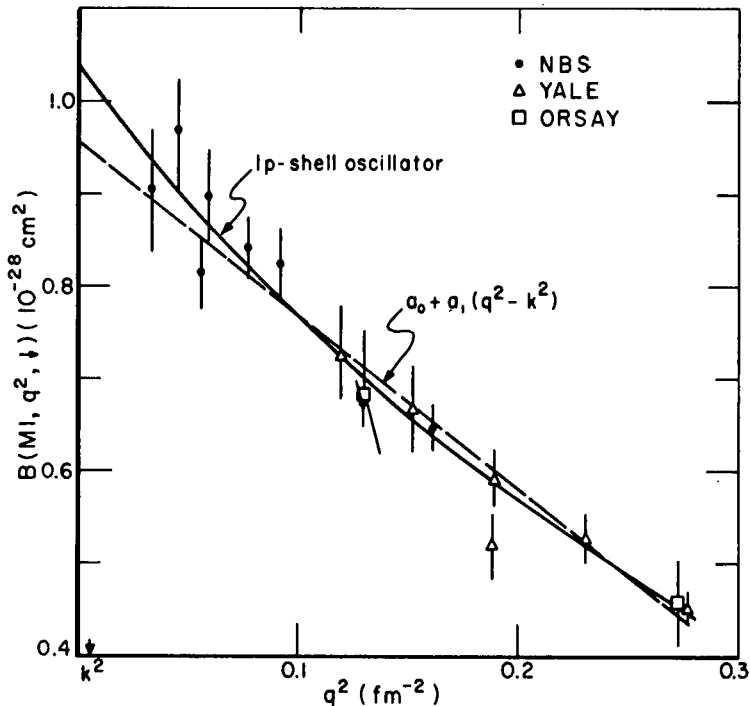


Fig. 25 — Fits to the experimental reduced transition probability vs q^2 . The solid curve is based on a $1p$ -shell harmonic oscillator model, while the dashed curve is given by $a_0 + a_1 (q^2 - \omega^2)$, where a_0 and a_1 are fitting parameters. (From Ref. 46.)

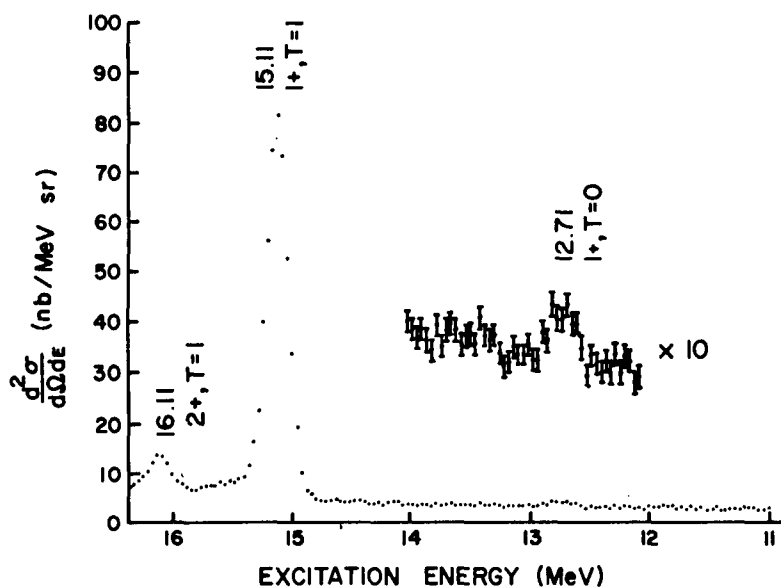


Fig. 26 — Spectrum of 50.5-MeV electrons scattered at 180° from ^{12}C . The region around the 12.7-MeV peak has been enlarged by a factor of 10. (From Ref. 71.)

$\Delta T = 1$ transition at 15.11 MeV. The principal result of this work was a model-dependent measurement of the isospin mixing between the $\Delta T = 0$ and 1 levels. Values for the mixing coefficient β were found to be $\beta = 0.194 \pm 0.011$ or 0.057 ± 0.011 .

Again it was early Stanford experiments [10, 47] at 180° which first gave electron scattering evidence of $M1$ transitions in ^{14}N (ground-state spin 1^+) at 9.2 and 10.5 MeV. Other workers [112] also studied these transitions at this angle. The Orsay group [123, 124] at more forward angles identified a weak $M1$ transition to a 0^+ , $T = 1$ level at 2.312 MeV, which is the analog of the β^- and β^+ decays from the ground states of C^{14} and O^{14} , respectively. Clerc and Kuphal [125] further examined the higher excitation region and reported $\Gamma_0 = 7.7 \pm 0.9$ and 12.1 ± 1.5 eV for the transitions to 2^+ states at 9.17 and 10.43 MeV, respectively. Again, therefore, considerable concentration of $M1$ strength is in evidence.

More recently, further observation was made of the 2.313-MeV transition by Ensslin et al. [126] using the NBS accelerator and a Be_3N_2 target. Their interest in a measurement of this transition strength arises from the fact that an accidental cancellation occurring in the β -decay matrix element of the ^{14}C decay imposes a strong constraint on the range of valid ^{14}C and ^{14}N ground-state wave functions. This constraint in turn makes it possible to test models of the nuclear force. Rose et al. [127], reviewing the β and γ -decay data on mass 14, concluded among other things that the smallness of the $^{14}\text{C} \rightarrow ^{14}\text{N}$ β -decay matrix element is due to the presence of a tensor force. Because of the low intensity of the 2.313-MeV transition, a measurement to an accuracy satisfactory to

Ensslin et al. [126] was not possible; however, they give a value of $B(M1, \omega) = (4.3 \pm 1.3) \cdot 10^{-30} e^2 fm^2$ for the transition. It is of interest to add that a useful theoretical approach to ^{14}N has been to regard it as a quasi-deuteron, i.e., a deuteron hole in an ^{16}O core [128].

We conclude this subsection with a remark about $M1$ strength in ^{16}O . Little such strength is expected here, as predicted by Kurath's sum rule; however, an $M1$ transition at 16.21 MeV has been reported by the Darmstadt group [129].

sd-Shell Nuclei — The convincing pattern of strong concentration of $M1$ strength present in the p -shell self-conjugate nuclei continues well into the sd -shell. In general in the sd shell, the lighter the self-conjugate nucleus, the greater the concentration of strength observed. However, there seems to be a somewhat larger increase in general fragmentation of this strength in passing from ^{28}Si to ^{32}S than in comparison with any other two such neighbors.

Thus, the concentration of strength in ^{20}Ne is quite comparable to that found in similar p -shell nuclei as can be seen in the spectrum taken at NRL [130] and presented in Fig. 27. The level excited at 11.24 MeV is probably the $T = 1$ analog of the 1^+ state at 1.057 MeV in ^{20}F [131]. The value of $\Gamma_0 = 11.2 \pm 2$ eV measured for this transition

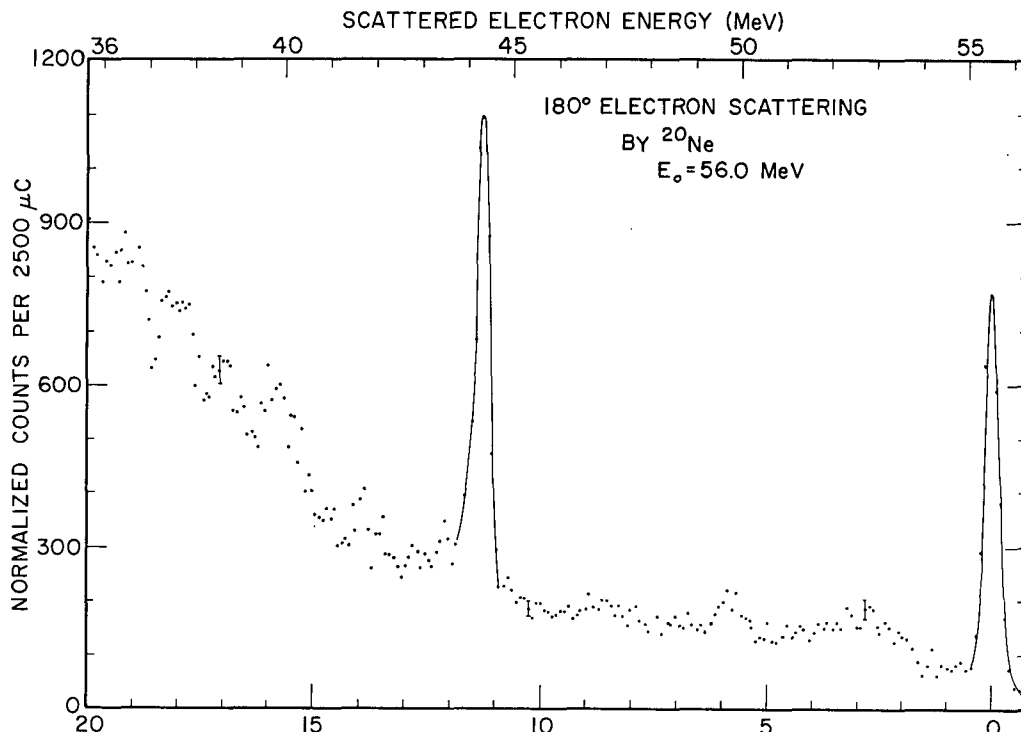


Fig. 27 — Spectrum of 56.0-MeV electrons scattered at 180° from ^{20}Ne . (From Ref. 130.)

represents about 67% of the total expected strength by Kurath's sum rule, assuming a spherical shell-model nucleus. Ritter et al. [132] have observed 1^+ states at 13.17 and 13.48 MeV using the $^{19}\text{F}(d, n)^{20}\text{Ne}$ reaction. Transitions to these states were too weak to be observed in the NRL data.

Using this rule with Nilsson wave functions (as discussed above in subsection 1), a calculation can be made of $\langle \sum \ell \cdot s \rangle$ as a function of the deformation parameter η . This is shown in Fig. 28 for two values of the parameter μ which is the coefficient of the orbit-orbit $\vec{\ell}^2$ term in the Nilsson Hamiltonian. Where the experimental value (given by the horizontal line) of the 11.24-MeV transition strength crosses these curves shows that this nucleus is no more prolate than is indicated by a value of $\eta = 4$. This is an example of how something can be said about nuclear shapes from $M1$ sum strength data. The value of $\eta = 4$ is in approximate agreement with that of 4.5 calculated by Drake and Singhal [133] for ^{20}Ne .

The strong concentration of $M1$ strength into one level in this nucleus also has a theoretical explanation given by Akiyama et al. [134] in terms of a shell model based on $SU(3)$ symmetry. They note that the dominant part of the $M1$ operator is given by $\sum_i \tau_{3i} \sigma_i$ (as mentioned in subsection 1 above), which cannot change the spatial symmetry.

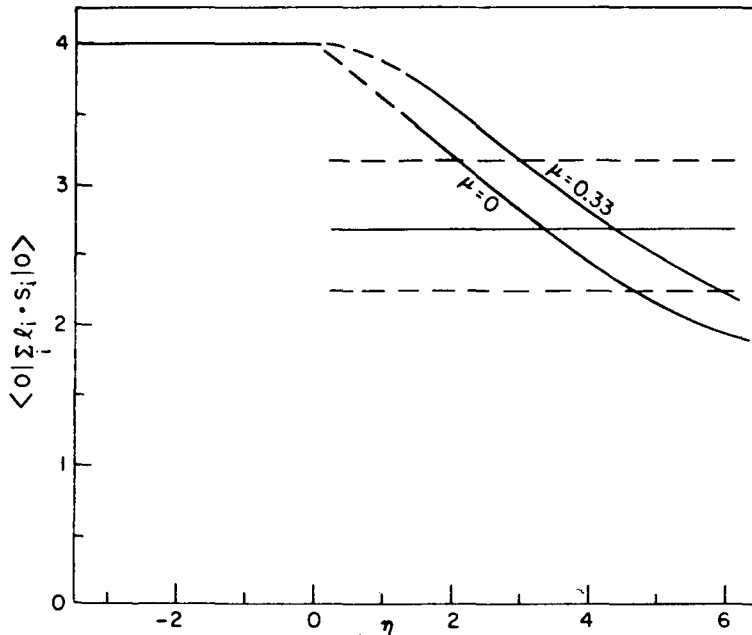


Fig. 28 — Curves of $\langle \sum \ell \cdot s \rangle$ vs η , the deformation parameter in the Nilsson model, for two values μ , the coefficient of the $\vec{\ell}^2$ term in the Nilsson Hamiltonian. The experimental value of the $M1$ transition strength sum from the 11.24-MeV transition alone is given by the horizontal solid line with the error limits given by the dashed lines. (From Ref. 130.)

In particular, this operator cannot excite the main component of the ground-state wave function to a $T = 1, 1^+$ state. It is then only by admixture of other states through spin-orbit coupling that an $M1$ transition can be effected by the above operator; one among these states was found to be dominant. Of the $T = 1, 1^+$ states available for transitions from the latter state, only one has nonvanishing strength, hence the observed concentration. In another shell-model calculation Maripuu and Wildenthal [135] show that the 11.24-MeV transition proceeds primarily by orbital recoupling and not by the spin-flip mechanism.

As is evident from the spectrum in Fig. 29, the $M1$ strength in ^{24}Mg is divided primarily between two transitions, at 9.96 and 10.72 MeV. The peaks in the spectrum corresponding to these transitions are comparable in height to the elastic peak, not shown. The two states which these transitions reach are probably $T = 1$ analogs of the 1^+ states at 0.472 and 1.347 MeV, respectively, in ^{24}Na [137, 138]. Using the $^{23}\text{Na}(p, \gamma)^{24}\text{Mg}$ reaction, Meyer et al. [139] observed 1^+ states at 12.182, 12.527, 12.816 and 12.894 MeV, transitions to which have not been detected in the 180° electron scattering studies.

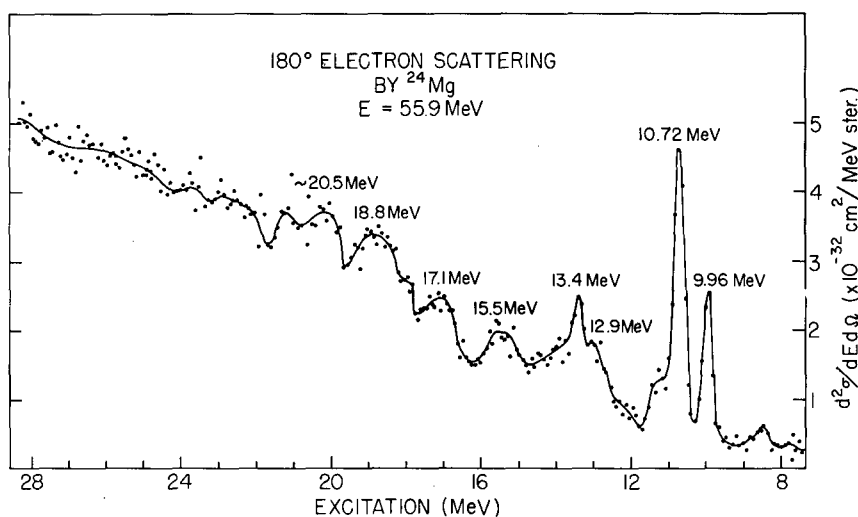


Fig. 29 — Spectrum of 55.9-MeV electrons scattered at 180° from ^{24}Mg . The 10.70-MeV peak is comparable in height to the elastic peak, not shown. (From Ref. 136.)

In Table 4 the values of Γ_0 for the 10.72-MeV transition given by the Darmstadt group [140] and Glasgow group [141] at more forward scattering angles are in good agreement with that of the NRL group [142] using 180° scattering. All three of these results, subjected to DWBA correction or analysis, agree with the earlier photon scattering value, $\Gamma_0 = 17.0 \pm 4.0$ eV [66]. However, the NRL value of Γ_0 for the 9.97-MeV transition is higher than the other two electron scattering values as well as the photon scattering result. The fact that the relatively poor resolution available at NRL made it impossible to resolve a weaker $M1$ transition at 9.85 MeV only partially explains the

Table 4
Ground-State Transition Widths of Electroexcited $M1$ Transitions
and Spin Assignments of States Excited

Nucleus, J_o^π, T_o	Excitation Energy, ω (MeV)	J^π, T	Γ_o (eV)	Γ_o/Γ_w	R_{tr} (fm)	θ_{max} (deg)	Reference	
${}^6\text{Li}, 1^+, 0$	3.56	$0^+, 1$				160	2	
						180	10	
						120	91, 123	
						180	93	
			8.36 ± 0.36	8.8	2.80 ± 0.10	155	94, 95	
	5.36	$2^+, (1)$	0.19 ± 0.04	0.059		153	96	
			0.08 ± 0.04	0.025		155	97	
${}^7\text{Li}, \frac{3}{2}^-, \frac{1}{2}$	0.478	$\frac{1}{2}^-, \frac{1}{2}$	$((2.74 \pm 0.40) \cdot 10^{-7}) [E2]$	17		80	98	
						120	91, 123, 145	
				$(6.30 \pm 0.31) \cdot 10^{-3}$	2.8	2.88 ± 0.07	162	147
			$((2.81 \pm 1.6) \cdot 10^{-7}) [E2]$	17		180	53	
${}^9\text{Be}, \frac{1}{2}^-, \frac{1}{2}$	11.28	$\frac{3}{2}^-, \frac{1}{2}$	1.3 ± 0.4^{ba}	0.043		153	147	
	2.44	$\frac{3}{2}^-, \frac{1}{2}$				160	2	
						180	47	
				$(8.9 \pm 1.0) \cdot 10^{-2}$	0.30	2.7 ± 0.5	165	148
				$(1.89 \pm 0.12) \cdot 10^{-3} [E2]$	23.8		165	148
	3.04	$\frac{1}{2}^-, \frac{1}{2}$	0.18 ± 0.09	0.30	2.9 ± 0.9	165	148	
	14.39	$\frac{3}{2}^-, \frac{3}{2}$				180	47	
				8.1 ± 0.8	0.13	1.9 ± 0.6	165	148
				6.2 ± 0.6	0.10		153	149
	15.97	$(\frac{3}{2}^-)$	2.6 ± 0.7	0.030		165	148	
	16.63	$(\leq \frac{3}{2}^-)$	$((2.0 \pm 0.5) g)$	$(0.021 g)$		153	149	
	16.97	$\frac{1}{2}^-, \frac{3}{2}$	8.6 ± 0.9	0.084	2.1 ± 0.6	165	147	
		11.5 ± 1.4	0.11		153	149		
17.28	$(\leq \frac{5}{2}^-)$	$((7.3 \pm 1.3) g)$	$(0.065 g)$		153	149		
${}^{10}\text{B}, 3^+, 0$	7.48	$2^+, 1$				180	112	
${}^{11}\text{B}, \frac{3}{2}^-, \frac{1}{2}$			12.0 ± 2.2^{ba}	1.4	2.70 ± 0.20^{ba}	165	111	
	2.12	$\frac{1}{2}^-, \frac{1}{2}$				180	47	
						165	111	
				0.16 ± 0.016^{ba}	0.79		180	112
				0.14 ± 0.04	0.70		145	150
	4.44	$\frac{5}{2}^-, \frac{1}{2}$				180	47	
						180	111	
				0.60 ± 0.09	0.32	2.60 ± 0.35^{ba}	165	151
				$(16.4 \pm 2.1) \cdot 10^{-3} [E2]$	7.9	3.44 ± 0.50^{ba}	165	151
				0.73 ± 0.07	0.39		145	150
				$(2.0 \pm 0.2) \cdot 10^{-2} [E2]$	9.7			
	5.02	$\frac{3}{2}^-, \frac{1}{2}$				180	47	
				1.73 ± 0.14	0.65	2.60 ± 0.15^{ba}	165	151
				2.12 ± 0.21	0.80		145	150
8.57	$\frac{3}{2}^-, \frac{1}{2}$		0.72 ± 0.30^{ba}	0.055		165	111	
			$0.4 \pm 0.1 [E2]^{ba}$	7.3	3.90 ± 0.50^{ba}	165	111	
			0.73 ± 0.07	0.06		145	150	
			$0.23 \pm 0.03 [E2]$	4.2		145	150	
8.93	$\frac{5}{2}^-, \frac{1}{2}$					180	112	
			4.0 ± 0.6	0.27	2.65 ± 0.21^{ba}	165	111	
			4.93 ± 0.50	0.33		145	150	
13.0	$(\frac{1}{2}^-), (\frac{3}{2}^-)$	(36 ± 7)	$(2.2 \pm 0.2) [E2]$	(0.78)				
			(18 ± 4)	(5.0)				
	$(\frac{3}{2}^-), (\frac{3}{2}^-)$		$(1.1 \pm 0.1) [E2]$	(0.39)				
				(2.5)				

Table 4 (Continued)

Nucleus, J_o^π, T_o	Excitation Energy, ω (MeV)	J^π, T	Γ_o (eV)	Γ_o/Γ_W	R_{tr} (fm)	θ_{max} (deg)	Reference
$^{12}C, 0^+$	12.7	$1^+, 0$	0.35 ± 0.05	0.008	2.70 ± 0.20^{ba}	165	152
	15.11	$1^+, 1$				180	72
						160	2, 113
			135	122			
			180	47			
			180	98			
	34.4 \pm 3.4		165	115			
			180	49, 153			
			36 \pm 3	0.50		150	117
			39.5 \pm 4 ^{ba}	0.55		180	115
35.74 \pm 0.86			0.49	180	119		
$^{13}C, \frac{1}{2}^-, \frac{1}{2}$	3.69	$\frac{3}{2}^-$,	37.0 \pm 1.1	0.51	162	46	
			0.358 \pm 0.047	0.34	2.76 \pm 0.16	165	154
	8.86	$\frac{1}{2}^-$,	(3.61 \pm 0.40) $\cdot 10^{-3}$ [E2]	3.52	3.50 \pm 0.37	165	154
			3.36 \pm 0.47	0.23	2.50 \pm 0.19	154	154
	9.90	$\frac{3}{2}^-$,	0.324 \pm 0.049	0.016	2.83 \pm 0.25	180	155
			(6.3 \pm 2.1) $\cdot 10^{-3}$ [E2]	0.045	165	154	
	11.07	$(\frac{1}{2}^-)$,	1.02 \pm 0.19	0.036	3.03 \pm 0.22	165	154
			$(\frac{3}{2}^-)$,	0.172 \pm 0.057	0.006	165	154
	11.80	$\frac{3}{2}^-$,	0.256 \pm 0.028 [E2]	1.03	4.01 \pm 0.27	180	155
			3.45 \pm 0.86	0.10	165	154	
15.11	$\frac{3}{2}^-$, $\frac{3}{2}$	25 \pm 7	0.35	150	117		
		22.7 \pm 2.7	0.31	2.55 \pm 0.20	165	154	
$^{14}C, 0^+, 1$	7.01	2^+			180	155	
	8.32	(1, 2) ⁺ ,			180	156	
	9.8				180	156	
$^{14}N, 1^+, 0$	11.3	(1 ⁺),				156	
	2.312	$0^+, 1$			120	123	
			(1.7 \pm 0.5) $\cdot 10^{-2}$	0.066	120	124	
9.17	$2^+, 1$			163	126		
				180	47		
10.43	$2^+, 1$			180	10		
				180	112		
		7.7 \pm 0.9	0.48	2.92 \pm 0.23	165	125	
$^{15}N, \frac{1}{2}^-, \frac{1}{2}$	6.32	$\frac{3}{2}^-$,	12.1 \pm 1.5	0.51	180	112	
			3.4 \pm 0.7	0.64	165	125	
	9.16	$\frac{3}{2}^-$ (-),	(6 \pm 2) $\cdot 10^{-2}$ [E2]	3.1	165	157	
0.75 \pm 0.45			0.046	165	158		
11.88	$\frac{3}{2}^-$,	0.10 \pm 0.05 [E2]	0.85				
		1.1 \pm 0.7	0.030	165	158		
$^{16}O, 0^+, 0$	16.21	1^+ ,	0.48 \pm 0.22	1.1			
	7.7	$\frac{3}{2}^+$,	5.1 \pm 0.8	0.05	3.2 \pm 0.3	165	129
1^+					180	10	
$^{19}F, \frac{1}{2}^+, \frac{1}{2}$	11.24	$1^+, 1$	11.2 \pm 2.1 - 1.8	0.38	2.53 \pm 0.15	180	130
	11.58	(1 ⁺)	0.65 \pm 0.18	0.020	180	130	
(2 ⁺)			0.40 \pm 0.13 [E2]	0.75	180	130	

LAWRENCE W. FAGG

Table 4 (Continued)

Nucleus, J_o^π, T_o	Excitation Energy, ω (MeV)	J^π, T	Γ_o (eV)	Γ_o/Γ_w	R_{tr} (fm)	θ_{max} (deg)	Reference
$^{22}Ne, 0^+, 1$	5.31	$1^+, 1$	0.127 ± 0.22	0.04	$2.51^{+0.18}_{-0.31}$	180	17
	6.82	$1^+, 1$	0.611 ± 0.096	0.092	$2.24^{+0.24}_{-0.42}$		
	9.14	$1^+, 1$	2.83 ± 0.26	0.176	$2.85^{+0.11}_{-0.14}$		
	10.08	$(1^+), 1$	(1.13 ± 0.14)	(0.042)	$3.15^{+0.15}_{-0.19}$		
	10.84	$1^+, 1$	$0.66^{+0.24}_{-0.17}$	0.025	$2.86^{+0.25}_{-0.30}$		
	12.56	$(1^+), 1$	$(1.34^{+0.86}_{-0.65})$	(0.032)	$3.14^{+0.32}_{-0.66}$		
$^{23}Na, \frac{3^+}{2}, \frac{1}{2}$	4.43	$(\frac{1^+}{2}),$	0.64 ± 0.06^{ba}	0.35		180	159
$^{24}Mg, 0^+, 0$	9.85	$1^+, 1$	1.05 ± 0.26	0.052		153	160
	9.97	$1^+, 1$	4.50 ± 0.73	0.22	3.05 ± 0.44	153	160
$^{24}Mg, 0^+, 0$			$7.6^{+1.6}_{-1.4}$	0.36	$2.94^{+0.18}_{-0.20}$	180	142
			4.6 ± 0.4	0.22	2.83 ± 0.30	153	141
	10.70	$1^+, 1$	15.9 ± 0.24	0.62	3.22 ± 0.47	153	160
			$17.6^{+3.5}_{-3.0}$	0.68	$2.94^{+0.13}_{-0.15}$	180	142
			13.4 ± 1.2	0.52	2.91 ± 0.04	153	141
	$^{25}Mg, \frac{5^+}{2}, \frac{1}{2}$	1.60	$\frac{7^+}{2}, \frac{1}{2}$	$(4.1^{+1.1}_{-0.9}) 10^{-2}$	0.48	$2.4^{+0.3}_{-0.4}$	180
5.77		$(\frac{3^+}{2}), \frac{1}{2}$	$0.92^{+0.42}_{-0.35}$	0.23	$2.0^{+0.6}_{-1.5}$		
7.03		$(\frac{5^+}{2}), \frac{1}{2}$	$2.2^{+1.0}_{-0.8}$	0.30	3.7 ± 0.5		
7.81		$\frac{3^+}{2}, \frac{5^+}{2}; \frac{3}{2}$	$(4.7^{+1.2}_{-1.0})/g$	$0.47/g$	$2.6^{+0.2}_{-0.4}$		
10.43			$(17 \pm 5)/g$	$0.72/g$	3.5 ± 0.3		
11.37			$(12^{+6}_{-5})/g$	$0.4/g$	$3.0^{+0.6}_{-0.8}$		
$^{26}Mg, 0^+, 0$	11.76		$(18^{+6}_{-6})/g$	$0.5/g$	$3.2^{+0.4}_{-0.6}$		
	8.22	(1^+)				153	160
	8.52	(1^+)				153	160
		(1^+)	$0.5^{+0.4}_{-0.3}{}^{ba}$	0.04	$3.2^{+0.6}_{-1.4}{}^{ba}$	180	52
		2^+				153	162
	9.24	(1^+)				153	160
			$3.3^{+0.9}_{-0.7}{}^{ba}$	0.19	$3.62^{+0.17}_{-0.19}{}^{ba}$	180	52
	9.29	2^+			$3.96 \pm 0.44 [E2]$	153	162
	9.67	(1^+)				153	160
			$1.7^{+0.8}_{-0.6}{}^{ba}$	0.091	$2.90^{+0.36}_{-0.54}{}^{ba}$	180	52
	10.20	1^+				153	160
			$5.7^{+1.3}_{-1.2}{}^{ba}$	0.26	$3.40^{+0.16}_{-0.18}{}^{ba}$	180	52
			4.8 ± 3.4	0.22	3.32 ± 0.20	153	162
	10.65	1^+				153	160
		$9.1^{+2.0}_{-1.7}{}^{ba}$	0.36	$3.47 \pm 0.14{}^{ba}$	180	52	
		6.4	0.25	3.34	153	162	
11.20	(1^+)	$3.9^{+1.3}_{-1.1}{}^{ba}$	0.13	$3.23^{+0.26}_{-0.33}{}^{ba}$	153	160	
					180	52	
13.33	(1^+)				153	160	
		$14.5^{+3.3}_{-3.0}{}^{ba}$	0.56	$3.10^{+0.17}_{-0.21}{}^{ba}$	180	52	
13.66	(1^+)	$2.3^{+2.4}_{-1.5}{}^{ba}$	0.043	$3.0^{+0.8}_{-3.0}{}^{ba}$	180	52	

Table 4 (Continued)

Nucleus, J_o^π, T_o	Excitation Energy, ω (MeV)	J^π, T	Γ_o (eV)	Γ_o/Γ_W	R_{Tr} (fm)	θ_{max} (deg)	Reference
$^{27}Al, \frac{5}{2}^+, \frac{1}{2}$	2.21	$\frac{7}{2}^+, \frac{1}{2}$				135	163,164
						180	165
	2.98	$\frac{3}{2}^+, \frac{1}{2}$					
	4.42	$\frac{5}{2}^+, \frac{1}{2}$					
	6.50						
	7.57						
	8.05						
	8.74						
	10.68						
	11.69						
	12.30						
$^{28}Si, 0^+, 0$	10.48	$1^+, 1$	$2.4^{+2.1}_{-0.9}$	0.099	3.9 ± 0.4	180	166
	10.86	$1^+, 1$				165	167
			$5.7^{+1.3}_{-1.1}$	0.21	$2.98^{+0.23}_{-0.27}$	180	166
	11.41	$1^+, 1$				180	47
						180	93
			25.7 ± 3.6	0.82	3.0 ± 0.3	165	167
						155	168
			$20.8^{+4.3}_{-3.7}$	0.67	$2.58^{+0.21}_{-0.25}$	180	166
	12.27	$1^+, 1$				165	167
			$7.3^{+2.0}_{-1.8}$	0.19	$2.93^{+0.32}_{-0.39}$	180	166
	12.79	$1^+, 1$	$3.3^{+2.3}_{-1.7}$	0.075	$3.2^{+0.7}_{-1.2}$		
14.01	$(1^+, 1)$	$(8.9^{+7.3}_{-5.0})$	(0.15)	$(3.8^{+0.9}_{-1.1})$			
$^{32}S, 0^+, 0$	8.13	$1^+, 1$	$2.8^{+1.8}_{-1.4}$	0.25	$3.4^{+0.5}_{-0.9}$	180	67
	10.82	$(1^+, 1)$	$(2.9^{+3.6}_{-1.4})$	(0.11)	$(2.0^{+1.2}_{-2.0})$		
	11.14	$1^+, 1$	$18.9^{+7.4}_{-6.3}$	0.66	3.9 ± 0.3		
	11.62	$1^+, 1$	$9.7^{+6.1}_{-4.8}$	0.30	$3.4^{+0.5}_{-0.9}$		
$^{36}Ar, 0^+, 0$	9.27	$(1^+, 1)$	$(1.8^{+0.9}_{-0.7})$	(0.11)	$(2.0^{+0.8}_{-2.0})$	180	169
	10.05	$1^+, 1$	$6.2^{+2.0}_{-1.7}$	0.29	$3.3^{+0.3}_{-0.4}$		
	10.55	$(1^+, 1)$	$(2.2^{+1.8}_{-1.0})$	(0.09)	$(1.9^{+1.1}_{-1.9})$		
	11.25	$1^+, 1$	$8.9^{+3.8}_{-3.1}$	0.29	$3.4^{+0.4}_{-0.5}$		
	12.09	$(1^+, 1)$	$(5.0^{+4.0}_{-2.6})$	(0.13)	$(2.3^{+0.9}_{-2.3})$		
$^{40}Ca, 0^+, 0$	10.34	$(1^+,)$	$(7.0^{+2.9}_{-2.2})$	(0.30)	$(3.5^{+0.4}_{-0.6})$	180	67
$^{55}Mn, \frac{5}{2}^-, \frac{5}{2}$	1.88	$(\frac{7}{2}^-,)$	$(0.96 \pm 0.21) 10^{-3} [E2]$	4.0		149	170
	2.29						
$^{58}Ni, 0^+, 1$	9.81	$1^+, 2$	(1.64)	(0.083)		180	171
	10.15	$1^+, 2$	2.30				
	10.55	$1^+, 2$					
	10.65	$1^+, 2$	6.72	0.27			
	11.15	$1^+, 2$	4.02	0.14			
$^{60}Ni, 0^+, 2$	11.89	$1^+, 3$	8.58	0.24		180	171
	12.31	$1^+, 3$	4.11	0.10			
	13.12	$(1^+, 3)$	(≤ 1.0)	(≤ 0.021)			
	13.36	$(1^+, 3)$	(≤ 1.0)	(≤ 0.020)			
	13.75	$(1^+, 3)$	(≤ 1.0)	(≤ 0.018)			

Table 4 (Continued)

Nucleus, J_o^π, T_o	Excitation Energy, ω (MeV)	J^π, T	Γ_o (eV)	Γ_o/Γ_w	R_{tr} (fm)	θ_{max} (deg)	Reference
$^{90}\text{Zr}, 0^+, 5$	~ 9					180	172, 173
$^{139}\text{La}, \frac{3}{2}^+, \frac{25}{2}$	~ 8					165	174-176
Ce^{nat}	8.7	($1^+, 1$)	(90)	(6)		165	174-176
$^{141}\text{Pr}, \frac{5}{2}^+, \frac{23}{2}$	~ 8					165	174-176
$^{197}\text{Au}, \frac{3}{2}^+, \frac{39}{2}$	7.9		(144)	(13.9)		180	177
$^{206}\text{Pb}, 0^+, 21$	6.1					180	178
	(6.9)						
	(7.3)						
	7.95						
$^{208}\text{Pb}, 0^+, 22$	6.2					180	173, 179, 206
	(7.3)						
	7.9						

Note: Table 4 summarizes the results of measurements on the electroexcitation of $M1$ transitions known to the author up to August 1974. While completeness has been attempted, no claim of it is made. When known, electroexcited $E2$ components have also been included (denoted by [$E2$] after the entry) as well as the maximum scattering angle θ_{max} of the experiment and the isospin quantum number T of the level excited. These three entries are somewhat more susceptible to lack of completeness than the others. When available, transition radii have been included for completeness, despite the doubt as to their physical reality as discussed in the section on DWBA (page 10). Continuum transition strengths such as that observed in ^3He are not included. Also not included are results not substantiated by later work on the same nucleus. The ground-state transition widths are given in both electron-volts and Weisskopf units (i.e., Γ_o/Γ_w). Doubtful values or ambiguous assignments are presented in parentheses. The ground-state spin, parity, and isospin are given along with each nucleus. In most cases when work by an author or group is followed shortly thereafter with more accurate and more complete results, only the later work is cited. When the results given issue from a PWBA analysis with no Coulomb distortion correction, a superscript ba is added to the value of Γ_o . In instances where the excited state is uncertain, the l_i are given times the statistical weighting factor $\mu = (2J_o + 1)/(2J + 1)$ (or $1/g$).

discrepancy [141]. In any event the value of $\langle \sum l \cdot s \rangle = 6.79$ given by Fagg et al. [142] should now be probably somewhat lower and thus in better agreement with the value of 6.04 calculated from the Nilsson model and with the value of 6.07 calculated in the projected Hartree-Fock formalism [68].

The structure around 13-MeV excitation in Fig. 29 is largely due to $M2$ transitions [141, 142]. However, the peaks beyond 15-MeV excitation are probably caused by $E1$ transitions, since they are at the same energies as those found at more forward angles [143]. This qualitative result supports what was discussed in page 6 concerning the enhanced ability to excite electric transitions at higher excitation energies using 180° electron scattering. In fact, it has been pointed out [144] that transverse form factors are considerably more sensitive than longitudinal ones to the configuration composition of the level wave functions in the giant resonance region. Thus there is a need for 180° electron scattering studies to exploit this situation.

Remarkably similar to the ^{24}Mg spectrum in Fig. 29 is that of ^{28}Si taken at NRL [166] and presented in Fig. 30. Again the peaks beyond 15 MeV are at the same energies as those found at more forward angles [180], while the structure at 14.7 and

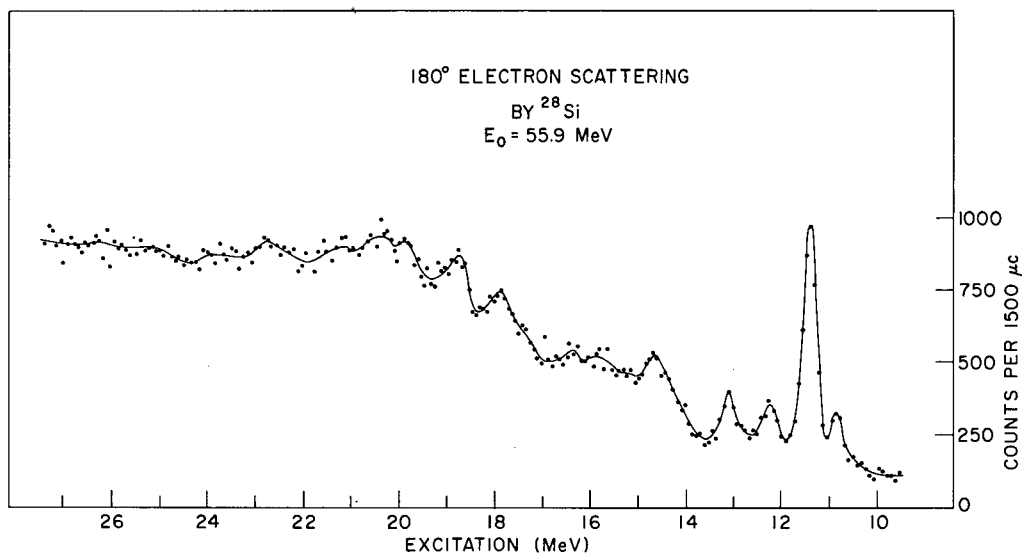


Fig. 30 — Spectrum of 55.9-MeV electrons scattered at 180° from ^{28}Si . The 11.41-MeV peak is comparable in height to the elastic peak, not shown. (From Ref. 166.)

13.1 MeV is due mostly to $M2$ transitions. The three peaks at lowest excitation energy, due to $M1$ transitions, are dominated by the 11.41-MeV peak, which again is comparable in height to the elastic peak.

In the early Stanford electron scattering investigations performed on this nucleus [2, 47, 93] an $M1$ transition was observed at 11.6 MeV. Later, with more forward-angle scattering this transition was observed at 11.42 MeV by Liesem [167], who reported for it a value of $\Gamma_0 = 32.4 \pm 4.5$ eV using a PWBA analysis. When corrected for Coulomb distortion, this value becomes 25.7 ± 3.6 , in agreement with the NRL [166] value of 20.8 ± 4.0 . Both values then also agree with the photon scattering [66] value of 22.9 ± 4.0 . The 11.42-MeV transition was also studied at higher momentum transfers by Drake et al. [168].

Inspection of Table 4 shows that the NRL group [166] also report $M1$ transitions corresponding to the two “satellite” peaks at 10.86 and 12.27 MeV on either side of the 11.41-MeV peak in Fig. 30. In addition, even weaker transitions are reported at 10.48 and 12.79 MeV. Using the $^{28}\text{Si}(t, ^3\text{He})^{28}\text{Al}$ reaction, Flynn et al. [181] have studied in ^{28}Al the charge-exchange mode of the above $M1$ resonances in ^{28}Si . They show that in ^{28}Al the intensities of the four resonances of lowest excitation energy follow approximately the same pattern as in the four of lowest energy in ^{28}Si .

The most likely identification of the lowest four states at 10.48, 10.86, 11.41, and 12.27 MeV with their analogs in ^{28}Al are to the states at 0.973, 1.372, 2.207, and 3.106 MeV, respectively [138, 182]. A value of $\langle \sum \ell \cdot s \rangle = 8.8$, obtained from the NRL results, is more consistent with the Nilsson model oblate value of 7.6 than with the

prolate (using $\eta = 4$) value of 4.3 (^{28}Si has been established as oblate [183, 184]). However, this experimental value is higher than the value calculated with the projected Hartree-Fock formalism, namely $\langle \Sigma \ell \cdot s \rangle = 6.05$ [68].

In ^{32}S the Stanford survey work at 180° reported possible $M1$ transitions at 5.7, 8.5, and 11.4 MeV [10] and, in a later work, at 4.7 and 5.55 MeV [112]. More recent work [67] showed $M1$ transitions at 8.13, 10.82, 11.14, and 11.62 MeV. Because of the low melting point of sulfur, a CaS target was used by Fagg et al. and a Ca spectrum subtracted to find that for S. Consequently, the resulting poor statistics made it impossible to observe the transitions to 1^+ levels at 7.00, 9.21, and 9.24 MeV [185, 186]. Thus nothing meaningful can yet be said from these data about the $M1$ sum strength in this nucleus.

The levels at 7.00 and 8.13 MeV and 1^+ analogs of the ground and 1.149 excited states, respectively, in ^{32}S [186]. A careful measurement of Γ_0 for the 7.00-MeV transition would be of considerable interest since the ^{32}P ground state, as in the case of the ^{14}C ground state mentioned earlier, exhibits an unexpectedly weak β -decay transition probability.

One clear quantitative result of the NRL work was that considerable fragmentation of the $M1$ strength is observed in ^{32}S . Kurath [71] offers a possible explanation for this increase in fragmentation. Using an adiabatic model of a triaxially deformed rotor, he showed that more fragmentation would occur in ^{32}S than for an axially symmetric model. Also, he felt that the inclusion of Coriolis coupling might induce further fragmentation.

Such fragmentation persists in the ^{36}Ar spectrum [169] presented in Fig. 31. Not all of the peaks in this spectrum correspond to $M1$ transitions. In fact only the transitions at 10.05 and 11.25 MeV are unambiguous from the analysis, with the transitions at 9.27, 10.55, and 12.09 being possibly $M1$. The transition widths for the latter three levels are given in Table 4, analyzed both as $M1$ and $M2$ transitions. Again, because of the marked fragmentation no discussion will be given here of the $M1$ sum strength.

The NRL results of $M1$ transition strength measurements for all of the self-conjugate sd shell nuclei are summarized in Fig. 32. Each column corresponds to an observed $M1$ transition. The height of each column is proportional to the percentage of maximum possible total $M1$ strength expected using Kurath's sum rule, corresponding to a spherical nucleus in the independent particle shell model. The increase in fragmentation in passing from ^{28}Si to ^{32}S is not as apparent here as it is on visual inspection of the spectra, but nevertheless seems to be present.

Finally, it might be commented that, just as with ^{16}O , $M1$ strength in ^{40}Ca is not expected to exist, according to the Kurath rule. However, analogous to the case of the 16.21-MeV transition in ^{16}O mentioned earlier, the NRL study of ^{40}Ca [67] shows an $M1$ transition at 10.34 MeV. Its existence is given some support by the report of a 1^+ level in ^{40}K [187-189] at 2.290 MeV, which may be the analog of the former level.

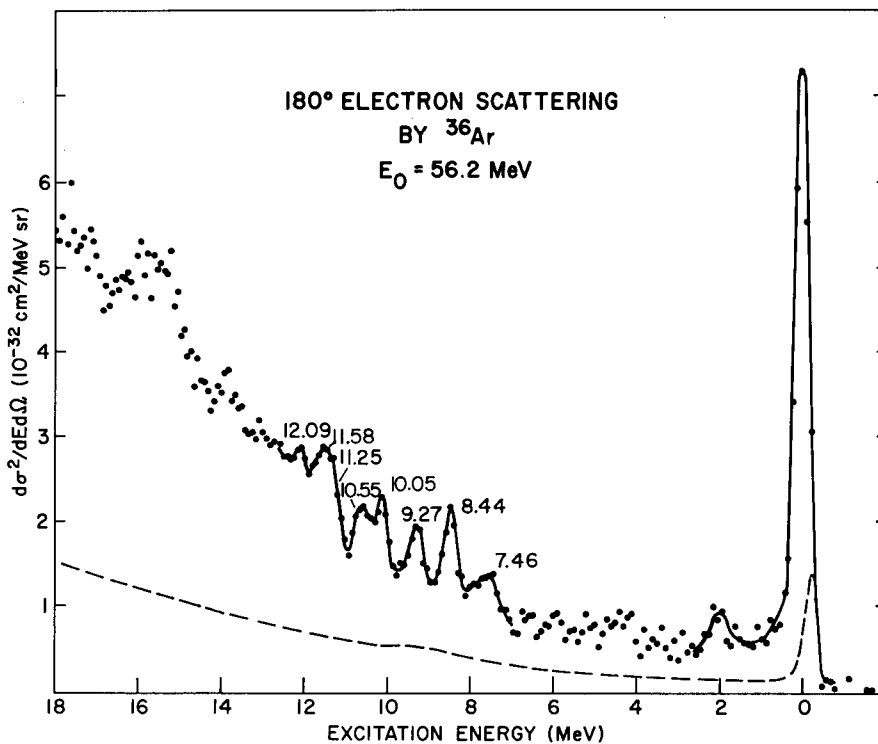


Fig. 31 — Spectrum of 56.2-MeV electrons scattered at 180° from ^{36}Ar . If the ordinate is regarded as arbitrary counting rate, the dashed curve gives a comparison of the counting rate resulting from the two Havar foils (target chamber evacuated [60]) with that resulting from the chamber-filled condition; it is not a cross-section curve. (From Ref. 169.)

Other Than Self-Conjugate Nuclei

Preliminary Remarks — A few general and qualitative features may be mentioned which are of interest in the study of these nuclei. First, it is important to understand how the $M1$ strength becomes fragmented with the addition of one to three nucleons to a self-conjugate nucleus. Corollary to this is an understanding of the behavior of $M1$ transitions in nuclei with a few valence nucleons or holes near closed shells or subshells. It is also of interest to see how 180° electron scattering can highlight some of the collective rotational features in odd- A nuclei and contribute to their understanding.

However, perhaps of most recent importance is the study of giant magnetic dipole resonances in heavy nuclei near or at closed shells. If one accepts for a qualitative definition of a giant resonance, one in which a majority of the transition strength resides in a relatively small excitation energy region, then some of these resonances appear to qualify. Because of the high-level densities in heavy nuclei, such resonances often represent the composite strength of several relatively closely grouped transitions, whereas the resonances seen in the p and sd shells usually correspond to discrete levels. Again, the nuclei examined in this section will be discussed in order of increasing A .

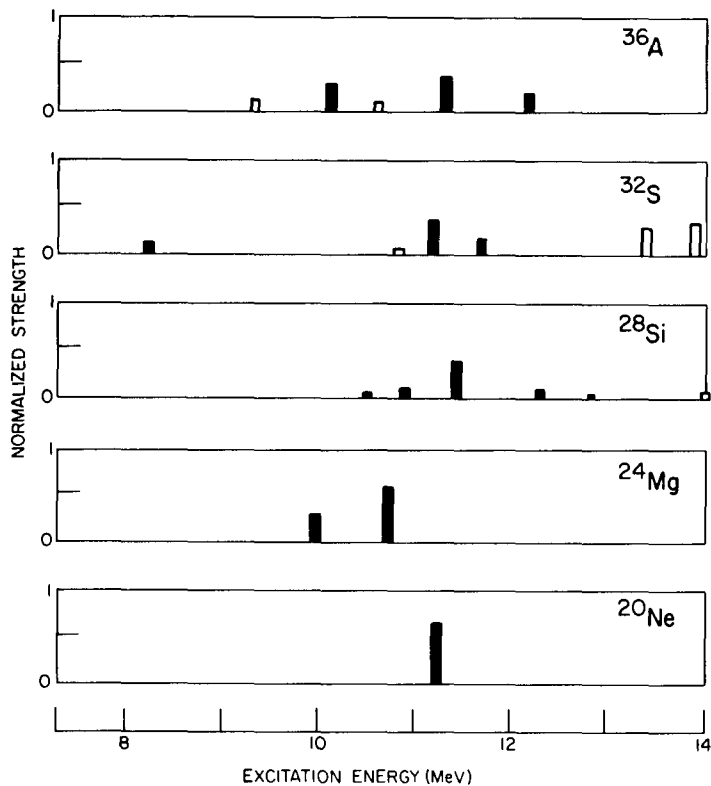


Fig. 32 — Strength of $M1$ transition vs excitation energy for self-conjugate nuclei of the sd shell. The strengths are normalized to the total $M1$ strength expected using Kurath's sum rule for a spherical nucleus in the independent particle shell model. (From Ref. 1.)

s-Shell Nuclei — The examination of ${}^3\text{He}$ using 180° electron scattering, the product of a joint American University-NRL effort [190], was the first study of the $M1$ continuum in this nucleus. The experiment was primarily a difference measurement between ${}^3\text{He}$ and ${}^4\text{He}$, the normalized spectra for which are shown in Fig. 33. In the elastic region can be seen the striking contrast between the magnetic scattering from ${}^3\text{He}$ and the pure charge scattering from ${}^4\text{He}$ at 180° . Such a phenomenon is only observable in the very light nuclei since the Z^2 charge-scattering dependence soon begins to produce elastic peaks in heavier nuclei due to the effects of finite solid angle and of multiple scattering and straggling in the target. The greater intensity of the ${}^3\text{He}$ continuum in the 0- to 5-MeV excitation region is due to magnetic bremsstrahlung. At 5.5-MeV and 7.7-MeV excitation are the two- and three-body breakup thresholds, respectively.

For some while the surprising continuum strength in ${}^3\text{He}$ was not adequately explained since selection rules prohibit an $M1$ transition from the 92% S -state component of the ground state to the continuum. The possibility that the strength could arise from the $< 2\%$ S' mixed symmetry component of the ground state and/or from meson exchange currents was suggested [190]. However, although the role that meson exchange

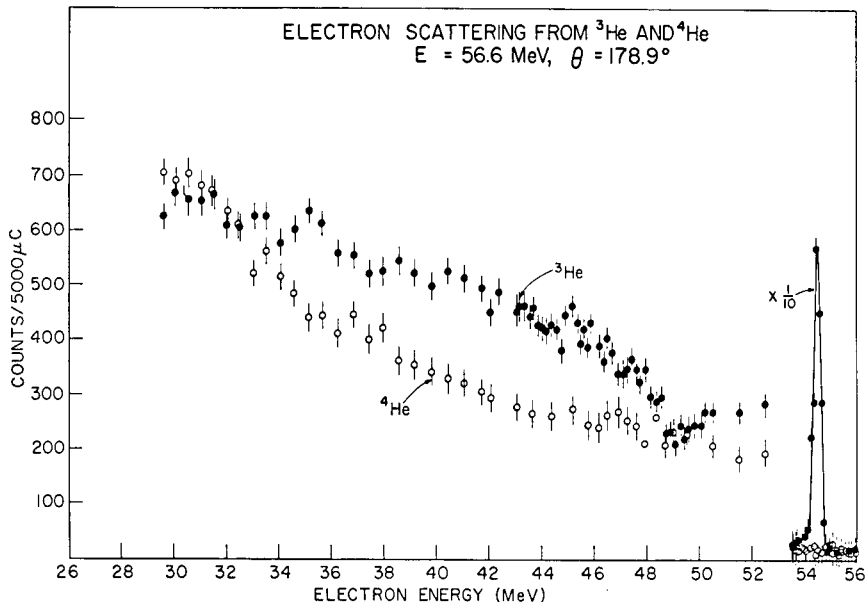


Fig. 33 — Normalized spectra of 56.6-MeV electrons scattered at 180° from ^3He and ^4He (here the average scattering angle of 178.9° is given). The filled circles correspond to ^3He and the unfilled circles to ^4He . (From Ref. 190.)

currents play here is still unclear, O'Connell and Gibson [191] have since shown that the above selection rule is only valid for $q = 0$ and rapidly breaks down as q is increased.

A further study of ^3He is presently under way at the National Bureau of Standards (NBS) with more forward-angle scattering as well as at 180° at NRL. Also, an investigation of ^3H is imminent at both of these laboratories.

p-Shell Nuclei — The 180° scattering system at Amsterdam was used to study the $M1$ transition [53, 192, 193] to the $\frac{1}{2}^-$ state at 0.478 MeV in ^7Li (ground-state spin, $\frac{3}{2}^-$). The spectrum presented in Fig. 34 separating the elastic and 0.478-MeV peaks exhibits the fine resolution of the Amsterdam system. A value of $\Gamma_0 = (6.30 \pm 0.31) \cdot 10^{-3}$ eV was measured. This number is based on the experimental value of the magnetic dipole moment of the ground state and agrees with the average value from the literature [194]. An $E2$ component of this transition was also electroexcited with values reported of $\Gamma_0 = (2.8 \pm 1.6) \cdot 10^{-7}$ eV [53] and $\Gamma_0 = (2.74 \pm 0.40) \cdot 10^{-7}$ eV [145]. A weaker $M1$ transition to a $\frac{3}{2}^-$ level at 11.28 MeV has been investigated by the Darmstadt group [147] using more forward-angle scattering. They reported a preliminary value of $\Gamma_0 = 1.3 \pm 0.4$ eV.

The relative lack of fragmentation in ^7Li is not present in ^9Be (ground-state spin $\frac{3}{2}^-$) in which several electroexcited $M1$ transitions have been reported. The $M1$ transition to the $\frac{5}{2}^-$ state at 2.44 MeV was first investigated by the Stanford group [2, 47]. Later the Darmstadt group [148, 195] reported the strength of the $E2$ component of this transition

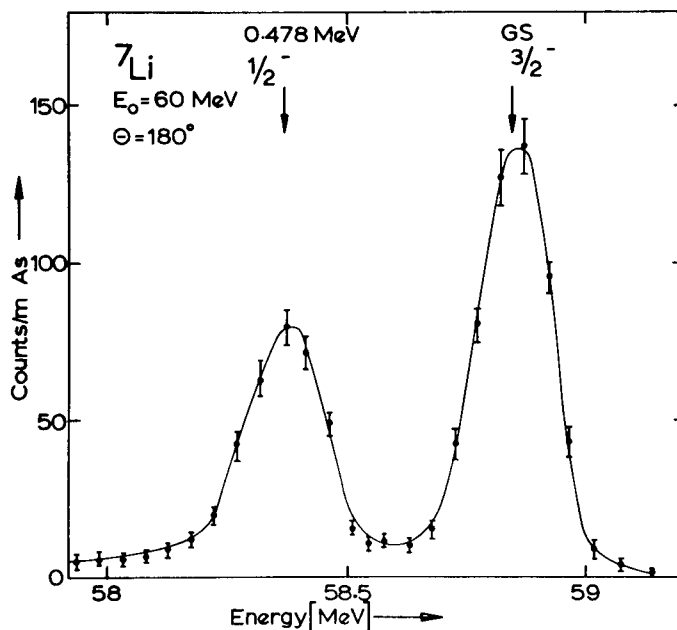


Fig. 34 — Spectrum of 60-MeV electrons scattered from ${}^7\text{Li}$ using the IKO Amsterdam 180° scattering system. The separation of the elastic peak and the 0.478-MeV inelastic peak is apparent. (From Ref. 193, © 1971 North-Holland Publishing Co., Amsterdam, The Netherlands. Used by permission.)

as well as the strength of $M1$ transitions to $\frac{1}{2}^-$, $(\frac{3}{2}^-)$, $(\frac{3}{2}^-)$, and $\frac{1}{2}^-$ states at 3.04, 14.39, 15.97, and 16.96 MeV, respectively (parentheses indicate tentative assignments). The states at 14.39 and 16.96 MeV were reported with isospin $T = \frac{3}{2}$, in general agreement with intermediate coupling calculations [99]. Part of the Darmstadt work [148] had as one of its goals determining the existence of a theoretically predicted [99, 196] strong $M1$ transition below 5-MeV excitation. Clerc et al. suggest the 3.04-MeV transition as a candidate for this transition. Since it was suggested [197] that the state at 2.44 MeV was an appropriate example for investigating the $1f$ admixture to $1p$ -shell states, another goal of this work [148] was an accurate determination of this admixture. They conclude that the $1f$ admixture is small enough to regard the state as being described essentially by a p -shell configuration. Also reported is the strength of the $E2$ component of this transition, $\Gamma_0 = (1.89 \pm 0.13) \cdot 10^{-3}$ eV.

More recent work at Saskatchewan [149] was designed to study a feature that ${}^9\text{Be}$ has in common with a few other nuclei, namely, the existence of several narrow states near 16-MeV excitation. Since isospin-conserving particle decay channels are energetically unfavored, the $T = \frac{3}{2}$ levels are expected to have very narrow widths. The Saskatchewan work roughly confirms that of Darmstadt on the 14.39- and 16.96-MeV levels and reports in addition possible $M1$ transitions to $\leq \frac{5}{2}^-$ levels at 16.63 and 17.28 MeV. The possibility of some $M2$ strength also exists at approximately these energies, again supporting earlier Darmstadt studies [195].

The Glasgow group also studied ${}^9\text{Be}$, finding transverse strength in the 2.2- to 3.6-MeV and 4.5- to 6.5-MeV excitation regions [198]. A summary of the results accumulated for ${}^9\text{Be}$ is presented in Table 4.

Considerable fragmentation of $M1$ transition strength also prevails in ${}^{11}\text{B}$ (ground-state spin $\frac{3}{2}^-$). The $M1$ transition to the $\frac{1}{2}^-$ state at 2.12 MeV was examined at Stanford [47, 112]. The transitions to the $\frac{5}{2}^-$, $\frac{3}{2}^-$, $\frac{3}{2}^-$, and $\frac{5}{2}^-$ states at 4.44, 5.02, 8.57, and 8.93 MeV, respectively, were investigated at Darmstadt [111, 151]. A more recent University of Massachusetts-NBS collaboration [150] reports confirmation of the $M1$ transition widths for the 2.12-, 4.44-, 5.02-, 8.57-, and 8.93-MeV transitions given by the earlier workers [111, 112, 151]. However, their value for the $E2$ component of the 8.57-MeV transition is considerably lower than that given by Spamer [111]. The Massachusetts-NBS group also observed a mixed $M1$ - $E2$ transition to a ($\frac{1}{2}^-$ or $\frac{3}{2}^-$) state at 13.0 MeV. Again the transition widths, along with those of the $E2$ components for the ${}^{11}\text{B}$ $M1$ transitions, are given in Table 4.

The strong $M1$ transition to the $\frac{3}{2}^-$ state at 15.11 MeV in ${}^{13}\text{C}$ (ground-state spin, $\frac{1}{2}^-$) was measured by Peterson [117] who reported a value of $\Gamma_0 = 25 \pm 7$ eV. This measurement was later supported at Darmstadt [154] where a value of $\Gamma_0 = 22.7 \pm 2.6$ eV was reported. In this experiment $M1$ transitions to the $\frac{3}{2}^-$, $\frac{1}{2}^-$, $\frac{3}{2}^-$, ($\frac{1}{2}^-$ or $\frac{3}{2}^-$), and $\frac{3}{2}^-$ states at 3.69, 8.86, 9.90, 11.07, and 11.80 MeV, respectively, were also investigated. Recent work using the 180° electron scattering facility at Amsterdam [155] has produced the spectrum presented in Fig. 35. The peaks corresponding to the $M1$ transitions to the 3.69- and 15.11-MeV states are especially prominent. The peak at 7.54 corresponds primarily to an $E2$ transition.

With the addition of a neutron (to ${}^{13}\text{C}$), not much more fragmentation of $M1$ strength seems to appear in ${}^{14}\text{C}$ than was already present in ${}^{13}\text{C}$. This is apparent from the 180° electron scattering spectrum shown in Fig. 36, which was the result of a Catholic University-NRL collaborative effort [156]. The peak at 11.3 MeV dominates the spectrum and is probably produced by an $M1$ transition. A target consisting of ${}^{14}\text{C}$ powder sandwiched between Be foils was used. Small capillaries containing filters to prevent passage of the ${}^{14}\text{C}$ particles made vacuum equalization possible.

Increased fragmentation of $M1$ strength still does not seem to occur in ${}^{15}\text{N}$ (ground-state spin, $\frac{1}{2}^-$), where the dominant transition is to the $\frac{3}{2}^-$ state at 6.32 MeV [157]. The properties of this state and its mirror state in ${}^{15}\text{O}$ provide a sensitive test of the purity of single-hole wave functions [157, Ref. 1]. Weaker transitions to the $\frac{3}{2}^-$ states at 9.16 and 11.88 MeV have also been studied [158]. All three of the above transitions have $E2$ components (see Table 4).

Clerc [158] gave a brief but quite useful review of the electron scattering data then available on the $1p$ -shell. He shows that there is a good agreement between the experimental $M1$ ground-state transition widths and those calculated in the shell model by Cohen and Kurath [196]. He also summarizes the $M1$ transition strengths in the $1p$ -shell as shown in Fig. 37, which gives a helpful overall picture of the strength distribution.

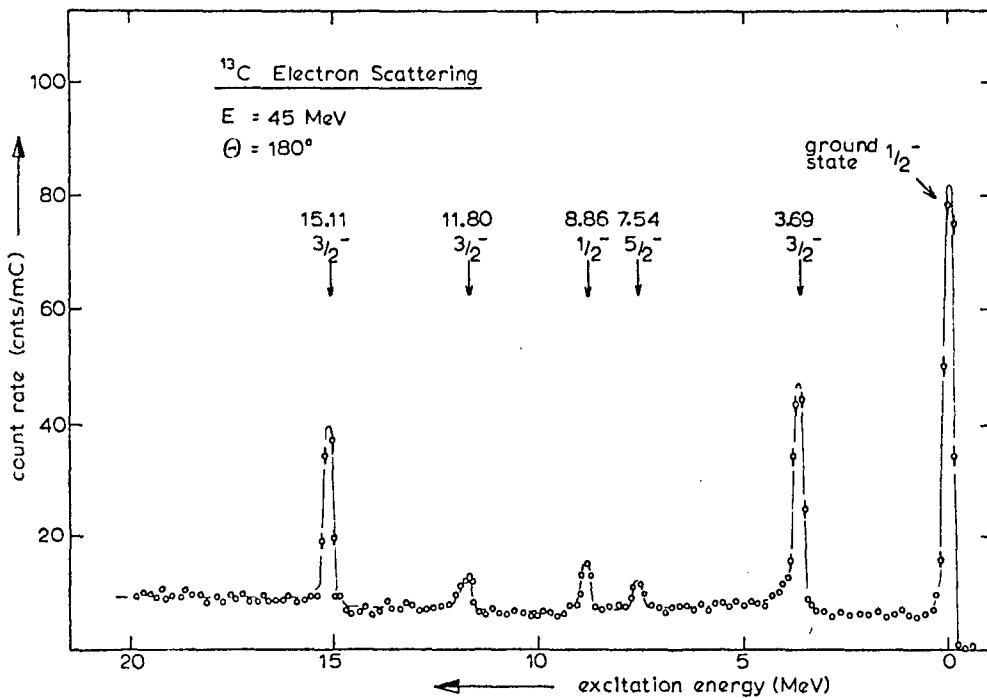


Fig. 35 — Spectrum of 45-MeV electrons scattered from ¹³C using 180° scattering system at IKO Amsterdam. (From Ref. 155.)

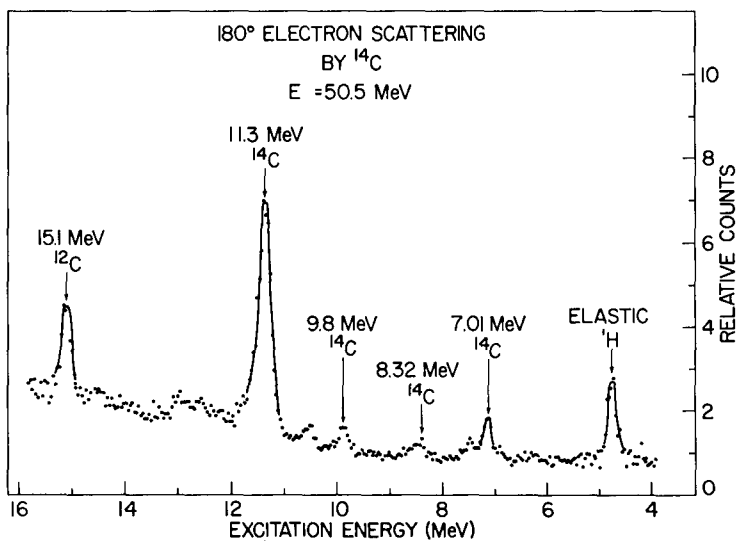


Fig. 36 — Spectrum of 50.5-MeV electrons scattered at 180° from ¹⁴C. Hydrogen and ¹²C contamination peaks are at 4.8 and 15.1 MeV, respectively. (From Ref. 156.)

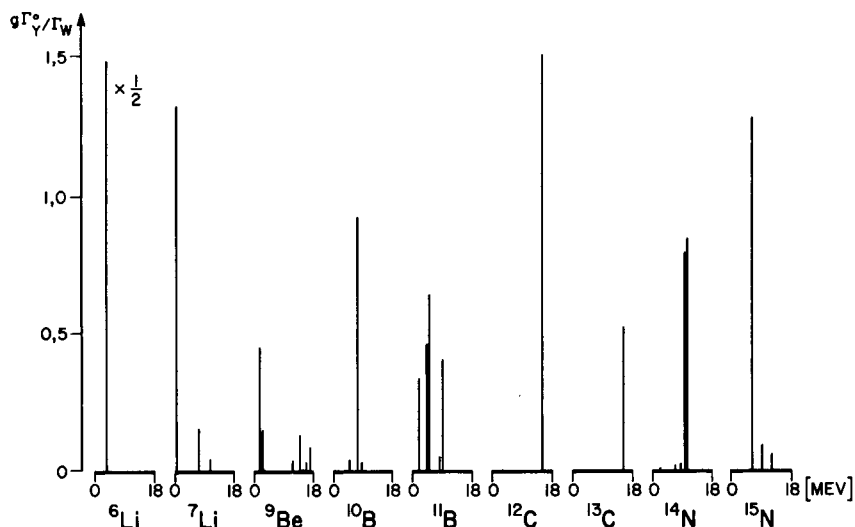


Fig. 37 — Strengths of $M1$ transitions in $1p$ -shell nuclei (in Weisskopf units) vs excitation energy. Most, but not all, transitions shown are from electro-excitation results: $g = (2J + 1)/(2J_0 + 1)$. (From Ref. 158.)

sd Shell Nuclei — Barber et al. [10] reported a probably $M1$ transition to the $\frac{3}{2}^+$ state at 7.7 MeV in ^{19}F . However, more recent work confirming this observation as well as extending the investigation of this nucleus has not been reported thus far.

The addition of two neutrons to ^{20}Ne , the spectrum of which was shown in Fig. 27, produces considerable fragmentation of the $M1$ strength. This can be seen in the ^{22}Ne spectrum taken at 180° [17] and presented in Fig. 38. In a PWBA analysis corrected for Coulomb distortion effects, unambiguous assignments of 1^+ were made for the states at 5.31, 6.82, 9.14, and 10.84 MeV. Ambiguous (1^+ or 1^-) assignments were given to states at 10.08 and 12.56 MeV. The experimental results were compared with the shell model calculations of Freedom and Wildenthal [199] who assume an ^{16}O core and a configuration space involving six nucleons in the sd shell. The energy positions of the theoretically predicted 1^+ levels in the excitation region under study ($\omega < 13$ MeV) are in good agreement with experiment. There is also general agreement as to relative transition strengths; however, the absolute theoretical strengths are on the average too high. The experimental $M1$ strength observed exhausts somewhat more than half of the Kurath sum rule calculated using the wave functions of the above shell model.

The only electroexcited $M1$ transition thus far reported in ^{23}Na (ground-state spin $\frac{3}{2}^+$) is that to the state at 4.43 MeV [159]. In a PWBA analysis a value of $\Gamma_0 = 0.64 \pm 0.06$ eV was determined for this transition.

An interesting example of how 180° electron scattering can highlight the rotational features in an odd- A nucleus is illustrated in the ^{25}Mg (ground-state spin, $\frac{5}{2}^+$) spectrum shown in Fig. 39 [161]. Although many levels exist in the 0- to 5.8-MeV

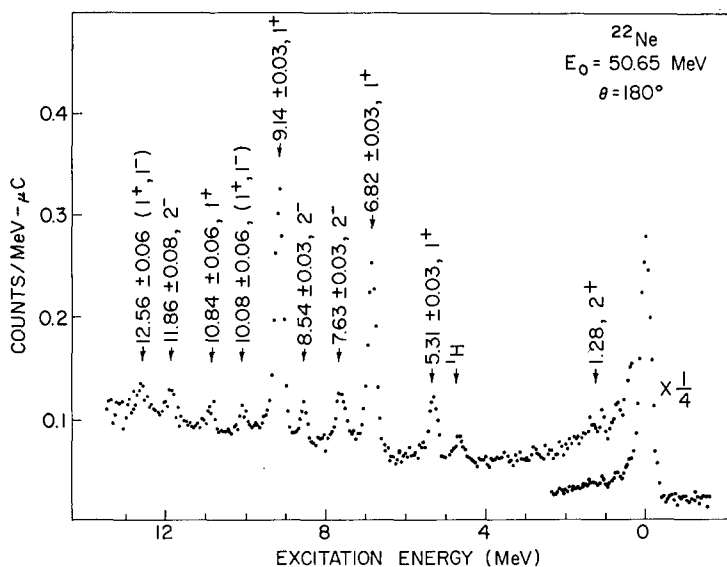


Fig. 38 — Spectrum of 50.65-MeV electrons scattered at 180° from ^{22}Ne . The spin assignments determined from the analysis described in the text are given for each of the levels corresponding to the peaks appearing in the spectrum, except that at 1.28 MeV. (From Ref. 17.)

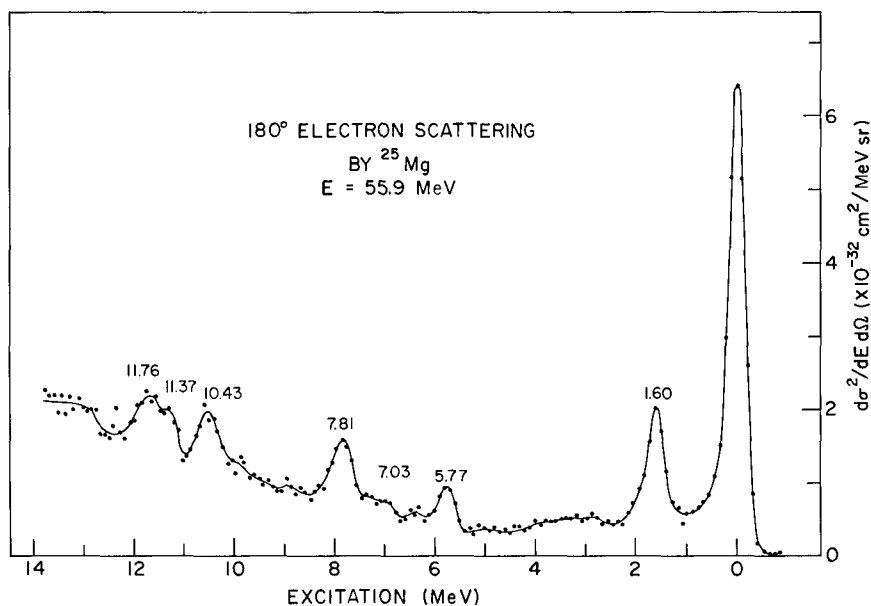


Fig. 39 — Spectrum of 55.9-MeV electrons scattered at 180° from ^{25}Mg . (From Ref. 161.)

excitation range that would ordinarily be reached by an $M1$ transition, only that at 1.60 MeV is excited. This result constitutes a convincing example of the $\Delta K = 0, \pm 1$ selection rule, for the 1.60-MeV level is the $\frac{7}{2}^+$ first excited state of the $K = \frac{5}{2}^+$ ground-state rotational band, while all other candidates in the 0- to 5.8-MeV region belong to $K = \frac{1}{2}^+$ bands. The peak at 7.81 MeV corresponds to the unresolved $T = \frac{3}{2}$ analogs of the ground $\frac{5}{2}^+$, and first excited $\frac{3}{2}^+$, states in ^{25}Na , which are 90 keV apart.

In an early 180° scattering survey of ^{27}Al by the Stanford group [10], peaks were observed at 4.8, 8.0, 10.6, and 12.8 MeV. In a later observation at Saclay [163, 164] a mixed $M1$, $E2$ transition at 2.21 MeV was reported. It might also be mentioned that spectra of 180° scattering from ^{27}Al have been observed more recently [165]. Analysis is not complete but peaks appear at 2.23-, 2.98-, 4.42-, 6.50-, 7.57-, 8.05-, 8.74-, 10.68-, 11.69-, and 12.30-MeV excitation levels.

The addition of two neutrons to the ^{24}Mg core leads to noticeably more fragmentation of $M1$ strength in ^{26}Mg than is observed in ^{22}Ne . The Darmstadt group [160] first observed some nine magnetic transitions in the excitation region between 8 and 14 MeV. These observations were generally confirmed using 180° scattering [52]. However, the latter study reports an $M1$ transition at 13.66 MeV in addition, while the Darmstadt results show a magnetic transition at 8.22 MeV not observed at NRL. Bendel et al. analyzed the data in a PWBA analysis and gave values of Γ_0 for nine transitions which are included in Table 4. Recently the Glasgow group [162] investigated the excitation region up to 11 MeV and reported more accurate values of Γ_0 for the 10.20- and 10.65-MeV transitions, which are in agreement with the NRL numbers, but found that the 8.52-MeV transition is transverse $E2$, not $M1$. It might be observed that while considerable fragmentation of $M1$ strength exists, nevertheless qualitatively there is some concentration, since all this strength resides within an energy range of about 5 MeV.

The early results of 180° electron scattering surveys on ^{31}P by Barber et al. [10] and Kossanyi-Demay and Vanpraet [200] are not in agreement as to the energies of the peaks observed. Consequently they are neither discussed here nor included in Table 4.

In a collaborative effort between the University of Massachusetts and NRL [201] the transition to the $\frac{1}{2}^+$ level at 2.53 MeV in ^{39}K (ground-state $\frac{3}{2}^+$) has been examined. This is an allowed $E2$, but an ℓ -forbidden $M1$, transition. Previous measurements [202] indicated that there might be considerable $M1$ excitation of this level due to violation of the forbiddenness arising from configuration mixing or, to a lesser extent, from modification of the $M1$ operator (by meson exchange currents, for example). Preliminary results, however, indicate that the $M1$ strength is indeed small. Finally, it might be mentioned that (γ, γ') experiments [203] have revealed several $M1$ transitions in ^{19}F , ^{23}Na , ^{27}Al , and ^{31}P .

A > 40 Nuclei — This region of the periodic table has been relatively unexplored by backward electron scattering techniques, and only in the last few years has a strong interest arisen as a result of observations of giant $M1$ resonances in some of the heavy nuclei.

In the fp shell, work done at Yale on ^{55}Mn (ground-state spin, $\frac{5}{2}^-$) [170] reveals evidence for some $M1$ strength in the 1.88- and 2.29-MeV transitions. As the first step in a systematic program to study the relative contributions of $M1$ strength to the $T_>$ and $T_<$ states among the isotopes of nickel, an NRL-NBS collaborative group [171] studied ^{58}Ni and ^{60}Ni using 180° , as well as more forward-angle, scattering. The spectrum presented in Fig. 40 shows structure in regions centered at 6.5, 8.5, and 10 MeV in ^{58}Ni . The two lower energy regions are, at least in part, tentatively associated with $M2$ transitions to $T = 1$ states, while peaks at 10.15, 10.55, 10.65 and 11.15 MeV result from $M1$ transitions to $T = 2$ states. Charge exchange resonances have been observed to these four states in ^{58}Co [204] using the (t , ^3He) reaction.

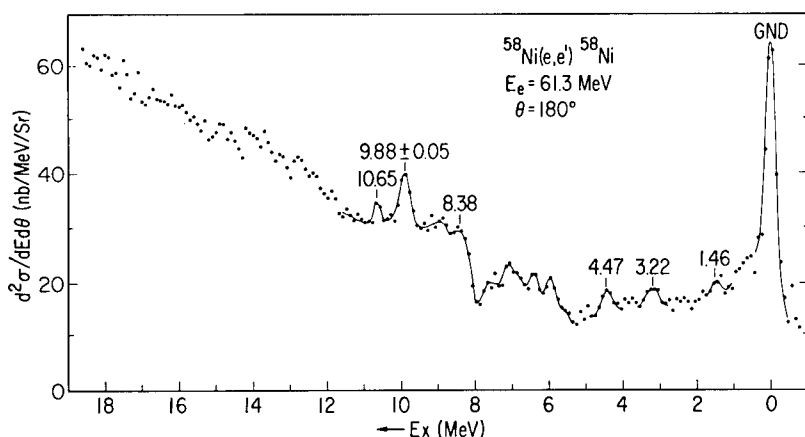


Fig. 40 — Spectrum of 61.3-MeV electrons scattered at 180° from ^{58}Ni . (From Ref. 171.)

A joint (State University of New York) SUNY-NRL investigation using 180° scattering [172, 173] was made to observe $M1$ strength produced by spin-flip transitions from the filled $g_{7/2}$ neutron shell in ^{90}Zr . A structure from 7.5 to 10.5 MeV, peaking at about 9 MeV, was observed in the spectrum (which extended to 14 MeV) at the highest incident energy ($E = 60$ MeV). However, no structure at all was in evidence at the lowest energy ($E = 37$ MeV). Thus, the extent to which these results represent $M1$ strength vs other multipolarities cannot be determined from these data alone.

In an experiment using natural targets of La, Ce, and Pr the Darmstadt group [174-176] observed an enhancement of the intensity of a broad peak at 9 MeV in their spectra at backward angles. This is evidence for a general $M1$ resonance among these nuclei at about that excitation energy. In Fig. 41 the broad peak (about 3 MeV FWHM) at 7.9 MeV was observed by Lone et al. [177] in a 180° scattering study of ^{197}Au . The analysis indicates that the structure is most consistent with the assumption of a group of $M1$ transitions in this excitation region. Spin-flip transitions primarily from the $h_{7/2}$ proton and $i_{13/2}$ neutron shells may be responsible for much of this strength. A tentative value of $\Gamma_0^2 = 144$ eV is given for the composite of this transition strength.

NRL REPORT 7878

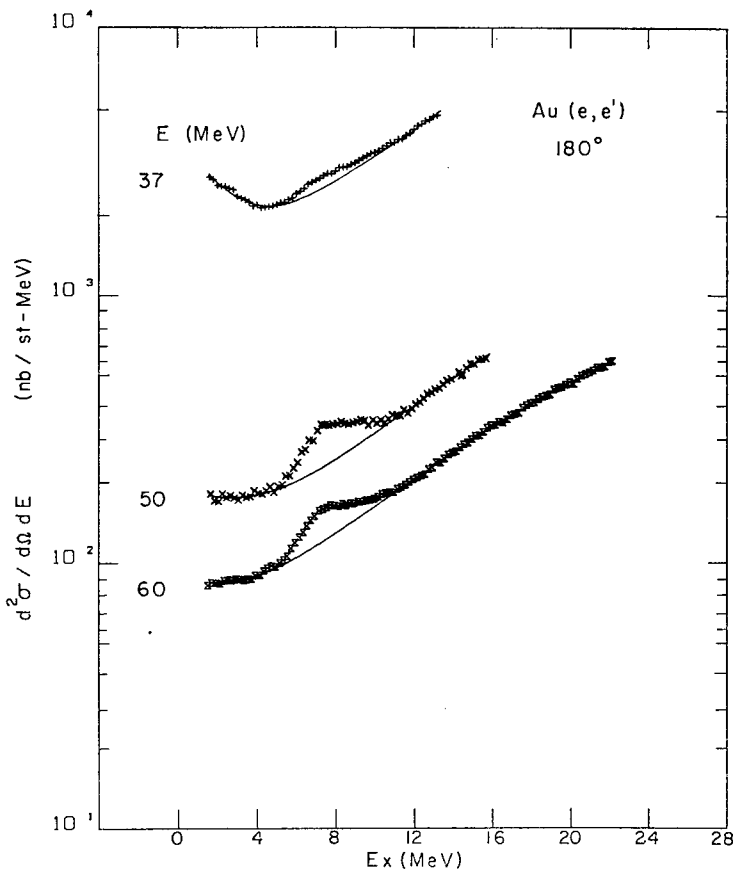


Fig. 41 — Spectra of 37-, 50-, and 60-MeV electrons scattered at 180° from ^{197}Au . (From Ref. 177.)

The possibility of spin-flip transitions from the proton $h\frac{11}{2}$ and neutron $i\frac{13}{2}$ shells is even greater for the lead isotopes. Both more forward-angle [205] and 180° [173, 179, 206] scattering observations have been made on possible $M1$ transitions in ^{208}Pb . In each observation, peaks are evident at 6.2, 7.3, and 7.9 MeV, e.g., as seen in Fig. 42. The structure at 7.3 MeV appears to be an unresolved group of transitions that increase in intensity much more rapidly with increasing q than the peaks at 6.2 and 7.9 MeV. Although analysis of the electron scattering results has not been completed, the peak at 7.9 MeV may be associated with the $M1$ structure observed at this excitation by threshold photoneutron techniques [207].

Vergados [208], in a calculation designed to examine configuration-mixing effects on $M1$ transitions in the Pb region, predicted such transitions at 5.5 and 7.5 MeV. Thus it was initially tempting to associate the peaks at 6.2 and 7.9 MeV with these transitions. However, in a resonance fluorescence experiment [209] an $M1$ transition at 4.8 MeV has

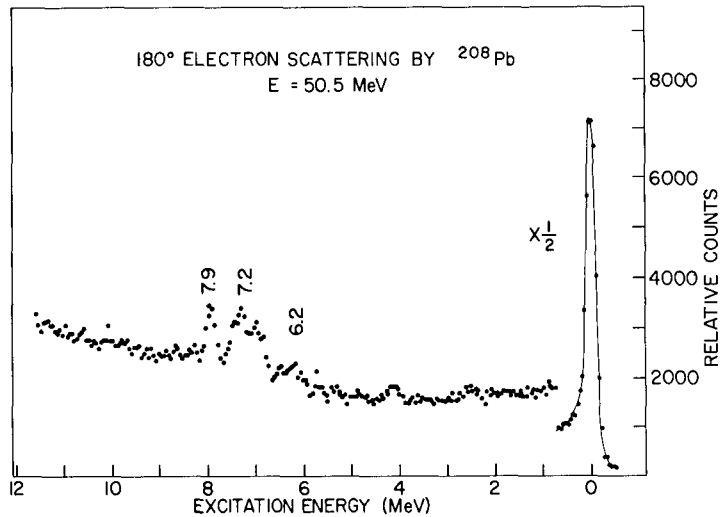


Fig. 42 — Spectrum of 50.5-MeV electrons scattered at 180° from ^{208}Pb . (From Refs. 173 and 179.)

been observed with a value of $\Gamma_0 = 5$ eV. Thus the picture of the $M1$ strength distribution in ^{208}Pb is as yet unclear. The Darmstadt group is at present reexamining this nucleus with their new high-resolution energy-loss system with the hope of contributing some clarification.

Still in progress is a study of ^{206}Pb using 180° scattering [178], which reveals peaks at about the same energies as in ^{208}Pb : 6.1, 6.9, 7.3, and 7.95 MeV. Although much work in this region of the nuclides remains to be done, the pattern that seems to be emerging is one which exhibits at least considerable $M1$ transition strengths in the 7- to 8-MeV excitation region. In this connection it should be noted that with (γ, γ') experiments [210], $M1$ strength in this excitation region has been observed in ^{141}Pr , ^{144}Nd , ^{205}Tl , ^{208}Pb , and ^{209}Bi .

Remarks on Some Closely Related Experimental $M1$ Studies

The purpose here is to call attention very briefly to a few types of closely related experiments designed to study $M1$ transitions besides the frequently cited nuclear reaction (γ, γ') and resonance fluorescence experiments. The study of final states excited in negative muon capture has proved a valuable complement to back-angle electron scattering observations of $M1$ transitions. This is typified in the work of Miller et al. [211] on $M1$ transitions in ^{24}Mg and ^{28}Si . A review of the study of nuclear structure by muon capture has recently been written by Überall [212]. The investigation of charge exchange $M1$ resonances to states which are analogs of those excited by back-angle electron scattering has generated considerable recent interest. Such studies using

the (t , ^3He) reaction have been made on the $M1$ transitions in ^{28}Al and ^{58}Co , for example [181, 204]. Also of considerable interest has been the study of $M1$ transitions from $T = 2$ states in self-conjugate nuclei. These transitions feed the $T = 1$ levels which are the subject of backward-angle electron scattering observations. In various nuclear reactions, such transitions from $T = 2$ levels have been observed in ^{20}Ne [213], ^{24}Mg [214], ^{28}Si [215], and ^{32}S [185].

CONCLUSIONS AND SUGGESTIONS FOR FURTHER STUDY

If one considers the early Stanford survey work on electroexcitation of $M1$ transitions to be the first phase of a progression to more refined measurements, then the second phase made possible by the laboratories at Darmstadt, Amsterdam, National Bureau of Standards (NBS), Saskatchewan, Glasgow, and NRL is now drawing to a close. The third phase generated by the development of the energy-loss (dispersion-matching) technique is already under way, with the first such system having recently become operational at Darmstadt.

Clearly, much of the work done in the second phase should be repeated. This is certainly true of work in the sd shell, particularly the upper part of the shell. A careful study of ^{32}S is especially needed. There are also some nuclei in the p -shell that should be reexamined, outstanding candidates being ^7Li , ^{10}B , and ^{14}N .

Although the high-energy electron scattering studies of nuclei in the s -shell command the most current interest, more accurate low- q measurements would still be useful. In this connection the work currently progressing on ^3He and ^3H at NBS and NRL should be helpful.

The nuclei with $A > 40$ constitute a relatively unexplored region. Closed-shell, or nearly closed, nuclei where spin-flip transitions are more possible have naturally been receiving the most attention. However, the situation among these nuclei needs much clarification, which will probably mean that they will remain in high priority for observation for some time.

ACKNOWLEDGEMENTS

The author expresses his deep gratitude for the support and invaluable interreaction that he received over the last eight years from his two primary coworkers, Drs. W. Bendel and E. Jones. Other coworkers who have been extremely helpful are Dr. N. Ensslin, Dr. R. Lindgren, Mr. R. Tobin, Miss S. Numrich, Dr. H. Kaiser, Dr. L. Cohen, and Dr. T. Godlove. The critical reading of the manuscript by Drs. G. Peterson, H. Überall, P. deWitt-Huberts, W. Bendel, and T. Godlove is greatly appreciated. The author is very grateful for enlightening discussions with Drs. H. Überall, R. Adler, and M. Rosen. He also wishes to express his gratitude to Ms. B. Sands and Ms. J. Sampson for their excellent typing, which was only exceeded by their gracious forbearance.

REFERENCES

1. L. W. Fagg, *Proceedings of the International Conference on Photonuclear Reactions and Applications*, Asilomar, Calif. (B. L. Berman, ed.), Vol. 1, 663, 1973.
2. W. C. Barber, F. Berthold, G. Fricke, and F. E. Gudden, *Phys. Rev.* **120**, 2081 (1960).
3. W. C. Barber, *Ann. Rev. Nucl. Sci.* **12**, 1 (1962).
4. J. Goldemberg and R. H. Pratt, *Rev. Mod. Phys.* **38**, 311 (1966).
5. H. Theissen, *Springer Tracts in Modern Physics* **65**, 1-59 (1972).
6. S. S. Hanna, in *Isospin in Nuclear Physics* (D. H. Wilkinson, ed.), North-Holland, Amsterdam, 1969.
7. S. Yoshida and L. Zamick, *Ann. Rev. Nucl. Sci.* **22**, 121 (1972).
8. G. A. Peterson, *Phys. Lett.* **2**, 162 (1962) and private communication.
9. M. Rosen, 1973, private communication.
10. W. C. Barber, J. Goldemberg, G. A. Peterson, and Y. Torizuka, *Nucl. Phys.* **41**, 461 (1963).
11. M. Rosen, R. Raphael, and H. Úberall, *Phys. Rev.* **163**, 927 (1967).
12. H. Úberall, *Electron Scattering from Complex Nuclei*, Academic Press, New York and London, 1971.
13. J. M. Blatt and V. F. Weisskopf, *Theoretical Nuclear Physics*, Wiley and Sons, New York, 1952.
14. R. J. Adler, *Phys. Rev.* **169**, 1192 (1968).
15. R. J. Adler, 1973, private communication.
16. L. W. Fagg and S. S. Hanna, *Rev. Mod. Phys.* **31**, 711 (1959).
17. X. K. Maruyama, R. A. Lindgren, W. L. Bendel, E. C. Jones, Jr., and L. W. Fagg, *Phys. Rev. C*, **10**, 2257 (1974).
18. B. H. Wildenthal, 1973, private communication.
19. T. H. Schucan, *Phys. Rev.* **171**, 1142 (1968).

20. M. A. Duguay, C. K. Bockelman, T. H. Curtis, and R. A. Eisenstein, *Phys. Rev.* **163**, 1259 (1967).
21. J. F. Ziegler and G. A. Peterson, *Phys. Rev.* **165**, 1337 (1968).
22. D. Drechsel, 1967, "Medium Energy Nuclear Physics with Electron Linear Accelerators," M.I.T. Summer Study, M.I.T.-2098-#470, p. 186 and D. Drechsel, *Nucl. Phys.* **A113**, 665 (1968).
23. S. T. Tuan, L. E. Wright, and D. S. Onley, *Nucl. Instrum. Methods* **60**, 70 (1968).
24. B. T. Chertok and W. T. K. Johnson, *Phys. Rev. Lett.* **22**, 67 (1969).
25. B. T. Chertok, *Phys. Rev.* **187**, 1340 (1969).
26. B. T. Chertok, W. T. K. Johnson, and D. Sarkar, *Phys. Rev. C*, **2**, 2028 (1970).
27. B. T. Chertok, W. T. K. Johnson, and D. Sarkar, "Table of Coulomb Distortion Corrections to Inelastic Electron Scattering Cross Sections for Magnetic Dipole and Quadrupole Transitions," American University, Washington, D.C., 1970.
28. L. Lapikás, A. E. L. Dieperink, and G. Box, *Nucl. Phys.* **A203**, 609 (1973).
29. P. Lee, 1974, private communication.
30. H. Andresen, 1974, private communication.
31. L. C. Maximon and D. B. Isabelle, *Phys. Rev. B*, **136**, 674 (1964).
32. L. C. Maximon, *Rev. Mod. Phys.* **41**, 193 (1969).
33. L. W. Mo and Y. S. Tsai, *Rev. Mod. Phys.* **41**, 205 (1969).
34. E. S. Ginsberg and R. H. Pratt, 1964, *Phys. Rev. B*, **134**, 773.
35. W. W. Gargaro and D. S. Onley, *Phys. Rev. C*, **4**, 1032.
36. G. A. Peterson and W. C. Barber, *Phys. Rev.* **128**, 812 (1962).
37. P. T. McCormick, D. G. Keiffer, and G. Parzen, *Phys. Rev.* **103**, 29 (1956).
38. J. W. Motz, H. Olsen, and H. W. Koch, *Rev. Mod. Phys.* **36**, 881 (1964).
39. R. E. Rand, R. Frosch, and M. R. Yearian, *Phys. Rev.* **144**, 859 (1966).
40. L. C. Maximon, 1970, unpublished notes.
41. E. Borie, *Phys. Rev. C*, **2**, 770 (1970).

42. H. Crannell, Nucl. Instrum. Methods **71**, 208 (1969).
43. D. B. Isabelle and J. Berthot, "Radiative Corrections from an Experimentalist's View Point," presented at Institute on Electron Scattering and Nuclear Structure, Cagliari, Italy, 1970.
44. J. T. O'Brien, H. Crannell, and F. J. Kline, Phys. Rev. C, **9**, 1418 (1974).
45. R. E. Rand, Nucl. Instrum. Methods **39**, 45 (1966).
46. B. T. Chertok, C. Sheffield, J. W. Lightbody, Jr., S. Penner, and D. Blum, Phys. Rev. C, **8**, 23 (1973).
47. R. D. Edge and G. A. Peterson, Phys. Rev. **128**, 2750 (1962).
48. C. de Vries, Stanford Linear Accelerator Center Report SLAC-25, 1963, p. 160, unpublished.
49. G. Proca, thesis University of Paris (Orsay) 1966.
50. D. Ganichot, D. Benaksas, B. Grossetete, J. Lorrain, and D. B. Isabelle, Nucl. Instrum. Methods **60**, 151 (1968).
51. D. Ganichot, B. Grossetete, and D. B. Isabelle, Nucl. Phys. A**178**, 545 (1972).
52. W. L. Bendel, L. W. Fagg, R. A. Tobin, and H. F. Kaiser, Phys. Rev. **173**, 1103 (1968).
53. G. J. C. Van Niftrik, H. de Vries, L. Lapikas, and C. de Vries, Nucl. Instrum. Methods, **93**, 301 (1971).
54. G. A. Peterson, Nucl. Instrum. Methods **59**, 341 (1968).
55. P. Leconte, Proceedings of M.I.T. Summer Study TID 24667, 1967, pp. 199-200.
56. L. A. C. Koerts, Nucl. Instrum. Methods **26**, 152 (1964).
57. J. C. Bergstrom, M.I.T. Laboratory for Nuclear Science Report LNS116 (May 1967) unpublished; and Proceedings of M.I.T. Summer Study TID 24667, p. 207.
58. S. Kowalski and H. Enge, *Proceedings of Fourth International Conference on Magnet Technology*, Upton, N.Y., 1972, p. 182.
59. G. A. Peterson and D. Vetter, 1974, private communication.
60. R. E. Rand, Rev. Sci. Instrum. **43**, 352 (1972).

61. L. W. Fagg, E. C. Jones, Jr., and W. L. Bendel, *Nucl. Instrum. Methods* **77**, 136 (1970).
62. E. C. Jones, 1974, private communication.
63. S. Penner, 1973, private communication.
64. G. Morpurgo, *Phys. Rev.* **110**, 721 (1958).
65. D. Kurath, *Phys. Rev.* **130**, 1525 (1963).
66. H. W. Kuehne, P. Axel, and D. C. Sutton, *Phys. Rev.* **163**, 1278 (1967).
67. L. W. Fagg, W. L. Bendel, L. Cohen, E. C. Jones, Jr., H. F. Kaiser, and H. Überall, *Phys. Rev. C*, **4**, 2089 (1971).
68. B. Castel, I. P. Johnstone, B. P. Singh, and J. C. Parikh, *Nucl. Phys.* **A157**, 137 (1970).
69. J. B. French and M. H. MacFarlane, *Nucl. Phys.* **26**, 168 (1961).
70. Ph. T. Nang, *Nucl. Phys.* **A185**, 413 (1972).
71. D. Kurath, *Phys. Rev. C*, **5**, 768 (1972).
72. F. E. Cecil, L. W. Fagg, W. L. Bendel, and E. C. Jones, Jr., *Phys. Rev. C*, **9**, 798 (1974).
73. P. O. Lipas, *Phys. Lett.* **8**, 279 (1964).
74. J. D. Murphy and H. Überall, 1974, to be published.
75. E. C. Jones and B. T. Chertok, 1968, unpublished.
76. V. Z. Jankus, *Phys. Rev.* **102**, 1586 (1956).
77. J. Goldemberg and C. Schaerf, *Phys. Lett.* **20**, 193 (1966).
78. L. Durand, III, *Phys. Rev.* **123**, 1393 (1961).
79. R. E. Rand, R. F. Frosch, C. E. Littig, and M. R. Yearian, *Phys. Rev. Lett.* **18**, 469 (1967).
80. B. Bosco, P. P. Delsanto, and F. Erdas, *Nuovo Cim.* **33**, 1240 (1964).
81. R. J. Adler and S. D. Drell, *Phys. Rev. Lett.* **13**, 349 (1964).
82. R. J. Adler, *Phys. Rev.* **141**, 1499 (1966).

83. R. Blankenbecler and J. F. Gunion, *Phys. Rev. D*, **4**, 718 (1971).
84. A. J. F. Siegert, *Phys. Rev.* **52**, 787 (1937).
85. J. Hockert, D. O. Riska, M. Gari, and A. Huffman, *Nucl. Phys.* **A217**, 14 (1973).
86. D. O. Riska, *Proceedings of the International Conference on Photonuclear Reactions and Applications*, Mar. 26-30, 1973, Asilomar, Calif. (B. L. Berman, ed.), Vol. 1, p. 337.
87. R. E. Rand, M. R. Yearian, H. A. Bethe, and C. D. Buchanan, *Phys. Rev. D*, **8**, 3229 (1973).
88. E. Hadjimichael, *Phys. Lett.* **46B**, 147 (1973).
89. S. A. Smirnov and S. V. Trubnikov, *Phys. Lett.* **48B**, 105 (1974).
90. H. G. Miller and H. Arenhovel, *Phys. Rev. C*, **7**, 1003 (1973).
91. M. Bernheim and G. R. Bishop, *Phys. Lett.* **5**, 294 (1963).
92. G. R. Bishop and M. Bernheim, *Phys. Lett.* **5**, 140 (1963).
93. J. Goldemberg, W. C. Barber, F. H. Lewis, Jr., and J. D. Walecka, *Phys. Rev. B*, **134**, 1022 (1964).
94. R. M. Hutcheon, T. E. Drake, V. W. Stobie, G. A. Beer, and H. S. Caplan, *Nucl. Phys.* **A107**, 266 (1968).
95. R. M. Hutcheon and H. S. Caplan, *Nucl. Phys.* **A127**, 417 (1969).
96. F. Eigenbrod, *Z. Phys.* **228**, 337 (1969).
97. R. M. Hutcheon, R. Neuhausen, and F. Eigenbrod, *Z. Naturforsch.* **25a**, 973 (1970).
98. R. Neuhausen and R. M. Hutcheon, *Nucl. Phys.* **A164**, 497 (1971).
99. F. C. Barker, *Nucl. Phys.* **83**, 418 (1966).
100. L. W. Fagg, W. L. Bendel, N. Ensslin, and E. C. Jones, Jr., *Phys. Lett.* **44B**, 163 (1973).
101. W. A. Fowler, *Nature* **238**, 24 (1972).
102. V. N. Fetisov and Yu. S. Kopysov, *Phys. Lett.* **40B**, 602 (1972).
103. R. Davis, Jr., L. C. Rogers, and V. Radenka, *Bull. Amer. Phys. Soc.* **16**, 631 (1971).

104. V. Trimble and F. Reines, *Rev. Mod. Phys.* **45**, 1 (1973).
105. L. S. Cardman, S. P. Fivozinsky, J. S. O'Connell, and S. Penner, *Bull. Amer. Phys. Soc.* **18**, 78 (1973).
106. G. R. Bishop, *J. Phys. A*, **6**, L21 (1973).
107. E. Spamer and F. Gudden, *Phys. Lett.* **14**, 210 (1965).
108. D. Kurath, *Phys. Rev.* **101**, 216 (1956).
109. W. F. Hornyak, C. A. Ludemann, and M. L. Roush, *Nucl. Phys.* **50**, 424 (1964).
110. D. Kurath, *Phys. Rev. B*, **134**, 1025 (1964).
111. E. Spamer, *Z. Phys.* **191**, 24 (1966).
112. P. Kossanyi-Demay and G. J. Vanpraet, *Nucl. Phys.* **81**, 529 (1966).
113. W. C. Barber and F. E. Gudden, *Phys. Rev. Lett.* **3**, 219 (1959).
114. T. W. Donnelly, J. D. Walecka, I. Sick, and E. G. Hughes, *Phys. Rev. Lett.* **21**, 1196 (1968).
115. G. J. Vanpraet and P. Kossanyi-Demay, *Z. Phys.* **222**, 455 (1969).
116. F. Gudden, *Phys. Lett.* **10**, 313 (1964).
117. G. A. Peterson, *Phys. Lett.* **25B**, 549 (1967).
118. C. de Vries, in "Nuclear Structure Studies using Electron Scattering and Photo-reaction," edited by K. Shoda and H. Ui, Tohoku University, Sendai, Japan, 1972, p. 405.
119. E. Spamer, K. Gravemeyer, C. W. deJager, and L. Dieperink, in *Proceedings of the International Conference on Nuclear Electron Scattering and Photoreaction*, Sendai, Japan, edited by K. Shoda and H. Ui (Research Report of Laboratory of Nuclear Science, Tohoku University), 1972.
120. J. S. O'Connell, T. W. Donnelly, and J. D. Walecka, *Phys. Rev. C*, **6**, 719 (1972).
121. M. Gell-Mann, *Phys. Rev.* **111**, 362 (1958).
122. B. Dudelzak and R. E. Taylor, *J. Phys. Radium* **22**, 544 (1961).
123. G. R. Bishop, M. Bernheim, and P. Kossanyi-Demay, *Nucl. Phys.* **54**, 353 (1964).
124. M. Bernheim, 1965, thesis, University of Paris (Orsay).

LAWRENCE W. FAGG

125. H. G. Clerc and E. Kuphal, *Z. Phys.* **211**, 452 (1968).
126. N. Ensslin, W. Bertozzi, S. Kowalski, C. P. Sargent, W. Turchinets, C. F. Williamson, S. P. Fivozinsky, J. W. Lightbody, Jr., and S. Penner, *Phys. Rev. C*, **9**, 1705 (1974).
127. H. J. Rose, O. Hausser, and E. K. Warburton, *Rev. Mod. Phys.* **40**, 591 (1968).
128. N. Ensslin, 1973, private communication.
129. M. Stroetzel and A. Goldmann, *Z. Phys.* **233**, 245 (1970).
130. W. L. Bendel, L. W. Fagg, S. K. Numrich, E. C. Jones, Jr., and H. F. Kaiser, *Phys. Rev. C*, **3**, 1821 (1971).
131. P. A. Quin, G. A. Bissinger, and P. R. Chagnon, *Nucl. Phys.* **A115**, 495 (1970).
132. R. C. Ritter, J. T. Parson, and D. L. Bernard, *Phys. Lett.* **28B**, 588 (1969).
133. T. E. Drake and R. P. Singhal, Internal Report, Kelvin Laboratory, University of Glasgow, Scotland, 1972.
135. Y. Akiyama, A. Arima, and T. Sebe, *Nucl. Phys.* **A138**, 273 (1969).
135. S. Maripuu and B. H. Wildenthal, *Phys. Lett.* **38B**, 464 (1972).
136. L. W. Fagg, W. L. Bendel, R. A. Tobin, and H. F. Kaiser, *Phys. Rev.* **171**, 1250 (1968).
137. P. J. M. Smulders, *Nucl. Phys.* **A210**, 579 (1973).
138. P. M. Endt and C. Van der Leun, *Nucl. Phys.* **A105**, 1 (1967).
139. M. A. Meyer, P. L. Reinecke, D. Reitmann, *Nucl. Phys.* **A185**, 625 (1972).
140. O. Titze, *Z. Phys.* **220**, 66 (1969).
141. A. Johnston and T. E. Drake, *J. Phys.* **7**, 898 (1974).
142. L. W. Fagg, W. L. Bendel, S. K. Numrich, and B. T. Chertok, *Phys. Rev. C*, **1**, 1137 (1970).
143. O. Titze, E. Spamer, and A. Goldmann, *Phys. Lett.* **24B**, 169 (1967).
144. Yu. I. Belyi and N. M. Kabachnik, *Nucl. Phys.* **14**, 619 (1972).

145. M. Bernheim and G. R. Bishop, *J. Phys. Radium* **24**, 970 (1963).
146. B. T. Chertok and E. C. Booth, *Nucl. Phys.* **66**, 230 (1965).
147. H. Artus, P. Brix, H. G. Clerc, F. Eigenbrod, A. Goldmann, F. Gudden, E. Spamer, P. Strehl, M. Stroetzel, O. Titze, K. J. Wetzel, 1967, in *Proceedings of International Nuclear Physica Conference*, Gatlinburg, 1966 (Academic Press, New York and London), p. 314.
148. H. G. Clerc, K. J. Wetzel, and E. Spamer, *Nucl. Phys.* **A120**, 441 (1968).
149. J. C. Bergstrom, I. P. Auer, M. Ahmad, F. J. Kline, J. H. Hough, H. S. Caplan, and J. L. Groh, *Phys. Rev. C*, **7**, 2228 (1973).
150. P. T. Kan, G. A. Peterson, and D. V. Webb, *Phys. Rev. C*, **11**, 323 (1975).
151. E. Spamer and H. Artus, *Z. Phys.* **198**, 445 (1967).
152. E. Spamer, 1973, private communication.
153. G. A. Proca and D. B. Isabelle, *Nucl. Phys.* **A109**, 177 (1968).
154. G. Wittwer, H. G. Clerc, G. A. Beer, *Z. Phys.* **234**, 120 (1970).
155. L. Lapikás, H. de Vries, and G. Box, 1974, to be published.
156. H. Crannell, P. L. Hallowell, J. M. Finn, J. T. O'Brien, N. Ensslin, L. Fagg, W. Bendel, E. Jones, *Bull. Amer. Phys. Soc.* **18**, 669 (1973).
157. G. A. Beer, P. Brix, H. G. Clerc, and B. Laube, *Phys. Lett.* **26B**, 506 (1968).
158. H. G. Clerc, "Habilitationsschrift," Technische Hochschule Darmstadt, Darmstadt, Germany, 1968.
159. W. C. Barber and G. J. Vanpraet, *Nucl. Phys.* **72**, 63 (1965).
160. O. Titze and E. Spamer, *Z. Naturforsch.* **21a**, 1504 (1966).
161. L. W. Fagg, W. L. Bendel, E. C. Jones, Jr., H. F. Kaiser, and T. F. Godlove, *Phys. Rev.* **187**, 1384 (1969).
162. E. W. Lees, A. Johnston, S. W. Brain, C. S. Curran, W. A. Gillespie, and R. P. Singhal, *J. Phys. A*, **7**, 936 (1974).
163. R. M. Lombard and G. R. Bishop, *Nucl. Phys.* **A101**, 601 (1967).
164. R. M. Lombard and G. R. Bishop, *Nucl. Phys.* **A101**, 625 (1967).

165. W. L. Bendel, E. C. Jones, Jr., and L. W. Fagg, *Bull. Amer. Phys. Soc. Ser. II* **19**, 999 (1974).
166. L. W. Fagg, W.L. Bendel, E. C. Jones, Jr., and S. Numrich, *Phys. Rev.* **187**, 1378 (1969).
167. H. Liesem, *Z. Phys.* **196**, 174 (1966).
168. T. E. Drake, E. L. Tomusiak, and H. S. Caplan, *Nucl. Phys.* **A118**, 138 (1968).
169. L. W. Fagg, W. L. Bendel, E. C. Jones, Jr., L. Cohen, and H. F. Kaiser, *Phys. Rev. C*, **5**, 120 (1972).
170. H. Theissen, R. J. Peterson, W. J. Alston, III, and J. R. Stewart, *Phys. Rev.* **186**, 1119 (1969).
171. R. A. Lindgren, W. L. Bendel, E. C. Jones, Jr., L. W. Fagg, X. K. Maruyama, J. W. Lightbody, and S. P. Fivozinsky, 1974, to be published.
172. F. E. Cecil, W. L. Bendel, E. C. Jones, Jr., and L. W. Fagg, 1974, to be published.
173. L. W. Fagg, W. L. Bendel, E. C. Jones, Jr., N. Ensslin, and F. E. Cecil, *Proceedings of the International Conference on Nuclear Physics*, Munich, 1973, p. 631.
174. R. Pitthan and T. Walcher, *Phys. Lett.* **36B**, 563 (1971).
175. R. Pitthan and T. Walcher, *Z. Naturforsch.* **27a**, 1683 (1972).
176. R. Pitthan, *Z. Phys.* **260**, 283 (1973).
177. M. A. Lone, H. C. Lee, L. W. Fagg, W. L. Bendel, E. C. Jones, Jr., X. K. Maruyama, and R. A. Lindgren, 1974, to be published.
178. M. A. Lone, W. L. Bendel, R. A. Lindgren, E. C. Jones, L. W. Fagg, and F. E. Cecil, 1974, to be published.
179. W. L. Bendel, E. C. Jones, L. W. Fagg, R. A. Lindgren, and F. E. Cecil, 1973, to be published.
180. I. S. Gulkarov, N. G. Afanasyev, G. A. Savitsky, V. M. Khvastunov, and N. G. Shevchenko, *Phys. Lett.* **B27**, 417 (1968).
181. E. R. Flynn, J. Sherman, and N. Stein, *Phys. Rev. Lett.* **32**, 846 (1974).
182. A. Tsveter, *Nucl. Phys.* **A185**, 433 (1972).
183. B. Rosner, K. Wittner, K. Bethge, and I. Tserruya, *Nucl. Phys.* **A218**, 1 (1974).

184. O. Häusser, T. K. Alexander, D. Pelte, B. W. Hootrn, and H. C. Evans, *Phys. Rev. Lett.* **23**, 320 (1969).
185. S. Gales, M. Langevin, J. M. Maison, and J. Vernatte, *Compt. Rend.* **271**, 978 (1970).
186. A. Graue, L. Herland, J. R. Lien, and E. R. Cosman, *Nucl. Phys.* **A120**, 513 (1968).
187. P. J. Twin, W. C. Olsen, and D. M. Sheppard, *Nucl. Phys.* **A143**, 481 (1970).
188. R. Wechsung, W. Strassheim, and R. Bass, *Nucl. Phys.* **A170**, 557 (1971).
189. A. N. James, P. R. Alderson, D. C. Bailey, P. E. Carr, J. L. Durell, W. A. Greene, and J. F. Sharpey-Schafer, *Nucl. Phys.* **A172**, 401 (1971).
190. B. T. Chertok, E. C. Jones, W. L. Bendel, and L. W. Fagg, *Phys. Rev. Lett.* **23**, 34 (1969).
191. J. S. O'Connell and B. F. Gibson, 1973, private communication.
192. L. Lapikás, Master's thesis, Instituut voor Kernfysisch Onderzoek, Amsterdam, 1970.
193. G. J. C. Van Niftrick, L. Lapikás, H. de Vries, and G. Box, *Nucl. Phys.* **A174**, 173 (1971).
194. S. J. Skorka, J. Hertel, and T. W. Retz-Schmidt, *Nuclear Data A*, **2**, No. 4, 347 (1966).
195. H. G. Clerc, K. J. Wetzel, and E. Spamer, *Phys. Lett.* **20**, 667 (1966).
196. S. Cohen and D. Kurath, *Nucl. Phys.* **73**, 1 (1965).
197. D. H. Wilkinson, J. T. Sample, and D. E. Alburger, *Phys. Rev.* **146**, 662 (1966).
198. A. G. Slight, T. E. Drake, and G. R. Bishop, *Nucl. Phys.* **A208**, 157 (1973).
199. B. M. Preedom and B. H. Wildenthal, *Phys. Rev. C*, **6**, 1633 (1972).
200. P. Kossanyi-Demay and G. J. Vanpraet, Stanford University Preprint HEPL 394, 1966.
201. D. V. Webb, G. A. Peterson, L. W. Fagg, W. L. Bendel, and E. C. Jones, 1974, to be published.
202. R. M. Tapphorn, M. Kregar, and G. G. Seaman, *Phys. Rev. C*, **3**, 2232 (1971).
203. N. Shikazono and Y. Kawarasaki, *Nucl. Phys.* **A188**, 461 (1972).

204. E. R. Flynn, J. D. Garrett, Phys. Rev. Lett. **29**, 1748 (1972).
205. T. Walcher, 1973, private communication.
206. N. Ensslin, W. L. Bendel, L. W. Fagg, T. F. Godlove, and E. C. Jones, Bull. Amer. Phys. Soc. Ser. II **18**, 670 (1973).
207. C. D. Bowman, R. J. Baglan, B. L. Berman, and T. W. Phillips, Phys. Rev. Lett. **25**, 1302 (1970).
208. J. D. Vergados, Phys. Lett. **36B**, 12 (1971).
209. C. P. Swann, Phys. Rev. Lett. **32**, 1449 (1974).
210. A. Wolf, R. Moreh, A. Nof, O. Shahal, and J. Tenenbaum, Phys. Rev. C, **6**, 2276 (1972).
211. G. H. Miller, M. Eckhause, P. Martin, and R. E. Welsh, Phys. Rev. C, **6**, 487 (1972).
212. H. Überall, in Springer Tracts in Modern Physics, **71**, 1-38 (1974).
213. H. M. Kuan, D. W. Heikkinen, K. A. Snover, F. Riess, and S. S. Hanna, 1967, Phys. Letters **25B**, 217.
214. F. Riess, W. J. O'Connell, D. W. Heikkinen, H. M. Kuan, and S. S. Hanna, Phys. Rev. Lett. **19**, 367 (1967).
215. K. A. Snover, D. W. Heikkinen, F. Riess, H. M. Kuan, and S. S. Hanna, Phys. Rev. Lett. **22**, 239 (1969).

GLOSSARY OF SYMBOLS

Some of the symbols listed below may be used at times to denote other quantities in the text. However, when this is the case, such use will be clear from the definitions accompanying them as well as from the context. Other symbols used only rarely are defined in the text.

a	spin-orbit coupling parameter
A	atomic number
$B(XL,q)$	reduced transition matrix element where $X = E$ (electric), or M (magnetic)
E, E'	incident and scattered electron energies, respectively
f_c	Coulomb distortion correction coefficient, $f_c = (d\sigma/d\Omega)_{\text{DWBA}} / (d\sigma/d\Omega)_{\text{PWBA}}$
H	nuclear Hamiltonian
J_0, J	ground- and excited-state spins, respectively
k	photon momentum
l	nuclear orbital angular momentum
L	transition multipolarity
m	electron mass
p, p'	incident and scattered electron momenta, respectively
q	momentum transfer
R_c	nuclear charge radius
R_m	nuclear matter radius
R_{tr}	nuclear transition radius
s	nuclear spin
T	isospin quantum number
Z	nuclear charge
α	fine structure constant
Γ_0	ground-state width for electromagnetic transitions
μ	nuclear magnetic moment operator
θ	angle of electron scattering
σ	general term for cross section
$\vec{\sigma}$	Pauli spin operator
τ	isospin operator (τ_3 , its third component)
ω	nuclear excitation energy
Ω	solid angle